Biomaterials Science: Studies on Injectable Biomaterials for Cardiac Tissue Engineering

A THESIS PRESENTED BY

Remya K

TO

SREE CHITRA TIRUNAL INSTITUTE FOR MEDICAL
SCIENCES AND TECHNOLOGY
THIRUVANANTHAPURAM
INDIA

IN PARTIAL FULFILMENT OF THE REQUIREMENTS
FOR THE AWARD OF
DOCTOR OF PHILOSOPHY

January 2017

DECLARATION

I, Remya K, hereby certify that I had personally carried out the work depicted in the thesis entitled, "Biomaterials Science: Studies on Injectable Biomaterials for Cardiac Tissue Engineering", except where due acknowledgment has been made in the text. No part of the thesis has been submitted for the award of any other degree or diploma prior to this date.

Thiruvananthapuram
06-01-2017

Remya K
Reg No: Ph.D/2014/01
Roll No: 6654

SREE CHITRA TIRUNAL INSTITUTE FOR MEDICAL

SCIENCES & TECHNOLOGY, TRIVANDRUM

Thiruvananthapuram – 695011, INDIA
(An Institute of National Importance under Govt. of India)
Phone-(91)0471-2520248 Fax-(91)0471-2341814
Email: jayabalan@sctimst.ac.in Web site – www.sctimst.ac.in

CERTIFICATE

This is to certify that **Mrs. Remya K**, in the Polymer Division, BMT Wing of this institute has fulfilled the requirements prescribed for the Ph. D. degree of the Sree Chitra Tirunal Institute for Medical Sciences and Technology, Thiruvananthapuram. The thesis entitled, "**Biomaterials Science: Studies on Injectable Biomaterials for Cardiac Tissue Engineering**" was carried out under my direct supervision. No part of the thesis was submitted for the award of any degree or diploma prior to this date.

* Clearance was obtained from the Institutional Ethics Committee/ Institutional Animal Ethics Committee for carrying out the study wherever it is required.

Thiruvananthapuram
06-01-2017

Dr. M Jayabalan Ph.D, D.Sc
(Research Supervisor)
Scientist - G & Head
Polymer Division, BMT wing
SCTIMST, Thiruvananthapuram

The thesis entitled

"Biomaterials Science: Studies on Injectable Biomaterials for Cardiac Tissue Engineering".

Submitted by

Remya K

for the degree of

Doctor of Philosophy

Of

SREE CHITRA TIRUNAL INSTITUTE
FOR MEDICAL SCIENCES AND TECHNOLOGY,
THIRUVANANTHAPURAM - 695011

is evaluated and approved by

……..	……..
Dr. M Jayabalan. Ph.D, D.Sc.	Examiner
(Research Supervisor)	

Dedicated to

My family, teachers & friends.....

A C K N OWL E D G EM E N T

I would like to express my heartfelt gratitude and respect to my supervisor Dr. M. Jayabalan, Scientist-G, Polymer Science Division-BMT wing, SCTIMST. His guidance, critical evaluations, suggestions and encouragement helped in nurturing my passion for science throughout the course of study. I thank him for his fatherly suggestions and entire support offered during my Ph. D programme.

I am grateful to the former and present Director of SCTIMST and the present Head and the previous Heads, BMT Wing for all support provided during the course of my work.

I thank members of the doctoral advisory committee, Dr. Ramesh P, (Scientist-G, Division of Polymeric Medical Devices) and Dr. Maya Nandkumar A (Scientist-G, Division of Microbial Technology) for their timely suggestions and critical comments.

I am thankful to Dr. George A.V, Registrar, Dr. Sundar Jayasingh, former Deputy Registrar, Dr. Santhosh Kumar, Deputy Registrar, Dr.Kumari T.V, Associate Dean for Ph.D affairs, Dr. Kalliyanakrishnan V, Dean, and all members of academic division and Director's office for their administrative support.

I thank all my friends from our laboratory Dr. Sunitha Prem Victor, Dr. Shivaram Selvam, Dr. Finosh G.T, Vineeth , Shamon , Jibin, Adarsh , Reesha, Girija and Gayathri for their help and support.

I am thankful to Dr.Prabha.D.Nair, Rakhi, Rahul (UV-Visible spectroscopy), Dr.K.Sreenivasan , P.R.Hari, Dr.C.Radhakumari (GPC, thermal analysis), Dr.Manoj Komath, Nishad KV (ESEM), Dr. Suresh Babu S (ICP analysis), Dr. Sabareeswaran (Cryosectioning of hydrogels), Dr. Lissy K. Krishnan, Dr. Anugya Bhatt, Priyanka A, Anilkumar V (Hemolysis), Dr. T.V Anilkumar, Reshma, Manju (Lyophilization, Cryopreservation of cells) for their for their assistance during the evaluations.

Thanks to the staff of various administrative departments and library of the Institute and fellow students in the campus for their lively companionship.

I thank The Director, RGCB, Thiruvananthapuram (Confocal analysis), The Director, NIIST, Thiruvananthapuram (NMR analysis) for extending their test facilities.

I am thankful to CSIR-New Delhi for JRF/SRF fellowships.

I am thankful to my parents (Reena, Rameshan), brother (Rahul), husband (Harikrishnan), family, friends and teachers for their, blessings, prayers, support and encouragements.

My immense gratefulness to the Lord Almighty for showering immeasurable blessings with ever loving family, caring supervisor, supporting friends, and so on for the successful completion of this endeavor.

Remya K

CONTENTS

Chapter 3 MATERIALS AND METHODS

Chapter 4 RESULTS

List of Figures

List of tables

ABBREVIATIONS

PP	Poly(propylene fumarate- co- ethylene glycol)
SP	Poly(propylene fumarate-co-sebacate-co-ethylene glycol)
PEAM	Mannitol-fumarate-poly (ethylene adipate)-fumarate-PEG
PEAX	Xylitol-fumarate-poly(ethylene adipate)-fumarate-PEG
PANI	Polyaniline
PANIE-P	Polyaniline emeraldine salt conjugated fumarate-PEG-sebacate
PANIS-P	Sulfonated polyaniline conjugated fumarate-PEG-sebacate
PEG	Poly(ethylene glycol)
PEGDA	Poly(ethylene glycol) diacylate
TEMED	N, N, N', N'-tetra ethyl methyl ethylene diamine
APS	Ammonium persulfate
PP6	Poly(propylene fumarate- co- ethylene glycol)/PEGDA hydrogel
SP 17	Poly(propylene fumarate-co-sebacate-co-ethylene glycol)/PEGDA hydrogel
PEAM-P	Mannitol-fumarate-poly (ethylene adipate)-fumarate-PEG/PEGDA hydrogel
PEAX-P	Xylitol-fumarate-poly(ethylene adipate)-fumarate-PEG/PEGDA hydrogel
PE50P	50% PANIE-P/PEGDA hydrogel
PS50P	50% PANIS-P/PEGDA hydrogen
EDC	1-Ethyl-3-(3-dimethylaminopropyl)carbodiimide
NHS	N-hydroxysuccinimide
MI	Myocardial infarction
HF	Heart failure
MSC	Mesenchymal stem cells

ESC	Embryonic stem cells
CSC	Cardiac stem cells
ADMSC	Adipose derived stem cells
iPSC	Induced pluripotent stem cells
EHT	Engineered heart tissue
OPF	Oligo(poly(ethylene glycol) fumarate
MTT	3-(4,5-Dimethylthiazol-2-Yl)-2,5-Diphenyltetrazolium Bromide
PBS	Phosphate buffered saline
FT-IR	Fourier transform infrared
^{1}H-NMR	Proton nuclear magnetic resonance
GPC	Gel permeation chromatography
DMSO	Dimethyl sulfoxide
$CDCl_3$	Deuterated chloroform
DSC	Differential scanning calorimetry
ESEM	Environmental scanning electron microscope
DPPH	1-1-diphenyl 2-picryl hydrazyl
EDTA	Ethylenediaminetetraacetic acid
DCFH-DA	2', 7' dichloro dihydro fluorescein diacetate
DCF	2', 7' dichloro dihydro fluorescein
DMEM	Dulbecco's Modified Eagle Medium
NCCS	National Centre for Cell Science
ROS	Reactive oxygen speceis
H_2O_2	Hydrogen peroxide
$FeCl_3$	Ferric chloride
TBA	Thiobarbituric acid

SYNOPSIS

Biomaterial science: Studies on injectable biomaterials for cardiac tissue engineering

American Heart Association reports ischemic heart failure as one of the major cause of death in the world. The current pharmacological and device-based cardiac therapy fails to prevent ventricular remodeling and recurrent heart failure. Cell based regenerative therapy is the practical solution for post-infarcted myocardial repair. However, the pathological free radicals generated at the infarct zone hinder the engraftment of delivered cells. Recently, various biocompatible materials have emerged as cell carriers to augment safe delivery of potential cells for cardiac regenerative therapy. Among these materials, the hydrogels are preferred due to the soft tissue-like viscoelasticity, high water holding capacity and porous morphology. The injectable hydrogels augment minimally invasive cell delivery in a one-step procedure.

So far, several groups have reported injectable hydrogels based on PEG-fibrin, chitosan and hyaluronic acid for cardiac cell delivery. The fibrin hydrogels are highly sensitive to fibrinolysis and degrades completely within 3-4 days in the presence of hydrolytic enzymes. However, PEGylation slightly slow down the degradation of fibrin, PEGylated-fibrin has poor compatibility with the encapsulated cells. The lower mechanical property of chitosan and hylauronic acid based hydrogels does not meet the required criteria for cardiac regeneration. Moreover, the decrease of mechanical moduli of shear thinning hylauronic hydrogels under cyclic deformations restricts their potential for cardiac

applications. In addition, these natural polymers may cause immune rejection and pathogen transfer on clinical applications. Therefore, the hydrogels prepared from synthetic polymers with tunable physical properties, low-cost bulk synthesis and fewer chances of immune rejection are preferred for injectable therapy. However, the synthetic hydrogels are rarely explored for cell encapsulation due to the poor cell adhesion and proliferation and toxicity of monomers when mixed with cells for injection. Further, the studies on the effect of mechanical stability of hydrogels on the fibrotic infarct size reveal the need for hydrogels with higher mechanical strength, better mechanical stability in biological fluid with high stress bearing property for cardiac regenerative therapy. For the successful engraftment of cells with myocardium, the injectable hydrogels with inherent free radical scavenging capability are preferable. Chitosan-glutathione based hydrogels and cellulose-trans ferulic acid hydrogels were reported with the free radical scavenging property. However, the short life span of glutathione and trans-ferulic acid limits the scavenging efficiency. Therefore, it is relevant to explore novel synthetic injectable hydrogels with inherent free radical scavenging property and cell encapsulation capability for cardiac regenerative therapy.

With this background, we aimed to develop synthetic injectable hydrogels with adequate physicochemical, mechanical properties and bulk morphology to scavenge free radicals and to promote adhesion and proliferation of encapsulated cells. The major objectives of the present investigation were to develop synthetic, biocompatible and injectable and mechanically viable hydrogels using polyester based comacromers, and to study the cytocompatibility, inherent free radical scavenging property and cell encapsulation efficiency of hydrogels.

The thesis consists of six chapters. Chapter-1 deals with the introduction of the investigation. This chapter describes the pathophysiology of heart failure, limitations of current pharmacological and surgical treatments and challenges in cardiac regenerative therapy.

Chapter 2 deals with the literature review on different engineering strategies used for cardiac regenerative therapy. This chapter describes the previously reported free radical scavenging injectable hydrogels for cardiac cell therapy. The objectives and scope of the present study are also described in this chapter.

Chapter 3 deals with the materials and methodology. This chapter consists of six sections. Section-1 describes the synthesis and characterization of polyester comacromers for hydrogel preparation. Three types of comacromers based on poly (propylene fumarate), sugar alcohol and polyaniline were synthesized. The poly(propylene fumarate- co- ethylene glycol) (PP), poly(propylene fumarate-co-sebacate-co-ethylene glycol) (SP), mannitol-fumarate-poly (ethylene adipate)-fumarate-PEG (PEAM), xylitol-fumarate-poly(ethylene adipate)-fumarate-PEG (PEAX), polyaniline emeraldine salt conjugated fumarate-PEG-sebacate (PANIE-P) and sulfonated polyaniline conjugated fumarate-PEG-sebacate (PANIS-P) comacromers were synthesized. The structural features of comacromers were analyzed using FT-IR and ^{1}H-NMR analysis. Section 2 describes the preparation of injectable hydrogels from the synthesized comacromers. The vinyl crosslinker, poly(ethylene glycol) diacrylate was used as a crosslinker. The setting characteristics of hydrogels; PP6, SP 17, PEAM-P, PEAX-P, PE50P and PS50P derived from PP, SP, PEAM, PEAX, PANIE-P and PANIS-P comacromers were

investigated. Section 3 deals with the characterization of physical properties of the hydrogels, studies on water swelling property, analysis of surface and cross-sectional morphology by environmental scanning electron micrograph, studies on *in vitro* ageing and biomechanical property of hydrogels in PBS. The state of water (free and bound water) present in the hydrogels was analyzed using differential scanning calorimetry. In addition, the electrical conductivity of polyaniline-based hydrogels was determined using a multimeter. Section 4 deals with the studies on cytocompatibility of hydrogels with L929 fibroblast cells evaluated by MTT assay, direct contact test, and live-dead assay as per ISO10993-5:2009. The hemolysis of hydrogels was also evaluated as per ISO 10993-4:2002 (E). Section 5 in this chapter deals with the studies on free radical scavenging property of hydrogels. The experiments conducted include biochemical assays on DPPH, hydroxyl, nitric oxide radicals and analysis on the protective effect of hydrogels over cardiomyoblast cells under oxidative stress. The intracellular ROS release from the cells under oxidative stress was studied by DCFH-DA assay in the presence and absence of hydrogels. Section 6 describes the studies on cell encapsulation efficiency of hydrogels. The cell proliferation, viability and extracellular matrix protein formation by the encapsulated cardiomyoblast cells were evaluated.

The chapter 4 and 5, deals with the results and discussion of the investigation respectively. These chapters are divided into different sections. Section 1, deals with the synthesis and spectral analyses of PP, SP, PEAM, PEAX, PANIE-P and PANIS-P comacromers. The presence of trans fumarate group in each comacromer, responsible for *in situ* gelation is confirmed with

structural characterizations. Section 2, deals with the schemes for the preparation of hydrogels by crosslinking comacromer with PEGDA to form hydrogels and variations in setting characteristics. Section 3, deals with the evaluation of physical and mechanical characteristics of hydrogels. The present hydrogels retain more than 75% water at equilibrium swelling. The SP 17 hydrogel has lower swelling ratio compared to PP6 hydrogel, due to the presence of hydrophobic sebacic acid in the former. The PEAM-P and PEAX-P hydrogels have similar swelling property, which may be due to the comparable water affinity of mannitol and xylitol. In the case of polyaniline-based hydrogels, the sulfonation has increased the water affinity of PS50P hydrogel in comparison with the non-sulfonated PE50P hydrogel. The degree of free and bound water present in the hydrogels influences the growth and adhesion of encapsulated cells inside the hydrogel. Relatively higher free water content and lower bound water is observed in all hydrogels. The ESEM analysis of present hydrogels reveals porous surface and cross-sectional morphology, which is favorable for vascularization and cell proliferation. The Young modulus of human heart muscle varies from 20-500 kPa at the end of diastole. The compressive Young moduli of the present hydrogels are in the range of human myocardium. The PEAM-P and PS50P hydrogels exhibit higher mechanical stiffness compared to other hydrogels, which is beneficial to provide better bulking effect on myocardium. The stress-strain curve indicates the extensibility of the present hydrogels, which increases with ageing; this is beneficial to prevent the collapse of hydrogels on forceful cardiac contractions. The PEAM-P and PS50P exhibit better mechanical stability under *in vitro* ageing. The electrically responsive matrices facilitate the electrical syncytium of engrafted cell with the existing myocardium. The electrical

conductivity of native myocardium is 1.6 x 10^{-5} S cm^{-1} longitudinally and 5 x 10^{-5} S cm^{-1} transversally. The electrical conductivity of PS50P hydrogel is 0.378± 0.030 x 10^{-3}, which is greater than the native human myocardium. Section 4 deals with the cytocompatibility of hydrogels with L929 cells. The present hydrogels are cytocompatible as per ISO10993-5. The PEAM-P and PS50P hydrogels cause 0.06% and 0.04% hemolysis, which are in the acceptable range as per ISO 10993-4.

Section 5 discusses the free radical scavenging property of hydrogels. The present hydrogels exhibit appreciable DPPH scavenging property comparable to ascorbic acid, which substantiate the reducing power of hydrogels. The SP17 and PEAM-P hydrogels exhibit better hydroxyl, nitric oxide radical scavenging property. The present hydrogels have appreciable reducing power, comparatively higher for PEAM-P hydrogel. The cardiomyoblast cells exhibit more than 80% viability with SP17 and PEAM-P hydrogel even in the presence of stress inducing media, which substantiates the role of hydrogels to reduce the free radical exposure to the cells. The presence of SP17 and PEAM-P hydrogels significantly reduces the release of intracellular reactive oxygen species from the cells under oxidative stress. The free π electrons, hydroxyl groups and free water associated with hydrogel plays significant role in free radical scavenging property of the present hydrogels. Section 6 presents the studies on cell encapsulation efficiency of hydrogels with cardiomyoblast cells. The cardiomyoblast cells encapsulated inside the hydrogel proliferate under *in vitro* culture. Relatively PEAM-P and PEAX-P favor cell proliferation with high cell density. The histological staining confirms the distribution of extracellular matrix proteins inside the hydrogel

matrix, which substantiate the tissue formation. The viability of cells inside the hydrogel under static culture substantiates better channeling of nutrients and gasses throughout the hydrogel, which is essential to retain the cell viability even under slow vascularisation conditions of infarct zone. Considering the synergistic properties of mechanical stability, free radical scavenging ability and cell proliferation, the PEAM-P hydrogel is more promising for cardiac regenerative therapy.

The chapter 6 deals with the summary, conclusion and future prospects of the present research work. The potential scope of standardization of most promising injectable PEAM-P hydrogel for *in vivo* evaluation and clinical translation by designing the suitable delivery vehicle for injecting the present hydrogel formulations through subxiphoid-epicardial method are emphasized. The scope of modification of PEAM-P hydrogel using cell adhesion peptides and angiogenic factors are presented. The applicability of PEAM-P hydrogel for the delivery of differentiation factors to induce *in situ* differentiation of myofibroblast at the infarct zone to cardiomyocytes is also discussed in this chapter.

CHAPTER 1

INTRODUCTION

1 Introduction

The molecular pathophysiology of heart failure is explained. The drawbacks of current pharmacological approaches and need for cardiac regenerative therapy for the repair of the post-infarcted myocardium are presented. The major challenges in cardiac regenerative therapy including selecting the population of cells, selecting the biomaterial for cell carriers, scaffolding approaches, need for vascularization, the significance of free radical scavenging and electroactive cell carriers are discussed in this chapter.

The heart is an organ less than the size of our fist, which is controlling the rhythm of life from the early embryonic stage to death. This pumping station of our body is the primary organ to form in an embryo. The human heart is a four-chambered muscular organ situated to the left of the midline of the thoracic cavity. The heart contracts more than 3 billion times in an average human lifespan and pumps over 7000 L blood per day along 160000 km of blood vessels (Venugopal *et al.*, 2012). However, the heart is one of the most susceptible organs, which can end our pulse without giving noticeable warning.

1.1. Heart failure statistics

Heart failure (HF) is the incapability of heart to maintain cardiac output required to meet the metabolic activities and systemic venous return. Heart disorder is more prevalent in male after 40 years of age and after 60 is equal in both sexes (Go *et al.*, 2014). The dramatic increase in the prevalence of heart failure is evident from the statistics in the 1970s to 1990s, which declared HF as an epidemic (Bui *et al.*, 2011). American Heart Association reports one death in every 40 seconds due to cardiovascular disease (CVD) in 2010 and 150000 silent deaths by myocardial infarction (MI) each year. In India 22.7 million people suffers end cardiac disorders (Pillai *et al.*, 2013). 1.4 million death followed by CVD was reported in 2004 which will be 2.1million in 2021 as per the statistics (Srivastava and Mohanty., 2013). The ultimate reason for HF is the irreversible loss of cardiomyocytes from the ventricular myocardium. The most prevalent etiologies are ischemic disorders, hypertension, and diabetes.

Table-1: ACC/AHA classification of heart failure

Class	Diagnosis	Treatment
Stage A	No structural disorders but high risk of developing heart failure	Exercise, avoid smoking, treatment for high blood pressure and cholesterol
Stage B	Patients with low ejection fraction and valve disease but without signs and symptoms of heart failure.	Treatment with angiotensin converting enzyme inhibitor (ACE inhibitor) or angiotensin II receptor blocker (ARB) along with beta-blockers. Or appropriate surgical treatments like coronary artery bypass and valve repair or replacement.
Stage C	Patients with systolic heart failure with symptoms like shortness of breath, Fatigue and reduced ability to exercise	ACE inhibitor and beta-blocker therapy supported with diuretics and digoxin. Surgical cues includes biventricular pacing or an implantable defibrillator
Stage D	Patients with systolic heart failure with advanced symptoms even after receiving medical care.	Heart transplantation, ventricular assist devices, continuous infusion of intravenous heart pump drugs and palliative care.

HF is classified by New York Heart Association (NYHA classification) and American College of Cardiology /American Heart Association (ACC/AHA classification) based on physical disability, evolution, and progression of disease respectively (Table-1) (Kemp and Conte., 2012).

1.2. Myocardial infarction: pathophysiology at molecular level

A profound knowledge of origin and prognosis of the disease is essential to formulate an effective treatment. A heart attack happens after a series of pathological events including coronary obstructions, which cause ischemic injury and necrosis of cardiomyocytes (Soukoulis *et al.*, 2014). The myocardial repair happens through an inflammatory, proliferative and maturation phase (Figure-1).The necrotic cardiomyocytes release high mobility group protein B1, heat shock proteins, ATP, hyaluronan and fibronectin fragments that function as proinflammatory signals via toll-like receptors (TLR2 and TLR4).

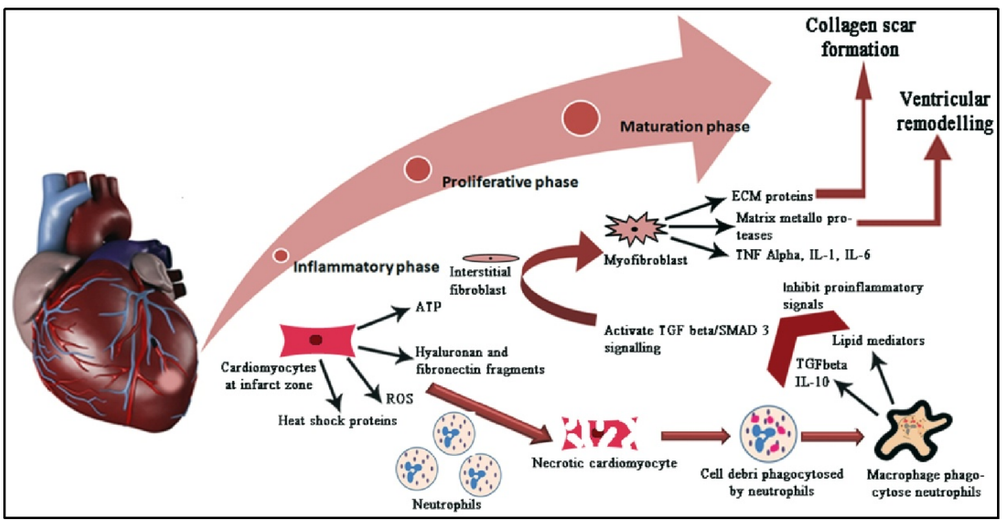

Figure-1: Repair of infarct zone followed by ischemic injury

The CXC chemokines and monocyte chemoattractant protein 1(MCP 1) expressed at the infarct zone can recruit neutrophils and monocytes to clear the cell debris. At the end of the inflammatory phase, the macrophages phagocytose the neutrophils and secrete TGFβ, IL -10 and lipid mediators (Shinde and Frangogiannis., 2014). The activation of TGF-β/ Smad 3 signaling induces the interstitial fibroblasts into myofibroblast. The myofibroblast proliferates and secretes ECM proteins, matrix metalloproteinases (MMP), TNF-α, IL- 1, IL-6 and TGF-β (Ma *et al.*, 2014). The MMP degrades collagen, laminin and other ECM proteins ensuing myocardial wall thinning. The structural variations of myocardium alter the biomechanical features, which significantly affect the cardiac output.

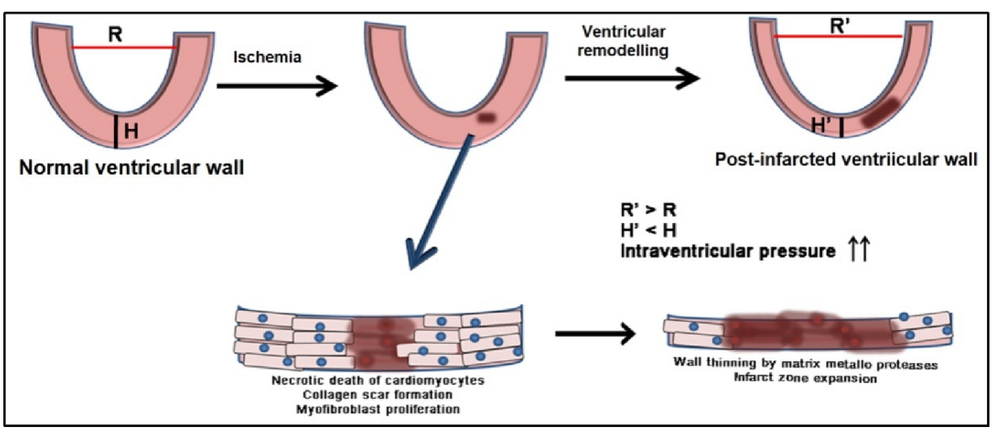

Figure-2: Ventricular remodeling followed by myocardial infarction.

As per Laplace theory (Leri *et al.*, 2011) slight variations in myocardial wall thickness drastically varies the wall stress (Eq.1).

$$\text{Ventricular wall stress} = \frac{\text{Ventricular chamber radius x intra-ventricular pressure}}{\text{2 x ventricular wall thickness}} \quad \text{(Eq.1)}$$

The wall thinning increases the chamber radius and the wall stress (Figure-2). The higher wall stress influences the generation of the sarcomere, alters the gene expression profile of cardiomyocytes, induce hypertrophy and reduces the elasticity of myocardium.

1.3. Pharmacological approaches

Heart failure is a complex disease condition, which is not yet under control of existing therapeutic approaches. The therapeutic interventions vary with different stages of HF. Stage A is associated with family history, smoking and food habits, which require treatment to modify the risk factors like blood pressure. The treatment of structural heart disease is recommended for stage B HF.

However, the patients with HF at stages C and D require strict attention to avoid mortality. Surgical interventions are recommended for stage C and D HF depending on the severity. The therapeutic interventions vary with different stages of HF. Stage A is associated with family history, smoking and food habits which require treatment to modify the risk factors like blood pressure. The treatment for structural heart disease is recommended for stage B HF. However, patients with HF at stages C and D require strict attention to avoid mortality. Surgical interventions are recommended for stage C and D HF depending on the severity.

Table-2: Pharmacological and surgical treatments for heart failure

Pharmacological Approaches	**Pharmacological Action**	**Function**	**Side effects**
Angiotensin Converting Enzyme (ACE) inhibitors (Yancy *et al.*, 2016)	Inhibit the conversion of angiotensin I to angiotensin II in RAAS system	Reduces water and sodium resorption from kidney, prevent aldosterone release	Cough, angioedema
Angiotensin receptor blocker (ARB) (Yancy *et al.*, 2016)	Prevent the action of angiotensin II	Dialation of blood vessels	Cough, angioedema,
Angiotensin receptor neprilysin inhibitor (ARNI) (Entresto) (Yancy *et al.*, 2016)	Inhibit the enzyme neprilysin and Valsartan act as ARB.	Dialation of blood vessels, prevent the degradation of natriuretic peptides	Angioedema, hypotension
Ivabradine (Tse *et al.*, 2015)	Inhibit sodium potassium channel at sinoatrial node	Inhibit cardiac pacemaker current at sinoatrial node	paroxysmal atrial fibrillation
Beta blockers (Gheorghiade *et al.*, 2003)	Block the β1, β2 and α1 receptors of sympathetic nervous system.	Reduces blood pressure , augment collateral blood flow, decrease the microvascular damage	Purpura, bronchoconstriction
Aldosterone antagonists (Maron and Leopold., 2010) (Spironolacton, Eplerenone)	Prevent the action of aldosterone	Retain potassium in blood, reduces water resorption in kidney	Dyspnea, Diarrhea.
Surgical procedures	**Method**	**Benefits**	**Risks**
Coronary artery bypass grafting	Internal mammary arteries, **saphenous veins** or **radial artery** sewn from aorta to the coronary artery below the site of blockage	Reconstruct the circulation towards infracted zone of myocardium.	chances of heart attacks during surgery. Risk of chest infection. Stroke in elderly patients.
Implantable cardiac defibrillators	device which monitors heart rate and provides extra electric shock when necessary	Useful to prevent sudden cardiac arrest by terminating ventricular tachyarrhythmias.	Inappropriate detection and subsequent delivery of a shock, infection at the site of implantation.
Adaptive cardiac resynchronization therapy (CRT) (Janaswamy *et al.*, 2016)	monitor heart rate, sends electrical impulses to both lower chambers of the heart	Increases blood flow, synchronized heart beating pattern, reduce mortality	Some patients are non responders.

The ACC/AHA/HFSA has derived a guideline for management of heart failure which include angiotensin converting enzyme inhibitors (ACE inhibitor), angiotensin receptor blocker (ARB), angiotensin receptor neprilysin inhibitor (ARNI) and Ivabradine in conjunction with beta-blockers and aldosterone antagonists for the treatment of stage A, B and C HF (Yancy *et al*, 2016). ACE inhibitor, ARB, and ARNI inhibit the formation and action of angiotensin II involved in the rennin-angiotensin system, which is intended to reduce the blood pressure in HF patients (Table-2). Entresto, an ARNI drug includes both ARB and neprilysin inhibitor which prevent the degradation of natriuretic peptides, bradykinin, adrenomedullin, and other vasoactive peptides. Ivabradine has recently approved by FDA, which is intended to reduce the heart rate by selectively inhibiting the cardiac pacemaker current at sinoatrial node (SA node) (Tse *et al.*, 2015). These treatments are combined with beta-blockers (Gheorghiade *et al.*, 2003), diuretics and aldosterone antagonists (Maron *et al.*, 2010) to improve the cardiac output and ejection fraction. The cardiac resynchronization therapy (Janaswamy *et al.*, 2016) and implantable cardiac defibrillators are employed to synchronize the heart-beating pattern to prevent the sudden cardiac death. Although once an infarct is formed, the drugs cannot repair or cease the ventricular remodeling, but only reduce the myocardial oxygen demand to protect the cells surrounding the infarct from hypertrophy. Heart transplantation is the gold standard treatment recommended for HF at the end stage. However, unavailability of donor organs, mortality of patients in waiting list, graft rejection reactions, lifelong immunosuppression and less survival rate add to the practical concerns. The OPTN/ SRTR annual data in 2010 and 2013 reported serious issues related to the long-term survival of patients after heart

transplantation. The number of patients in waiting list has increased by 34.2% from 2003 to 2013 (Colvin *et al.*, 2013). In the year 2005-2009, only 50% of patients in waiting list were undergone heart transplantation in which acute rejection happened in 24% of patients within 1 year of implantation. Therefore, the current situation demands the validation of an efficient, practical and cost effective treatment for heart failure. The ultimate aim of treatment for ischemic heart failure is the complete removal or reduction of fibrotic infarct from the myocardium to regain the normal cardiac performance. Now, tissue engineering comes up with innovative ideas to regenerate the infarct in the myocardium.

1.4. Cardiac regenerative therapy

The current therapeutic status for HF treatments initiated an active research on regenerative therapy of myocardium through tissue engineering approaches. The basic principles of tissue engineering include cells for tissue formation, scaffolds for cell adhesion and growth signals to improve the proliferation and differentiation of seeded cells.

1.4.1. Selecting the population of cells for cardiac regenerative therapy

The intrinsic repair mechanism of infarcted cardiac tissue cannot regenerate or replace the massive loss of specialized cardiomyocyte on infarction. Moreover, the adult mammalian cardiomyocytes are terminally differentiated binucleate cells with poor proliferation rate (Burridge *et al.*, 2012). Therefore, exogenous stem cell and progenitor cell population are explored for cardiomyocyte generation. The cells with immune tolerance, which evoke a minimal adverse response with host immune system, are required for cell therapy.

Therefore, autologous adult stem cells have a promising role in cell therapy especially for cardiac repair since most of the patients are above 50 years old. The first isolated adult stem cells are bone marrow-derived mesenchymal stem cells (BMSC), which have both myogenic, and vasculogenic potential. Later stem cell population is isolated from adipose tissue (ADMSC), circulating blood, joint synovium, muscle fibers, and even skin. BMSC, ADMSC, and skeletal myoblast have both myogenic and the vasculogenic potential suitable for cardiac regeneration. Further, the challenge lies incomplete differentiation of adult stem cells to highly specialized contractile cardiomyocytes.

1.4.2. Selecting biomaterial for cell carriers

The direct injection of cells to the infarct zone has reduced the cell engraftment rate due to the loss of cells in circulation and oxidative stress by the hypoxic microenvironment. Therefore, suitable and degradable cell carriers comparable with the native myocardium are required for the delivery of cells to the infarct zone. Tissues are organized by extracellular matrix (ECM) components, which form the basic frame to align cells, blood vessels, and nerves to construct structurally and functionally matured tissues. However, the complex architecture and dynamic nature of ECM is difficult to mimic. Therefore, the substrate for cell delivery is custom designed using natural or synthetic biomaterials to mimic the ECM of target tissue partially. Naturally derived biomaterials have a better cellular response to augment tissue formation, however, the fast degradation of the substrate by the enzymes in body fluid and loss of mechanical property limit their applications in cardiac tissue engineering. Moreover, the natural polymers of animal origin may cause the transmission of

pathogens and transplantation rejection. Therefore, synthetic polymers with tunable degradation property, suitable mechanical characteristics, and biodegradability are used to design tissue engineered constructs. However, the poor cellular response due to the absence of cell recognition moieties raises issues. The challenge lies in the apt selection of biomaterial with favorable characteristics of both natural and synthetic polymers.

1.4.3. Scaffolding approaches

The nature of the scaffold plays a vital role in tissue engineering. The different scaffolding approaches include porous scaffolds, decellularised extracellular matrices, and hydrogels. The porous scaffolds are generally prepared by 1) solvent casting, particulate leaching, gas foaming, freeze-drying or phase separation techniques, 2) rapid prototyping technology including selective laser sintering, stereolithography and 3D printing and 3) electrospinning techniques. However, the pre-formed scaffolds are not desirable for soft tissue engineering especially for cardiac applications due to its poor tissue integration, which cause severe arrhythmia after implantation.

The decellularized allogenic or xenogenic heart with native ultrastructure and three-dimensional architecture is employed as the scaffold for cardiac tissue engineering. Ott *et al* have first reported successful decellularization and recellularization of rat and porcine heart by perfusion method (Ott *et al.*, 2008*)*. However, the challenges include the selection of decellularization technique, selection of cells for recellularization of construct and chances of damage and infection to the vasculature of heart on perfusion culture (Montón *et al.*, 2013).

Moreover, the complex network of microvasculature in myocardium increases the risk of occlusions on recellularization.

The hydrogels are soft and crosslinked three-dimensional networks of a hydrophilic polymer, which can absorb a huge amount of water. Hydrogels are different from gels in retaining the three-dimensional structure in water (El-Sherbiny and Yacoub., 2013). The hydrogels are crosslinked by covalent bonds or physical intramolecular or intermolecular attractions to retain the three-dimensional structure even after equilibrium swelling. Wichterle and Lím (1960) have reported the first hydrogel based on poly(2-hydroxyethyl methacrylate) for contact lens applications. Later dramatic development has happened in the field of hydrogels in tissue engineering. Hydrogels are classified into different groups based on the origin, durability, and response to environmental stimuli. The dried and lyophilized hydrogels are termed as xerogels and aerogels respectively, which form a porous substrate for *in vitro* tissue formation. The hydrogels possess tissue like visco-elasticity, cytocompatibility, tissue mimetic water content and controllable physical characteristics. The hydrogels with *in situ* gelation characteristics can be employed for minimally invasive injectable therapy (Hunt *et al.*, 2014). The injectable hydrogels are prepared by physical, chemical, enzyme mediated or ionic crosslinking mechanism. Physical crosslinking is initiated by physical stimuli like pH or temperature.eg. poly(N-isopropyl acrylamide), pluronic, agarose and self-assembling peptides hydrogels. The chemical hydrogels are prepared by free radical initiated polymerization, Michael addition reactions, and Schiff-base reactions. The chemical hydrogels are mechanically stronger than physical hydrogels. Enzyme-mediated crosslinking occurs with transglutaminases

and horseradish peroxidases. Fibrin is an established biomaterial crosslink via transglutaminases. The ionic crosslinks are observed in water-soluble polymers with di or trivalent ions.eg. chitosan–polylysine, chitosan–glycerol phosphate.

1.4.4. Need for vascularization

Vascularisation is detrimental for tissue formation *in vitro* and *in vivo*. Within the body, cells are found within 100-200 μm away from the blood vessel, which ensures the availability of nutrients and essential gasses to each cell (Lovett *et al.*, 2009). Proliferation and tissue formation by the cells in tissue-engineered constructs also depends on the extent of vascularization. There are different approaches to augment vascularization of tissue-engineered constructs, which includes material functionalization with pro-angiogenic factors, scaffold fabrication with channeled porosity (Muehleder *et al.*, 2014), coculture with endothelial cells, the microfluidic design of scaffold with capillary network and modular assembly of reendothelialized microtissues (Lovett *et al.*, 2009). The porosity of injectable hydrogels also influences the vascularisation. However, the *in situ* vascularisation of hydrogels used for injectable therapy further raises the issue related to the condition of the site of injection. Especially, with infarcted myocardial applications, the *in situ* vascularisation of injected construct is challenging due to the hypoxic microenvironment at the infarct zone.

1.4.5. Free radical scavenging property

Followed by acute Mi, the oxidative stress develops in infarcted and non-infarcted myocardium significantly contributes to the infarct expansion and remodeling. The ischemic injury causes the upregulation of free radical

generating enzymes and critically impairs the existing antioxidant system in the myocardium. During the inflammatory phase of myocardial repair, the macrophages and neutrophils migrate to the infarct zone to augment proper clearance of necrotic cells. However, the over-expression of NADPH oxidase in inflammatory cells results in the huge release of superoxides (O2-) at the infarct zone. Moreover, the macrophage-derived inducible nitric oxide synthase releases nitric oxides (NO), which readily reacts with superoxides to form harmful peroxynitiles (Sun., 2009). The concentration of free oxy-radical in the healthy myocardium is 1.8 ± 0.8 μM. Grill *et al.*, 1992 have reported that the concentration of free oxy-radicals increases to 13.0 ± 2.5 μM after within 30 min of ischemic injury. These free radicals are generally released at the border zone of infarct, which attacks the cell membrane, proteins and genetic materials of cardiomyocytes and vascular cells even in non-infarcted myocardium cause infarct expansion. Lu *et al.* (2004) have reported the progressive decrease of antioxidants like superoxide dismutase (SOD), catalase, glutathione peroxidase and vitamin E in infarcted myocardium, which is extended slowly in the non-infarcted myocardium. Therefore, antioxidant therapy has a significant role in balancing the oxidative radical at infarct zone. The probucol, vitamin E or C, and N-acetyl cysteine are currently recognized for antioxidant therapy (Sun., 2009). However, the clinical trials using these antioxidant molecules failed to satisfy the issue. The major reasons are, firstly, the free radicals are generated from multisource at the infarct zone. The antioxidant molecules are designed to scavenge specific free radicals cannot reduce the oxidative stress generated by different types of radicals at infarct zone. Secondly, the given antioxidant molecules are not consistent to scavenge the radicals at its recommended dose to

reduce the oxidative stress at infarct zone. Therefore, the current scenario necessitates an antioxidant with an inherent, consistent, and wide range of free radical scavenging property.

1.4.6. Electromechanical function

The rhythmic contractions and relaxation of cardiac muscle are responsible for the cyclic pumping of blood. The synergy of electrical and mechanical functions of heart ensures the cyclic beating action (Novakovic *et al.*, 2010). The cardiomyocytes in myocardium responds to the electrical impulses and syncytial coupling augment synchronous contraction of cells. The challenging criterion is the electromechanical coupling of implanted or injected cells with the native myocardium. Poor integration of construct with the native cardiac tissue leads to arrhythmia. The selection of cell population and material for construct fabrication has a crucial role in electromechanical integration followed by cell transplantation. Gepstein *et al.* (2010) have reported better coupling of cardiomyocytes derived from human embryonic stem cells with the native cardiomyocytes. The formation of gap junctions supported by connexin 43 proteins is responsible for the coupling between cardiomyocytes. Moreover, the electrically conductive matrices can also improve the integration of implanted cells with the native myocardium (Zhou *et al.*, 2014).

1.5. Strategies for cardiac regenerative therapy

Cardiac tissue engineering proposes different approaches for cell-based regenerative therapy of infarcted myocardium. The approaches include both invasive and minimally invasive therapy. The selected cell population can be

implanted through *in vitro* matured engineered heart tissue or cell sheets, which require invasive surgical procedures. The injectable cell therapy using *in situ* forming cytocompatible hydrogels can facilitate minimally invasive cardiac cell therapy.

The present work deals with the synthetic, cytocompatible and injectable hydrogels for cardiac cell therapy.

CHAPTER 2

REVIEW OF LITERATURE

2 Review of literature

The potential of different stem cells reported for cardiac regenerative therapy is presented. The different strategies for cardiac regenerative therapy including engineered heart tissue, cell sheet engineering, and injectable hydrogels are discussed. The detailed review on injectable hydrogels as a bulking agent, cell carrier, free radical scavenging and electro-active cell carriers are discussed in the chapter.

2.1. Stem cells for cardiac regenerative therapy

Embryonic stem cells, cardiac stem cells, bone marrow-derived mesenchymal stem cells (Boyle *et al.*, 2010), adipose-derived stem cells (Liu *et al.*, 2014) and induced pluripotent cells (Lundy *et al.*, 2014) have the potential for cardiac regeneration. Embryonic stem cells (ESC) are pluripotent cells isolated from 5-7 day old blastocyst. The aggregation of ESC in suspension cultures to the embryoid body signals the generation of germ layers. Further post plating along with suitable differentiation signals induces the generation of contractile cardiomyocytes in adherent culture (Vidarsson *et al.*, 2010). However, ethical and political issues, chances of teratoma formation and poor availability of embryos limit the use of ESC in cell therapy (Lo *et al.*, 2009). Later, to avoid the ethical

issues and practical concerns, stem cells derived from adult tissues are considered for cell therapy. Cardiac stem cells (CSC) are the progenitor cells of cardiomyocytes. They are clonogenic, multipotent cells, which can differentiate into myocytes, vascular smooth muscle cells, and endothelial cells. Bolli *et al* (2011) have used CSC for a phase 1 clinical trial (SCIPIO) in patients with MI, reported 23.8% reduction in infarct size compared to control. However, the isolation of cardiac stem cells is not feasible for the autologous cell therapy. Mesenchymal stem cells (MSC) from bone marrow (BMSC) and adipose tissues (ADMSC) are also explored for cardiac differentiation. MSC are immune privileged cells lack co-stimulatory molecules and immunogenic surface markers. Moreover, the engrafted MSC secrets bFGF, VEGF, HGF, IGF-I, and adrenomedullin, which enhances the resident cardiac stem cell survival and proliferation at infarct zone (Williams *et al.*, 2012). Williams *et al* have reported a significant reduction in infarct size followed by the co-injection of CSC with BMSC in the infarcted heart of Yorkshire swine. The clinical trials coded BONAMI, BOOST, FINCELL and HEBE was reported with the direct injection of BMSC in patients with ischemic cardiac disorders. However, the painful bone marrow aspiration for autologous BMSC isolation is not preferred for ischemic HF patients. Over this concern, adipose derived stem cells (ADMSC) are desirable than BMSC for autologous stem cell therapy in HF patients. ADMSC can be easily isolated and expanded from subcutaneous adipose tissue fragments, lipoaspirate blood and saline fraction (Francis *et al.*, 2010). ADMSC can differentiate into various cell lines including myocytes. Wang *et al.* (2014) have reported the cardiac differentiation of ADMSC to cardiomyocytes on chitosan scaffold. They have observed the spontaneous differentiation of CD 29^{+} brown

ADMSC into cardiomyocytes with high efficiency. As the adult stem cells are lineage specific, the complete differentiation of adult stem cells to beating cardiomyocytes are rarely observed. The pluripotent stem cells are the ideal source for functional cardiomyocyte generation. Later the revolutionary finding of induced pluripotent stem cells (iPSC) by Takahashi and Yamanaka (2006) solved the issue. They have designed a protocol for the generation of iPSC from adult mouse fibroblast by retroviral assisted expression of Oct3/4, Sox2, Klf4 and c-Myc (OSKM) transcription factors. iPSC resemble ESC in pluripotency and proliferative capacity. Besides, the somatic origin nullifies the ethical issues and autologous origin reduces the risk of transplantation rejection (Wang *et al.*, 2013). The ventricular cardiomyocytes are generated from iPSC by embryoid body method and matrix sandwich method, in which the later yield 95% differentiation to beating cardiomyocytes (Knollmann., 2013). The iPSC-derived cardiomyocytes exhibit action potential parameters and ionic current similar to the ventricular myocytes. The recent research in iPSC focuses on the generation of clinical-grade patient-specific iPSC using alternative reprogramming factors assisted with non-viral vectors (episomes, minicircle vectors, transposons and human artificial chromosome vectors) (Rony *et al.*, 2015). The patient-specific iPSC is the ideal candidate for cardiac regenerative therapy.

2.2. Direct cell delivery

The selected population of cells can be transplanted to infarcted myocardium via direct surgical intramyocardial injection, catheter-based intramyocardial administration, trans-endocardial injection, trans-coronary venous injection, intravenous infusion, and intracoronary artery administration. However,

the harsh hypoxic microenvironment at the infarct zone and loss of cells in circulation results in poor engraftment of delivered cells (Sheng *et al.*, 2012). Visage *et al.* (2012) have compared the engraftment of MSC delivered to the rat myocardium through scaffold with that of direct endocardial injection. Comparatively, the cell engraftment was lower with direct injection than scaffold approach. Here, the tissue engineering strategies play a significant role to improve the cell engraftment rate through custom designed cytocompatible matrices.

2.3. History of cardiac regenerative therapy

The concept of tissue engineering was first proposed by Vacanti and Langer in 1991, initiated with cartilage tissues. The attempt on cardiac regenerative therapy was initiated with the isolation and *in vitro* culture of functional cardiomyocytes. In late 1950's Moscona (1959) have generated spheroid cell aggregates from embryonic chick heart. However, the tendency of cardiomyocytes to detach from the culture dish created difficulties for later studies. In late 1980's, Vandenburgh *et al.* (1988) have identified the role of freshly neutralized collagen type1 to overcome the detachment problem of cardiomyocyte culture. Terracio *et al.* (1988) have cultured cardiomyocytes on silastic membranes coated with laminin under cyclical stretch. They have identified the role of mechanical load on cardiomyocyte differentiation and orientation. Moreover, Simpson *et al.* (1994) have cultured the cardiomyocytes in cardiac tissue-like orientation on pre-oriented collagen layer. The elastomeric polyurethane film printed with laminin lanes were also used for the aligned growth of cardiomyocytes *in vitro* (McDevitt *et al.*, 2003). Further studies were

reported engineered heart tissues, cell sheets, and injectable hydrogels to deliver the cells for regenerative repair of the myocardium.

2.4. Engineered heart tissue (EHT)

The implantable construct with viable and proliferating cardiac cells are employed for regenerative repair of infarcted myocardium. The EHT is *in vitro* matured, biodegradable, biocompatible and porous scaffolds with mechanical property comparable to the native myocardium. The natural and synthetic biomaterials are used for the fabrication of scaffolds.

2.4.1. Natural biomaterials

Collagen I, fibrin, hyaluronic acid, alginate, matrigel and decellularized matrices are predominantly used for EHT (Hasan *et al.*, 2015). Collagen 1 is FDA approved protein used for skin and bone applications, which is the major component of myocardial ECM. It is used for the preparation of hydrogel and sponge-like engineered construct. Fibrin glue and hydrogels are the attractive matrices for cardiac cell proliferation. Matrigel is the tumor extract that contains growth factors promoting cell attachment and differentiation, which is not considered safe for clinical applications (Ye *et al.*, 2011). The decellularized matrices of myocardial tissue, small intestinal submucosa, and urinary bladder were reported for fabrication of engineering cardiac tissue. However, the high risk of pathogen transfer, transplantation rejection, rapid degradation in body fluid and poor tissue availability limits the use of decellularized matrices. Though, the natural polymers exhibit a better cellular response, the complicated isolation

procedures from animal tissues, the risk of contamination, poor mechanical stability and fast degradation by proteases limits the clinical applications.

2.4.2. Synthetic biomaterials

Synthetic biomaterials are easily available with tunable degradation and mechanical property suitable for constructing pathogen free, porous scaffolds. Poly(N-isopropyl-acrylamide) (Fujimoto *et al.*, 2009), poly(lactic-co-glycolic acid) (Xing *et al.*, 2012), poly(glycerol sebacate) (Rai *et al.*, 2013) and poly(caprolactone) (Yeong *et al.*, 2010) were employed for the fabrication of engineered cardiac construct. However, the absence of cell adhesion sites in synthetic biomaterials challenges the seeded cell proliferation. Therefore, the biosynthetic polymers containing both synthetic and natural biomaterials have gained promise in tissue engineering. Our group has previously reported a polyvinyl alcohol-calcium alginate hydrogel with adequate mechanical property, fatigue life and blood compatibility was reported as a promising scaffold for cardiac applications (Thankam and Muthu, 2013). They have also studied the factors influencing the penetration, proliferation, distribution and long-term viability of cells on the EHT (Thankam and Muthu, 2014). Crowder *et al* (2013) have proposed an electrically conductive biocompatible scaffold prepared from poly(ε-caprolactone) incorporated with carbon nanotube for the cardiac application. The electrically responsive scaffold has improved the expression profile of cardiomyocytes derived from MSC. Martins *et al.,* (2014) have fabricated a conductive, elastic and biocompatible scaffold using chitosan containing carbon nanotube. The neonatal cardiomyocytes cultured over the scaffold showed better electrical coupling with each other. Pok *et al.,* (2014) have

optimized the concentration of carbon nanotube (CNT) in chitosan scaffold for proper action potential propagation without compromising the cytocompatibility. As the studies confirmed the better maturation and coupling between the cardiomyocytes on electrically responsive scaffolds, the recent studies on EHT focuses on designing electrically responsive and biocompatible scaffolds using conducting polymers.

2.5. Cell sheet engineering

Cell sheet engineering is a promising approach to constructing viable tissues with better cell-cell interaction. Poly(N-isopropyl acrylamide) (PIPAAm), a thermo-responsive polymer with lower critical solution temperature (LCST) at 32 ^{0}C is used for the preparation of cell sheets. The cells are grown over the cell culture plastics coated with PIPAAm film of thickness <100 nm at 37 ^{0}C. The PIPAAm film becomes hydrophilic at a temperature below 32 ^{0}C and inhibits the cell adhesion, which detaches the cells as a monolayer cell sheet (Hannachi *et al.*, 2010). The 3-4 cell monolayers can be stacked together to prepare cell sheet with 80-100 μm thickness for direct transplantation. The upper limit for stacking is 3 layers due to the hypoxic cell damage. However, the thin cell sheets are not suitable for cardiac implantation due to poor mechanical characteristics. Later, Matsuo *et al.* (2015) have reported an alternative method to fabricate the thick viable cardiac tissue from pluripotent stem cells. They have inserted gelatin hydrogel microspheres in between the cardiac cell sheets to prepare 15 layer cell sheets with a thickness greater than 1 mm. They have observed long-term survival of thick cell sheets in infarcted myocardium of athymic nude rats.

The major issues related to the clinical translation of implantable EHT or cell sheets are the delay *in vitro* maturation of constructs, the need for complicated surgical procedures chances of infection and cardiac arrhythmia after implantation. Therefore, current attraction relies on the injectable hydrogels for minimally invasive intramyocardial delivery of cells for cardiac regenerative therapy.

2.6. Injectable hydrogels

The injectable hydrogels are emerged as tissue bulking agent and as a carrier of cells or growth factors in cardiac regenerative therapy (Choi *et al.*, 2015). Injectable hydrogels are delivered at the infarct zone of myocardium through minimally invasive approaches, which can reduce the discomfort of patients. Other advantages of injectable hydrogels therapy over preformed scaffold approach are given in table-3:

Table-3: Advantages of injectable hydrogels over preformed scaffold

	Pre-formed scaffold	**Injectable hydrogels**
Advantages	Most diversified choices of biomaterials Precise design for architecture	Ease of incorporating cells or growth factors by simple mixing. Minimally invasive therapy. Fast and simple procedure. Intimate cell –material interactions
Disadvantages	Time-consuming cell seeding procedure Inhomogeneous distribution of cells Presence of residual solvents used for purification Need for surgical procedures Chances of contamination	Soft structures, difficult to handle

2.6.1. Injectable hydrogels as a bulking agent.

Injectable hydrogels can act as a bulking agent at the infarct zone to prevent extensive ventricular remodeling (Tous *et al.*, 2011). Studies were reported with the injection of acellular hydrogels in animals of induced MI. Christman *et al.* (2004a) have initiated the acellular hydrogel therapy with fibrin hydrogels in a rat myocardium after 1 week of induced MI. They have observed increased arteriolar density and decreased infarct size after 5 weeks. Later alginate (Tsur-Gang *et al.*, 2009), hyaluronic acid (Yoon *et al.*, 2009) and collagen (Dai *et al.*, 2005) were reported as a bulking agent at the infarct zone, which facilitated improved LV ejection fraction with reduced scar size. Wang *et al.* (2009) have evaluated the role of a novel thermosensitive hydrogel prepared with dextran grafted poly(caprolactone)-2-hydroxyethyl methacrylate copolymerized with poly(N-isopropyl acrylamide) (Dex-PCL-HEMA/PNIPAAm) in 4-day post-MI rabbit model; have observed significant improvement in ejection fraction and LV end diastolic and systolic diameter of the myocardium. Further, the hydrogels prepared using poly(NIPAAm-co-acrylic acid-co-hydroxyethyl methacrylate-poly(trimethylene carbonate)) (Fujimoto *et al.*, 2009), α-cyclodextrin mixed with MPEG-PCL-MPEG triblock copolymer (Jiang *et al.*, 2009) and vinyl sulfone derivatized PEG (Dobner *et al.*, 2009) were evaluated in rat MI model. Ifkovits *et al.* (2010) has assessed the influence of mechanical property of injectable hydrogel to augment bulking effect at the infarct zone. They have injected the hyaluronic acid (MeHA) hydrogels with a compressive modulus of 43 kPa and 7.7 kPa into the ovine MI model. Higher cardiac output and significantly lower infarct area were observed in ovine heart treated with hyaluronic acid hydrogels

with higher compressive modulus, which substantiate the role of mechanical stiffness of hydrogels in bulking effect. Landa *et al.*, (2008) have studied the efficacy of acellular hydrogel therapy in new (immediately post-MI) and old infarct (2 months post-MI) by injecting alginate hydrogel; have observed better outcome in new infarct compared to old infarct. The repair of old infarct requires an external supplement of growth factors or potential cells to accomplish the regeneration of infarct zone.

2.6.2. Injectable hydrogels as cell carriers

The hydrogel formulation with the cells or growth factors can be used for the regenerative therapy. The hydrogels crosslink via fast, mild and selective chemical reactions are considered for injectable cell therapy to reduce the exposure of delivered cells with the monomers (Yang *et al.*, 2014).

Injectable cell therapy using injectable hydrogel is challenging since it demands strict criteria (Hastings *et al*, 2014). The hydrogels are injected using a catheter through intracoronary, epicardial or trans-endocardial methods. Therefore, the hydrogel formulation must be less viscous sufficient to easily pass through the catheter and must undergo fast gelation at the site of injection. Here the challenge is to avoid premature gelation, which may block the catheter. Moreover, after the *in situ* gelation, the hydrogel must retain the intact structure without collapsing. The shredded hydrogel particle may cause embolization that can result in infarction at another zone of the myocardium. The hydrogel should have the adequate mechanical property to withstand the fatigue cycles of the heart during and after surgery. Another major concern is the compatibility of an

injectable solution containing monomeric units with the cells selected for injection. The viability of cells mixed with injectable formulation during injection and gelation is crucial to ensure the success of cell therapy. The retention, proliferation and differentiation of injected cells at the infarct zone determine the suitability of injectable matrix for therapy.

The biomaterials from both natural and synthetic origin are used for injectable hydrogel therapy. The fibrin, alginate, chitosan, hyaluronic acid and collagen (I & III) includes injectable hydrogels of natural polymers (Tous *et al.*, 2011). However, uncontrolled gelation rate, fast and uncontrolled degradation rate in body fluid, chances of immunogenicity, transplantation rejection, and pathogen transfer limits the clinical translation. These issues can be overcome by biocompatible and biodegradable synthetic biomaterials with tunable gelation, degradation, and mechanical characteristics. However, the absence of cell adhesion moieties in synthetic polymers may resist the cell adhesion and proliferation of encapsulated cells. With this scenario, several groups have reported injectable hydrogel prepared using natural, synthetic and biosynthetic (combination of both natural and synthetic polymers) biomaterials for cell therapy.

Christman *et al.* (2004b) have reported fibrin glue for injectable cell therapy in postinfarcted myocardium of rat. They have injected the thrombin solution containing 5 x 10^6 skeletal myoblast cells along with fibrin component using Baxter's supplied duploject applicator. They have observed ~ 2-fold increase in cell retention after 5 weeks of injection compared to saline control. However, the fibrin hydrogels are highly sensitive to fibrinolysis and degrade

completely within 3-4 days in the presence of hydrolytic enzymes. Therefore, fibrin glue cannot provide the necessary mechanical support to attenuate ventricular remodeling. Later in 2011, Habib *et al.* have reported the PEGylated fibrinogen for the culture of neonatal rat ventricular cardiomyocytes and delivery of human embryonic stem cell-derived cardiomyocytes to the myocardium. In PEGylated-fibrin; PEGylation slightly slows down the degradation of fibrin, however, exhibit poor compatibility with the encapsulated cells. Lu *et al.* (2009) have used injectable, thermoresponsive chitosan hydrogel to deliver embryonic stem cells to the myocardium. They have observed 2 fold increases in cell retention compared to PBS control. The infarct area was decreased from 51.7 ± 2.3% to 22.9 ± 3.5% when treated with chitosan + ESC. Wang *et al.* (2014) have observed the role of chitosan in cardiac differentiation of brown adipose-derived stem cells (BADSC). The chitosan components have improved the collagen synthesis and matrix modeling for BADSC proliferation and differentiation. However, the in vivo bioluminescence imaging of BADSC engrafted with chitosan hydrogel, reveal a significant reduction in cell density after 28 days of injection, which indicate the loss of engrafted cells at the infarct zone. The inability of chitosan hydrogel to protect the cells from reactive free radicals in the infarct zone and the fast degradation or collapse of hydrogen may account for the drastic loss of cells at the site of injection. Gaffey *et al.* (2015) have reported a shear thinning hyaluronic acid (STG-EPC) hydrogel for the injection of endothelial progenitor cells into the ischemic rat myocardium. The adamantine- and b-cyclodextrin–modified HA improved the cell engraftment rate and vasculogenesis at infarct zone. The reduced scar fraction and enhanced ventricular performance have observed in STG-EPC hydrogel group compared to cell alone

group. However, the decrease of mechanical moduli of shear thinning hyaluronic hydrogels under cyclic deformations limits their potential for cardiac applications.

The injectable hydrogels for cardiac application require high mechanical strength, elastic nature, porous interconnected bulk morphology, slow bulk degradation with a gradual increase in bulk space in line with tissue formation. As these requirements are diagonally opposite and need rigorous standardizations, the natural biomaterials fail to form an ideal hydrogel for cardiac regenerative therapy. In addition, natural polymers may cause immune rejection and pathogen transfer on clinical applications. Therefore, the hydrogels prepared from synthetic polymers with tunable physical properties, low-cost bulk synthesis and fewer chances of immune rejection are preferred for injectable therapy. However, the synthetic hydrogels are rarely explored for cell encapsulation due to the poor cell adhesion, proliferation and toxicity of monomers when mixed with cells for injection. In 2012, Wang *et al.* have reported a purely synthetic hydrogel prepared from oligo(poly(ethylene glycol) fumarate (OPF) for the transplantation of mouse embryonic stem cells to the infarcted myocardium. The infarct size has reduced from 52.4 ± 4.6% to 23.8 ± 2.3% after 4 weeks of implantation of ESC encapsulated OPF hydrogel. However, they have observed the poor proliferation of cell inside the hydrogel. Here the present study reports the purely synthetic, cytocompatible, biodegradable and injectable hydrogels for long-term cell encapsulation.

2.6.3. Free radical scavenging injectable hydrogels

The novel approaches propose reinforcing free radical scavenging property in injectable hydrogels for cardiac regenerative therapy. However, the hydrogels with inherent free radical scavenging property and cell encapsulation efficiency are rarely reported. Chitosan-glutathione based hydrogels (Li *et al*, 2013), cellulose hydrogel with trans-ferulic acid (Trombino *et al*, 2009) and cerium oxide nanoparticle hydrogels (Weaver *et al*, 2015) are reported with the radical scavenging property. Chitosan and cellulose constructs have negligible radical scavenging property in the absence of antioxidant mediators like glutathione and ferulic acid. However, the short lifespan of these small molecules limits the application. Cerium oxide nanoparticle hydrogels have favorable scavenging properties; however, the cytotoxicity of heavy metal oxide and its deleterious effects on cell internalization challenges the long-term *in vivo* application. Therefore, it is highly relevant to explore novel injectable hydrogels with inherent free radical scavenging characteristics for regenerative therapy. The present study relies on synthetic injectable hydrogel with inherent antioxidant property for regenerative therapy.

2.6.4. Electrically responsive injectable hydrogel.

The proper interaction and coupling of delivered cells with the surrounding myocardium are essential to establish the functional regeneration of infarct zone. The cardiomyocytes are electrically responsive and coupled with tight junctions to facilitate the synchronous beating. However, the engrafted cells, even if differentiated to cardiomyocytes, remains isolated inside the carrier

hydrogel from surrounding myocardium. Therefore, the researchers aim to develop electrically responsive hydrogels for myocardial cell delivery to ensure the proper alignment, growth, and coupling of engrafted cells with the surrounding cardiomyocytes. The polymeric scaffolds are electrically non-conductive in nature. Therefore, different strategies have evolved to reinforce the electrical conductivity in polymeric injectable hydrogels. The electrically conducting carbon nanotubes (Stout *et al.*, 2012) and gold nanowires (Dvir *et al.*, 2011) were employed to construct electro-responsive tissue engineered constructs by different grafting techniques. However, inhomogeneous distribution, non-biodegradability and unknown long-term effects of these nanomaterials limit the therapeutic potential (Qazi *et al.*, 2014). Electroactive conducting polymers with properties of both metals (electrical and optical properties) and polymers (flexibility in processing and ease of synthesis) are evolved to resolve the issue (Balint *et al.*, 2014). However, the major issue is poor biocompatibility and non-biodegradability of conducting polymers. The polypyrrole, polyaniline, and polythiophene were evaluated for biocompatibility and electrical conductivity, in which polyaniline with ease of synthesis, processibility, antibacterial effect and cost effectiveness is recommended for preparation of electro-responsive matrices (Qazi *et al.*, 2014). Still, the generation of injectable formulations from conducting polymers is challenging due to its poor water solubility and cytotoxicity. Cui *et al.* (2014) have reported an injectable thermoresponsive electroconductive hydrogel using the pNIPAAM based copolymer conjugated with tetra aniline by EDC-NHS reaction. They have ensured the viability of cardiomyoblast cells inside the conducting hydrogels, moreover, have evaluated the *in vivo* gelation and histological responses. However, they have observed

leaching of tetra aniline within 2 days on *in vitro* ageing experiment of hydrogels, which changed the color of incubation medium to dark blue. The subcutaneously injected hydrogel elicited an acute inflammatory response in the first week, which may be due to the leaching of tetraaniline at the injection site. The current situation necessitates the development of a single component injectable hydrogel containing polyaniline with better cytocompatibility and mechanical stability.

2.7. Clinical translation of injectable cardiac cell therapy

With the increasing publications in injectable hydrogel aided cardiac regenerative therapy, very few hydrogels have reached up to the preclinical studies. Chang *et al.* (2016) have injected human cord blood mononuclear cells in hyaluronan hydrogel to the infarcted myocardium of pig. This approach showed left ventricle ejection fraction of 51.32% ± 0.81% in injected group with improved hemodynamic data than cell alone or hydrogel alone groups. The major hurdles, which limit the clinical evaluations in a large animal, are the safety issues related to the route of administration. As the current method delivers hydrogels though intracoronary trans-endocardial method, the risk of formation of emboli by the injectable formulation limits the clinical translation.

2.8. Routes of cell delivery

The safe injection of hydrogel along with cells into the myocardium of ventricular wall is challenging. The injectable hydrogels can be delivered via intracoronary, trans-endocardial or epicardially to the myocardium. Leor *et al.* (2009) have injected alginate hydrogel using catheters by an intracoronary method in swine MI model. Seif-Naraghi *et al.* (2013) have successfully delivered

myocardial matrix derived hydrogel by percutaneous, trans-endocardial method to the infarcted ventricular wall of a pig. Even if these methods do not show any emboli formation, theoretically, the chance of regurgitation of injectable formulation into the blood is higher for these methods. Recently, Zhu *et al.* (2016) have proposed a practicable and safe epicardial methods using robotic catheter system for injectable cell therapy of infarcted myocardium of pig. They have used subxiphoid trans-epicardial approach without passing the catheters through the blood vessels, which avoid the chances of emboli formation. A thermosensitive poly(NIPAAm -co- N-vinylpyrrolidone -co- methacrylate-polylactide) polymer solution is injected through the robotic catheter equipped with the coaxial cooling fluid pathway, to retain the low viscosity till the point of injection. This novel technique is promising to bring the injectable cardiac cell therapy from preclinical to clinical practice. The extensive clinical studies on injectable hydrogels are explicitly required to uphold the injectable cardiac cell therapy for cardiac regeneration.

2.9. Objectives of the present study

Cell-based regenerative therapy could be considered as a better option for post-infarcted myocardial repair. However, an efficient cell carrier with optimum characteristics is not yet reported for clinical translation. So far, several groups have reported injectable hydrogels based on PEG-fibrin, chitosan and hyaluronic acid for cardiac cell delivery. These hydrogels support excellent cell growth and proliferation. However, these hydrogels fail to meet the desired mechanical strength and degradation required to attenuate ventricular remodeling. Therefore, the major hurdle is to design an injectable hydrogel with maximum interconnected porosity and high mechanical stability, which are conflicting characteristics to establish. In this context, the synthetic polymers with broad chances of characterizations are preferred for designing cell carriers. However, the synthetic hydrogels are rarely explored for cell encapsulation due to the poor cell adhesion, proliferation, and toxicity of monomers when mixed with cells for injection.

As the mechanical strength and porosity are reversibly related, the preparation of hydrogel with higher mechanical strength with higher internal porosity is difficult. Especially, the hydrogels with higher water affinity swell in an aqueous medium and loose the mechanical modulus. The oligo(poly(ethylene glycol) fumarate) (OPF) based hydrogel, reported for cardiac cell therapy has a high swelling ratio which significantly reduces the mechanical modulus. Therefore, it is necessary to control the swelling property of hydrogel without compromising the porosity. In this milieu, a practical solution is to design an *in*

situ crosslinkable amphiphilic macromers to prepare hydrogel, which can control super swelling to retain higher mechanical stiffness. Hence, one of the objectives of this study is to synthesize oligomeric macromers with balanced hydrophilic and hydrophobic units. Sebacic acid, poly (ethylene adipate) and polyaniline are used to reduce the hydrophilicity of macromers.

Another disadvantage of the synthetic polymer is poor adhesion, growth, and proliferation of cells seeded or encapsulated inside the hydrogels. The extracellular matrix contains specific sites for adhesion and proper alignment of cells during tissue formation. The polymers of synthetic origin have no cell adhesion sites. Here, one option is to incorporate biological molecules with cell adhesion sites, which is attempted previously. Direct mixing or encapsulation of biological molecules with the injectable formulation can result in burst release of molecules from the hydrogel matrix. The covalent conjugation of biological molecules with the synthetic polymers may alter their specific action. Therefore, here we have attempted on a different strategy to improve the cell adhesion property of hydrogels. It is reported that the serum protein adsorption is higher for amphiphilic surfaces than extremely hydrophilic or hydrophobic surfaces, which assist cell adhesion and proliferation. Therefore, in this study, the hydrogels are prepared using biocompatible and hydrophobic monomers along with hydrophilic PEG and sugar alcohols to accomplish amphiphilicity.

In injectable hydrogels, the cells are cultured inside the hydrogel under extremely stressful condition. Therefore, the long-term viability and proliferation of cells are crucial for injectable cell carrier. So far, no studies have reported the long-term cell viability and proliferation inside the hydrogel under *in vitro* culture

conditions. In the present study, one of the objectives is to study the long-term viability and proliferation of cells encapsulated inside the hydrogel. The long-term cell viability is accomplished when the porosity and degradation of the bulk hydrogel are balanced for nutrient diffusion and metabolite exclusion.

The chosen cardiac cells are directly mixed with the injectable formulation just before injection. In this process, even the biocompatible polymers may cause toxicity if it remains in monomeric form. Therefore, the major concern is the compatibility of the injectable formulation containing monomeric units with the cells selected for injection. This issue is more serious in synthetic hydrogels, as most of the synthetic monomers are toxic to the cells. Hence, the monomers for the synthesis of in situ crosslinkable macromer are cautiously selected to avoid cytotoxicity.

The regenerative therapy combined with an antioxidant having an inherent, consistent and wide range of free radical scavenging property is advantageous for cardiac repair. The oxidative stress at infarct zone significantly reduces the retention of injected cells even with cell carriers. So far, in situ crosslinkable macromers conjugated with free radical scavenging glutathione or trans-ferulic acid are reported for the preparation of cell carriers. However, these soluble factors have a short time of action and higher chances of degradation by proteases. Moreover, the slight structural changes during conjugation can reduce the site-specific action of these factors. Therefore, an objective of the present study is to design injectable hydrogels with inherent free radical scavenging property of different types of free radicals. The hydrogels with high reducing power are preferred for the neutralization of free radicals.

Electrically responsive matrices are desirable for better integration of injected cells with the native myocardium. However, the electroactive, injectable hydrogels are rarely reported for cell encapsulation. The poor solubility and loss of electrical conducting property of conducting polymers in aqueous media are the limiting factors to design injectable hydrogels. In the present study, the objective is to design an injectable hydrogel containing polyaniline for cardiac cell encapsulation.

The major objectives of the present study are the development of biocompatible and injectable hydrogels with variable free radical scavenging and cell encapsulation characteristics for cardiac cell therapy.

The detailed objectives are as follows:

1) Development of biocompatible and injectable hydrogel materials, which include the following studies

- Preparation of injectable hydrogels based on poly(propylene fumarate), sugar alcohol and polyaniline.
- Evaluation of free water content, mechanical property, surface and cross-sectional morphology and *in vitro* ageing profile of injectable hydrogels.
- Evaluation of electrical conductivity of hydrogels based on polyaniline.
- Evaluation of cell viability with hydrogels.

2) Studies on free radical scavenging property of hydrogels under oxidative stress environment, which includes

- Evaluation of DPPH, hydroxyl, nitric oxide radical scavenging property and reducing power of hydrogels by biochemical assays.
- Evaluation of protective effect of hydrogels on cardiomyoblast cells treated with stress inducing media.
- Evaluation of intracellular ROS release from cardiomyoblast cells treated with stress inducing media in the presence of hydrogels.

3) Studies on cell encapsulation with hydrogels, which includes

- Studies on the proliferation of cardiomyoblast cells encapsulated inside the hydrogels under *in vitro* culture conditions.
- Evaluation of viability and distribution of cells inside the hydrogels after long-term *in vitro* culture.
- Assessment of extracellular matrix modeling by the encapsulated cells inside the hydrogels by histological analysis.

CHAPTER 3

MATERIALS AND METHODS

3 Materials and methods

Synthesis and characterization of three types of comacromers based on poly (propylene fumarate), sugar alcohol and polyaniline polyester comacromers and preparation of hydrogels with a vinyl crosslinker, poly(ethylene glycol) diacrylate are presented. The experimental studies on setting characteristics of the hydrogels, physical properties of the hydrogels, such as swelling in water, surface and cross-sectional morphology, in vitro ageing and biomechanical stability, the state of water (free and bound water) present in the hydrogels are presented. The experimental studies on cytocompatibility, hemolysis and free radical scavenging property of hydrogels are presented. The studies on cell encapsulation efficiency of hydrogels, cell proliferation, viability and extracellular matrix protein formation by the encapsulated cardiomyoblast cells are also presented.

3.1. Materials

PEG 300, dihydroxy terminated poly(ethylene adipate), ammonium persulfate, 1-Ethyl-3-(3-dimethylaminopropyl)carbodiimide (EDC), N-hydroxysuccinimide (NHS), PEG diacrylate, sodium bicarbonate, DPPH, deoxyribose, ascorbic acid, Griess reagent, potassium ferricyanide, ferric chloride, acridine orange and 2', 7' dichloro dihydro fluorescein diacetate (DCFH-DA)

were supplied by Sigma-Aldrich pvt.ltd. Propylene glycol and aniline were purchased from S.D Fine chemicals pvt.ltd. Maleic anhydride, conc. sulfuric acid, thiobarbituric acid, trichloroacetic acid and hydrogen peroxide were provided by Merck specialties Pvt. Ltd. Sebacic acid, mannitol, xylitol, N, N, N', N'-tetraethyl methyl ethylenediamine (TEMED), DMEM, Fetal bovine serum (South American origin), antibiotic-antimycotic solution, MTT, calcein AM and ethidium bromide, hematoxylin stain and eosin were purchased from HiMedia laboratories Pvt. Ltd, India. All other chemicals used were of analytical grade.

3.2. Synthesis of in situ crosslinkable comacromers

3.2.1. Synthesis of poly(propylene fumarate) based comacromers

3.2.1.1. Synthesis of poly(propylene fumarate-co-ethylene glycol) comacromer

Poly(propylene fumarate-co-ethylene glycol) comacromer was synthesized by melt condensation reaction. 1 M propylene glycol and 2 M maleic anhydride were refluxed at 160 ^{0}C for 1 h. Then vacuum condensation was done at 180 ^{0}C for 5 min under nitrogen atmosphere. The reaction was catalyzed by morpholine and sodium acetate. The reaction product was then dissolved in acetone and precipitated with 25% aqueous methanol. The product was reprecipitated with petroleum ether to remove the unreacted low molecular weight reactants. Then filtered and dried at 60 ^{0}C. The purified poly(propylene fumarate) resin was condensed with polyethylene glycol (300) at 160 ^{0}C for 1 h followed by vacuum condensation for 5 min to get poly(propylene fumarate -co- ethylene glycol) coded as PP comacromer. (Komeri, Thankam, Muthu., 2015)

3.2.1.2. Synthesis of poly(propylene fumarate-co-sebacate-co-ethylene glycol) comacromer

The poly(propylene fumarate-co-sebacate-co-ethylene glycol) comacromer was synthesized in a three neck round bottom flask. 1, 2 propylene glycol and maleic anhydride were refluxed at 1:1 ratio for 1 h at 160 ^{0}C. The reactants were vacuum condensed at 180 ^{0}C for 10 min. The further reaction was carried out with sebacic acid and PEG 300 at 160 ^{0}C for 1 h each, followed by vacuum condensation for 5 min. The comacromer was precipitated with 25% methanol and washed with petroleum ether. The poly (propylene fumarate-co-sebacate-co-ethylene glycol) comacromer is coded as SP. (Komeri, Muthu., 2016)

3.2.2. Synthesis of sugar alcohol based comacromers

The comacromer, mannitol-fumarate-poly ethylene adipate-fumarate-PEG (coded as PEAM) and xylitol-fumarate-poly ethylene adipate-fumarate-PEG (coded as PEAX) were synthesized by two-step condensation reaction to getting the resultant comacromer as block comacromer. Initially, the 1.5 M dihydroxy terminated poly(ethylene adipate) (PEA) was reacted with excess 3.0 M maleic anhydride by refluxing for 1 h at 160 ^{0}C. The reactants were vacuum condensed at 180 ^{0}C for 5 min. The second step reaction was carried out at 160 ^{0}C for 1 h with the addition of an equal quantity of mannitol (1.5 M), PEG 300 (1.5 M) for PEAM and xylitol (1.5 M), PEG 300 (1.5 M) for PEAX comacromers. The reaction was completed by vacuum condensation for 5 min at 160 ^{0}C. The comacromer was dissolved in acetone and precipitated in cold diethyl ether. (Komeri, Thankam, Muthu., 2017)

3.2.3. Synthesis of polyaniline based comacromers

3.2.3.1. Synthesis of polyaniline

Polyaniline was synthesized by free radical polymerization of anilinium hydrochloride as per the protocol of Stejskal and Gilbert, 2002. Briefly, anilinium hydrochloride was prepared by reacting 0.2 M aniline with 0.2 M hydrochloric acid in distilled water. 0.25 M ammonium persulfate was added drop wisely into anilinium hydrochloride. The reaction was conducted overnight in round bottom flask at 4 ^{0}C. Polyaniline emeraldine salt coded as PANIE was purified by vacuum filtration and washed with 100 ml of 0.2 M hydrochloric acid, 100 ml of acetone and 100 ml of distilled water to remove the unreacted aniline. The precipitate was dried at 40 ^{0}C for 48 h. The filtrate was crushed using motor and pestle to a fine powder.

3.2.3.2. Sulfonation of polyaniline emeraldine salt

The polyaniline emeraldine salt was sulfonated to improve the solubility and electrical conductivity in aqueous media. 0.5 g of polyaniline emeraldine salt (PANIE) was reacted with 10 ml cold conc. sulfuric acid. The mixture was kept at 4 ^{0}C for 1 h with intermittent shaking. The sulfonated polyaniline was precipitated over 75:25 ratio of ice: water mixture. The fine precipitate was collected by centrifugation at 3000 rpm. The supernatant was removed and the pellet was washed with distilled water twice. Sulfonated polyaniline is coded as PANIS.

3.2.3.3. Synthesis of carboxy terminated in situ crosslinkable comacromer

Carboxy terminated *in situ* crosslinkable comacromer, fumarate-co-PEG-co-sebacate, was synthesized by one-step melt condensation reaction. 1.5 M maleic anhydride, 1.5 M sebacic acid and 3.0 M polyethylene glycol 300 were refluxed in round bottom flask for 1 h at 160 ^{0}C in a nitrogen atmosphere. 0.5 g morpholine and 0.25 g sodium acetate were used as a catalyst. Vacuum condensation was done at 180 ^{0}C for 5 min. The polymer was dissolved in acetone and precipitated in cold diethyl ether. The solvent was evaporated using rotor evaporator at 40 ^{0}C and stored in airtight container at 4 ^{0}C.

3.2.3.4. Preparation of electrically conducting in situ crosslinkable comacromers

The fumarate-co-PEG-co-sebacate comacromer was conjugated with polyaniline to prepare *in situ* crosslinkable, electrically conducting comacromer. 0.5 g *in situ* crosslinkable comacromer was neutralized with 3 ml sodium bicarbonate and diluted with 5 ml PBS. The reaction was conducted in a round bottom flask at room temperature. Carboxyl groups of comacromer were activated with equal volumes of 0.4 M EDC and 0.1 M NHS for 10 min. 300 mg PANIE/PANIS was dissolved in 1 ml distilled water and reacted for 24 h. The reaction mixture was dialyzed against PBS, lyophilized and stored at 4 ^{0}C. The comacromers conjugated with PANIE and PANIS are coded as PANIE-P and PANIS-P respectively.

3.3. Structural characterisation of comacromers

3.3.1. FT-IR and ^{1}H-NMR analysis

The structural analysis of comacromers was carried out using Fourier transform infrared spectrophotometer (FT/IR-4200, Jasco, USA) in the range of 4000-400 cm^{-1}. The comacromers were smeared over KBr pellet and spectral analysis was performed with JASCO's proprietary Spectra Manager TM II software. The nuclear magnetic resonance spectrum (^{1}H-NMR) of comacromers was recorded using Bruker 500 MHz spectrophotometer (Bruker Biospin, Billerica, MA).

3.3.2. UV-visible spectra

The structural characteristics of polyaniline-based comacromer were analyzed using UV-Visible spectrum. The PANIE, PANIS, PANIE-P, and PANIS-P were dissolved in distilled water at 5 mg/ml concentration. The spectra were recorded from 200-800 nm wavelengths at 600 nm/min scan rate using Varian Cary 100 Conc UV-Visible spectrophotometer.

3.3.3. Determination of molecular weight of comacromers

The molecular weight of comacromers was determined by gel permeation chromatography (GPC, Waters) system equipped with a 600 series pump, refractive index detector (Waters 2414), Rheodyne injector and Sytragel columns (HR-5E/4E/2/0.5). 2 mg/ml of comacromer solution in tetrahydrofuran was run at the flow rate of 1 ml/min. The chromatogram was compared with Dextran standards for relative calibration and analyzed by Empower 2 software.

3.4. Preparation of injectable hydrogels

3.4.1. Preparation of hydrogels from poly(propylene fumarate) based comacromers

0.25 g of PP comacromer and 0.1 g of SP comacromer were neutralized with 1 M sodium bicarbonate. The solution was dialyzed (float dialyzer with a molecular weight cut-off = 1 kDa) for 48 h against PBS to remove free ions and monomers. The purified comacromers were freeze-dried and resuspended in 1 ml distilled water. 200 µl of PP comacromer was mixed with 14 mg of PEGDA to prepare a PP6 hydrogel. 200 µl of SP comacromer was mixed with 17 mg of PEGDA to prepare SP 17 hydrogel. The crosslinking reaction was initiated by 10 µl of 0.4 M APS and 1 µl of 6 M TEMED. The time taken for the sol-gel transition was identified by tube tilting method. Temperature rise during polymerization was detected by a thermometer.

3.4.2. Preparation of hydrogels from sugar alcohol based comacromers

0.1 g of purified comacromer was neutralized with 4 ml, 1 M sodium bicarbonate. The excess salt was removed by dialysis against PBS using float dialyzer (Spectrum laboratories). The dialyzed product was lyophilized and resuspended in 8 ml PBS. 200 µl of the injectable formulation was vortex mixed with 5 mg PEGDA, 5 µl, 0.4 M APS and 1 µl, 6 M TEMED. The hydrogel prepared with PEAX and PEAM comacromers were coded as PEAX-P and PEAM-P respectively.

3.4.3. Preparation of hydrogels from polyaniline based comacromers

0.02 g of PANIE-P and PANIS-P comacromers were neutralized with 1 ml sodium bicarbonate. The excess salt was removed by dialysis. The comacromers were lyophilized and redissolved in 5 ml distilled water. Three hydrogels were prepared using PANIE-P comacromer and distilled water by mixing with distilled water in the comacromer: water ratio of 20:80, 50:50 and 100:0. 200 µl of comacromer solution was reacted with 20 mg PEG diacrylate, 10 µl, 0.4 M APS and 3 µl, 6 M TEMED to prepare the hydrogels. Similarly, three hydrogels were prepared using PANIS-P. The hydrogels prepared using PANIE-P with 20%, 50%, and 100% comacromer concentrations are coded as PE20P, PE50P and PE100P respectively. Similarly, the hydrogels prepared using PANIS-P with 20%, 50%, and 100% comacromer concentration are coded as PS20P, PS50P and PS100P.

3.5. Physico-chemical characterization of injectable hydrogels

3.5.1. Swelling percentage and equilibrium water content of hydrogels

The swelling ratio and equilibrium water content of PE50P and PS50P hydrogels was determined using the gravimetric method. The lyophilized hydrogel discs were weighed (W_d) and immersed in PBS for 24 h at 37 ^{0}C. The weight of hydrogel after swelling was measured (W_s). The swelling ratio and equilibrium water content was calculated as per the equations 2 and 3.

$$\text{Weight swelling ratio} = \frac{\text{Wet weight}}{\text{Dry weight}} \qquad \text{(Eq 2)}$$

$$EWC = \frac{\text{Wet weight-Dry weight}}{\text{Wet weight}} \times 100 \qquad \text{(Eq 3)}$$

3.5.2. Crosslink density of hydrogels

The crosslink density and number average molecular weights between crosslinks were calculated for each hydrogel. The lyophilized circular hydrogels discs were swelled in different solvents (acetone, DMSO, methanol, ethanol, dimethylacetamide and distilled water) for 48 h at 37 ^{0}C. The swelling ratio in each solvent was calculated. The maximum swelling was observed in distilled water and the readings were used for calculating crosslink density. The diameter and thickness of circular hydrogel discs were measured using digital vernier calipers before and after swelling. Maximum swelling coefficient (Q) was calculated as the ratio of the volume of the solvent in the swollen material to that of the swelled material. The crosslink density was calculated from modified Flory-Rehner's equation (Eq 4).

$$\text{Crosslink density } (\gamma) = -\frac{[Vr+\chi Vr^2 + \ln(1-Vr)}{drVo\left(\sqrt[3]{Vr}-\frac{Vr}{2}\right)} \qquad \text{(Eq 4)}$$

Here V_r is the volume fraction of the polymer in the swollen hydrogel equals to 1/1+Q. dr, the density of the polymer; χ , the polymer lattice interaction parameter (0.34 for the maximum swelling) and V_0 , the molar volume of the solvent. The number average molecular weight between crosslinks (M_C) was calculated as the reciprocal of crosslink density (mol/cm^3).

3.5.3. State of water inside the hydrogels

The phase transition of water inside the hydrogels was studied using differential scanning calorimetry (DSC Q20 V24.4 Build 116, TA Instruments) to determine the free and bound water content inside the present hydrogels. The lyophilized hydrogels were swelled in distilled water for 24 h. 5 mg of sample was cooled to (-) 60 ^{0}C and gradually heated to 100 ^{0}C at a rate of 5 ^{0}C/min in a nitrogen atmosphere. The thermogram was scanned from -60 ^{0}C to 100 ^{0}C using an empty aluminum pan as a reference. (Komeri, Thankam, Muthu., 2015). The freezable water content [free water (FW) + freezable bound water (FBW)] and bound water fraction [non-freezable bound water (NBW)] are calculated using the following equations.

$$\text{Freezing-free water} = \frac{\Delta H \text{ Endo}}{\Delta H_w} \times 100 \qquad \text{(Eq 5)}$$

Where ΔH_{Endo} is the enthalpy of melting of frozen water in the hydrogel. ΔHw is the enthalpy of melting of frozen pure water (334 Jg^{-1}).

$$\text{Bound water} = (\text{Equilibrium water} - \text{Freezing water}) \times 100 \qquad \text{(Eq 6)}$$

3.5.4. Surface and cross-sectional morphology of hydrogels

The morphology of surface and cross-section of hydrogel was determined using environmental scanning electron microscope (ESEM, FEI QUANTA 200, USA). The hydrogels were prepared in cylindrical shape using a syringe mold. The hydrogels were immersed in distilled water for 24 h and partially dried at room temperature to remove the surface adhered water molecules. The hydrogels

were cut horizontally to analyze the internal morphology. The distribution of pore diameter was analyzed by image J software.

3.5.5. *In vitro* ageing and biomechanical analysis

The compressive mechanical property of the present hydrogels with ageing was determined to analyze the mechanical stability of hydrogels under physiological conditions. The hydrogels (1 cm diameter x 1 cm height) were fabricated in a cylindrical mold. The hydrogels were incubated in 20 ml PBS (pH 7.4) at 37 ^{0}C for 24 h. The uniaxial compression testing (Instron 3345, Bioplus) was performed to identify the Young modulus. The height and diameter of hydrogel after swelling was measured using digital vernier calipers. The samples were compressed to 60 % of its height at a rate of 5 mm/min using 500 N load cell at room temperature. The maximum load at break, compressive stress at maximum load and the compressive Young modulus of each sample was identified using Bluehill 3.13 software. The variation in Young modulus of hydrogels with *in vitro* ageing (n = 6 per group) was also determined. The stress-strain graph of hydrogels was plotted. (Komeri, Thankam, Muthu., 2017).

3.5.6. Electrical resistance of polyaniline based hydrogels

The electrical resistance of PANIE-P and PANIS-P based hydrogels was measured using digital multimeter having a range from 0.1 to 4 x 10^{7} ohms. The PANIE-P and PANIS-P based hydrogels were prepared in cylindrical syringe mold with 0.5 cm diameter and 1.5 cm length. The electrical resistivity and conductivity of hydrogels were calculated as per the equations 7 and 8.

$$\text{Resistivity} = \frac{\text{Resistance} \times \text{Area of cross-section}}{\text{Length of hydrogel}} \quad \text{(Eq 7)}$$

$$\text{Conductivity} = \frac{1}{\text{Resistivity}} \quad \text{(Eq 8)}$$

3.6. Cytocompatibility of hydrogels

The cytocompatibility of hydrogels was evaluated with L929, rat fibroblast cells (NCCS, Pune). The cells were cultured in Dulbecco's modified eagles medium containing high glucose supplemented with 0.37% sodium bicarbonate, 10% fetal bovine serum and 1% antibiotic-antimycotic solution. Cells were cultured at 37 ^{0}C and 5% CO_2 in a humidified incubator.

3.6.1. Evaluation of cytocompatibility of hydrogel extract

The cytocompatibility of the present hydrogels was determined as per ISO10993-5, annexure C. The injectable formulation of each comacromers was sterile filtered. The initiators were also filtered through 0.22 µm bacterial filter. The hydrogel samples were prepared in 24 well plates and incubated in 1 ml DMEM media for 72 h at 37 ^{0}C. This hydrogel extract was used for the following assay. Around 1x10^4 cells were seeded and cultured in a 96 well plate to reach 80% confluent. The hydrogel extract was diluted with fresh DMEM media to different concentrations. The cells were incubated with the hydrogel extract for 24 h at 37 ^{0}C and 5% CO_2. After 24 h, the culture media was removed and washed with PBS. The cells were incubated with 5 mg/ml of MTT solution in PBS for 4 h at 37 ^{0}C. The formazan crystals were extracted in 200 µl DMSO for 30 min at room temperature. The absorbance was measured at 540 nm using ASYS UVM

340 plate reader. (Komeri, Muthu., 2016). The viability of cells was calculated using the following equation (Eq 9).

$$\text{Cell viability} = \frac{\text{Absorbance of test group}}{\text{Absorbance of control cells}} \times 100 \qquad \text{(Eq 9)}$$

3.6.2. Direct contact assay

The direct contact assay was carried out to demonstrate the influence of present hydrogels over morphology and confluence of cells under contact. 10 mg of hydrogels were incubated with L929 cells ($1x10^4$) in 96 well plate for 24 h at 37 ^{0}C. The phase contrast micrographs were taken to assess the morphology of the cells.

3.6.3. Live dead assay

Live dead assay was carried out to study the viability and apoptotic death of cells incubated with the present hydrogels. L929 cells ($1x10^4$) were seeded in 96 well plate and cultured till 80% confluence. 10 mg of hydrogels were incubated with L929 cells for 24 h at 37 ^{0}C. The cells were stained with 2 µM calcein AM and 4 µM ethidium bromide for 10 min. Cells were observed under an epifluorescence microscope (Optika, Italy).

3.7. Hemolysis study

The hemolytic potential of hydrogel materials with human blood is analyzed as per ISO 10993-4:2002 (E) guideline. The blood from human volunteer was collected into an anticoagulant, citrate phosphate dextrose adenine solution (CPD-A). The hydrogel materials were taken in a polystyrene culture plate and washed with PBS for 5 min. The hydrogels were incubated with 4 ml of

blood for 30 min under agitation at a speed of 70 ± 5 rpm at 35 ± 2 ^{0}C. 3 ml of blood was centrifuged at 4000 rpm for 15 min and platelet poor plasma was aspirated. The blood in polystyrene culture plate is taken as reference. The free hemoglobin liberated into the plasma after 30 min of exposure was measured in each sample using a spectrophotometer. The percentage of hemolysis was calculated using the formula (Eq 10).

$$\% \text{ hemolysis} = \frac{\text{Free hemoglobin} \times 1000}{\text{Total hemoglobin}} \times 100 \qquad \text{(Eq 10)}$$

3.8. Studies on free radical scavenging characteristics of hydrogels

The free radical scavenging property of hydrogels was assessed by biochemical methods. The protective effect of hydrogels over cardiomyoblast cells under oxidative stress was investigated by *in vitro* tests.

3.8.1. Biochemical assays

The scavenging property of hydrogel on DPPH, hydroxyl, and nitric oxide radicals was assessed by biochemical assays. The hydrogel discs of 1 cm diameter x 0.5 mm thickness and 0.1 g weight were used for biochemical assays.

3.8.1.1. DPPH (1-1-diphenyl 2-picryl hydrazyl) radical scavenging property

The DPPH scavenging assay was carried out as per the method reported by Li *et al*, 2013. The hydrogel discs (1cm diameter x 0.5 mm thickness, 0.1 g weight) were immersed in 1 ml absolute ethanol and incubated with 100 µl of DPPH radical solution (0.5 mM in ethanol). 100 µl of 0.5 mM DPPH in 1 ml ethanol was used as a control. The hydrogels immersed in 1.1 ml ethanol was

served as blank. Ascorbic acid (5-100 μM) was taken as positive control. All the samples were incubated for 100 min in dark. The absorbance (optical density or OD) was measured at 517 nm using a plate reader (ASYS UVM 340, UK). The DPPH radical scavenging potential of the test sample was determined as per the equation 11.

$$\text{Scavenging effect (\%)} = \frac{\text{OD of control - OD of test}}{\text{OD of control}} \times 100 \qquad \text{(Eq 11)}$$

3.8.1.2. Hydroxyl radical scavenging property

The hydroxyl radical scavenging activity of hydrogels was determined by deoxyribose assay as per Gutteridge and Halliwell, 1988. The reaction mixture consists of 1 mM Ferric chloride, 30 mM deoxyribose, 1 mM ascorbic acid, 1 mM EDTA and 20 mM H_2O_2 in 0.2 M phosphate buffer. The hydrogel discs (1cm diameter x 0.5 mm thickness, 0.1 g weight) were incubated with 1 ml of the reaction mixture at room temperature for 1 h. The reaction mixture containing 0.2 ml phosphate buffer instead of hydrogel was used as a control. Then 1 ml of reagent mixture containing 1% thiobarbituric acid (TBA) and 15% trichloroacetic acid (TCA) reagent in 0.25 N HCl was added to all the tubes and incubated in boiling water bath for 20 min. The reduction in color due to the scavenging of hydroxyl radical was read at 532 nm. Ascorbic acid at different concentrations (5-100 μM) was used as the standard. The hydroxyl radical scavenging ability was determined using the equation (11).

3.8.1.3. Nitric oxide radical scavenging property

The nitric oxide radical scavenging assay was based on Griess reaction as reported by Sangameswaran *et al.*, 2009. The hydrogel discs (1 cm diameter x 0.5

mm thickness, 0.1 g weight) were incubated with 125 µl methanol and 750 µl sodium nitroprusside (5mM) in PBS at 25 ^{0}C for 30 min. The hydrogel discs in 875 µl PBS was served as blank. The reaction mixture without hydrogel was used as a control. Ascorbic acid (5-100 µM) was taken as positive control. After 30 min of incubation 375 µl Griess reagent (1% sulphanilamide, 2% H_3PO_4 and 0.1% naphthyl ethylenediamine dihydrochloride) was added to all the tubes. The absorbance was measured at 546 nm. The scavenging percentage was calculated as per equation (11).

3.8.1.4. Total reducing power

The total reducing power of hydrogel was carried out as reported by Jose *et al.*, 2015. The hydrogel discs (1 cm diameter x 0.5 mm thickness, 0.1 g weight) were incubated in reaction mix containing 2.5 ml, 1% potassium ferricyanide and 2.5 ml phosphate buffer (0.2 M, pH 6.6) at 50^{0}C for 20 min. 2.5 ml 10% trichloroacetic acid (TCA) was added to all the tubes. Then centrifuged at 3000 rpm for 10 min. 2.5 ml of the upper layer was mixed with equal volume of distilled water. 0.5 ml Ferric chloride (0.1%) was added to all the tubes and vortexed. The absorbance was read at 700 nm. The reaction mixture without hydrogel disc served as blank. The reducing power was calculated as per equation 11 and compared with ascorbic acid (100 µM).

3.8.2. *In vitro* studies

The metabolic activity, viability and intracellular ROS generation of cardiomyoblast cells treated with stress inducing media in the presence of hydrogels were studied by MTT assay, live dead assay and DCFH-DA assay. The

present hydrogels (1cm diameter x 0.5 mm thickness, 0.1 g weight) were sterilized with 70% ethanol and washed thrice with sterile PBS.

3.8.2.1. Stress inducing media

A stress inducing media was prepared using optimum concentration of Fenton reagents to induce oxidative stress on the cardiomyoblast cells. Initially, the concentration of hydrogen peroxide (H_2O_2) and ferric chloride ($FeCl_3$) which induce 50% death of cardiomyoblast cells was identified by MTT assay. Cardiomyoblast cells were seeded in 24 well plate at $1x10^3$ density and cultured to 80% confluence. The stress inducing media was prepared by mixing 12.5, 25, 50, 100 and 200 µM of hydrogen peroxide and ferric chloride in PBS. The cardiomyoblast cells were incubated with stress inducing media for 15 min. Then the cells were cultured in serum-containing DMEM media for 19 h. The cells were stained with MTT (5 mg/ml) for 4 h and digested with DMSO for 30 min. The absorbance was measured at 540 nm using spectrophotometer (ASYS UVM 340, UK). The concentration of stress inducing media for 50% cell death (LD 50) was determined (Komeri, Thankam, Muthu., 2017).

3.8.2.2. Effect on cell metabolic activity under oxidative stress

The metabolic activity of cardiomyoblast cells treated with stress inducing media in the presence of the present hydrogels was determined by MTT assay. The oxidative stress was induced on H9c2 cells using 70 µM hydrogen peroxide and 70 µM ferric chloride in PBS (stress inducing media as determined above) for 15 min. The hydrogel discs (1 cm diameter x 0.5 mm thickness, 0.1 g weight) were added along with stress inducing media. The stress inducing media was

removed after 15 min. The hydrogel was retained in a well plate. Cells were washed with PBS and incubated with serum containing DMEM media for 19 h. Ascorbic acid (50 µM) treated cells were taken as positive control. The cells were washed with PBS and incubated with MTT solution (5 mg/ml) for 4 h. Formazan crystals were digested in DMSO for 30 min under continuous shaking. The absorbance was measured at 540 nm using spectrophotometer (ASYS UVM 340, UK). (Komeri, Thankam, Muthu., 2017). The cell viability was calculated using equation 12.

$$\text{Cell viability (\%)} = \frac{\text{OD Test}}{\text{OD control}} \times 100 \qquad \text{(Eq 12)}$$

3.8.2.3. Effect on cell apoptosis under oxidative stress

The apoptotic death of cardiomyoblast cells treated with stress inducing media in the presence of hydrogels was assessed by live dead assay. The control cells, cells treated with stress inducing media, cells under oxidative stress treated with ascorbic acid (50 µM) and cells under oxidative stress treated with the present hydrogels were stained with 5 ug/ml acridine orange and 5 ug/ml ethidium bromide in PBS for 5 min. The fluorescence images were taken under an epifluorescent microscope (Optika, Italy). (Komeri, Thankam, Muthu., 2017). The number of cells in each image was determined using image J software supported with ITCN automated cell counting application.

3.8.2.4. Studies on intracellular ROS generation

The degree of reactive oxygen species generated in cardiomyoblast cells by the external inducement of H_2O_2 was determined by 2', 7' dichloro dihydro

fluorescein diacetate (DCFH-DA) assay. The fluorescence from 2', 7' dichloro dihydro fluorescein (DCF) trapped inside the cells indicates the presence of ROS inside the cells. The cardiomyoblast cells at $1x10^3$ density were seeded in 96 well plate and cultured till 80% confluence. The cells were incubated with DCFH-DA (20 μM) in serum free media for 20 min at 37 ^{0}C in dark. The cells were treated with stress inducing media (70 μM H_2O_2 and 70 μM $FeCl_3$) for 15 min to induce oxidative stress. The cells were treated with 10 mg of the present hydrogels. Ascorbic acid at 50 μM concentration was used as positive control. Cells treated with serum free media for 20 min was taken as cell control. The media was removed and cells were washed with PBS. The fluorescence emission from each well was identified using spectrofluorimeter equipped with a multiwell plate reader. DCFH excites at 480 nm and emits at 530 nm. The fluorescence intensity was compared with control groups.

3.9. Encapsulation of cardiomyoblast cells.

H9c2 cardiomyoblast cells were encapsulated in the present hydrogels to assess the cell proliferation and viability under long-term culture. H9c2 cells were cultured in Dulbecco's Modified Eagle's Medium at 37 ^{0}C and 5% CO_2. Filtered comacromers with PEGDA, APS and TEMED were mixed with $1x10^7$ cardiomyoblast cells in PBS. The cell-encapsulated hydrogels were prepared in 24 well plate and cultured for 30 days (Komeri, Thankam, Muthu., 2015).

3.9.1. Proliferation of encapsulated cells

The proliferation of cardiomyoblast cells inside the hydrogels was studied by MTT assay. The cell-encapsulated hydrogels were cultured for

30 days. The hydrogels cultured for 1, 2, 3 and 4 weeks intervals were taken for analysis. The cell encapsulated hydrogels were washed with PBS and incubated with 1 mg/ml MTT solution in serum free DMEM media for 24 h at 37 ^{0}C. The hydrogels were homogenized in 1 ml DMSO and kept for 30 min at room temperature to extract formazan crystals. Then centrifuged at 1500 rpm and absorbance of the supernatant was measured at 540 nm. The absorbance of acellular hydrogels was taken as blank and subtracted from the test samples. (Komeri, Thankam, Muthu., 2015). The viability of encapsulated cells was determined against the control cells under 2D culture.

$$\text{Cell viability (\%)} = \frac{\text{OD Test- OD blank}}{\text{OD control}} \times 100 \qquad \text{(Eq 13)}$$

3.9.2. Live dead assay

The viability of cells encapsulated inside the hydrogels was assessed by live dead assay. Cell-encapsulated hydrogels cultured for 30 days were taken for live dead assay. The hydrogels were washed with PBS and incubated in a staining solution containing 2 µM calcein AM and 4 µM ethidium bromide for 45 min. The hydrogels were washed with PBS and observed under confocal laser scanning microscope (ZEISS LSM 510 META). The images were taken at 488 nm and 514 nm excitation wavelengths with emission filters at 507-550 nm and 539-614 nm respectively. The images were analyzed using ZEISS LSM Image Examiner software. (Komeri, Muthu., 2016). The density of cells in each image was determined using image J software supported with ITCN automated cell counting application.

3.9.3. Histological evaluation

The cell distribution and extracellular matrix modeling by the encapsulated cells inside the present hydrogels were studied by H & E staining. The cardiomyoblast cell-encapsulated hydrogel after 30 days of culture was used for histological evaluation. The cryosections of cell-encapsulated hydrogels of 10 μm thickness were taken using LEICA CM 3050S microtome on a poly lysine coated glass slide. The sections were stained with hematoxylin stain for 2 min, washed with tap water for 2 min, destained with acid alcohol until the sections look red and washed under tap water. The slides were dipped in the bluing solution for 2 min and rinsed with tap water. The slides were rinsed in 95% ethanol followed by eosin counterstaining for 30 sec. The slides were dehydrated using 70, 80, 95 and 100% ethanol. The sections were mounted and Images were taken using an inverted microscope (Optika, Italy). The acellular hydrogel kept in DMEM media for 30 days was processed and stained in a similar way for comparison. (Komeri, Muthu., 2016).

3.10. Statistical analysis

All experiments were performed at least 3 times and the data were reported as mean ± standard deviation. The significance in difference was analyzed by student's t-test using GraphPad QuickCals t-test calculator. The values of $p < 0.05$ were considered significant. * Sign was given for the data that exhibit significant difference compared to other groups.

CHAPTER 4

RESULTS

4 Results

The synthesis and structural analyses of the new comacromers based on poly(propylene fumarate), sugar alcohol and polyaniline and preparation and the gelation characteristics of injectable hydrogels are presented. The results on swelling of hydrogels in water, surface, and cross-sectional morphology, a variation of biomechanical property with in vitro ageing and state of water inside the present hydrogels are presented. The electrical conductivity of polyaniline-based hydrogels is also specified. The results of the studies on cytocompatibility, hemolysis and free radical scavenging property of the present hydrogels are presented. The morphology, proliferation, viability and extracellular matrix modeling by the encapsulated cardiomyoblast cells are also given in this chapter.

4.1. Synthesis and structural characterization of in situ crosslinkable comacromers for hydrogels

4.1.1. Synthesis and characterization of poly(propylene fumarate) based comacromers

The poly(propylene fumarate-co-ethylene glycol) and poly(propylene fumarate-co-sebacate-co-ethylene glycol) comacromers were synthesized by melt condensation reaction. The reaction involves esterification and cis-trans

isomerisation of maleate groups to fumarate. The vacuum condensation was done at each step to ensure the complete removal of water during esterification reactions. The poly(propylene fumarate-co-ethylene glycol) comacromer was synthesized by two-step condensation reaction (Figure-3), whereas, poly(propylene fumarate-co-sebacate-co-ethylene glycol) comacromer was synthesized by three step condensation reaction (Figure - 4). The additional step in poly(propylene fumarate-co-sebacate-co-ethylene glycol) account for the condensation with sebacic acid. The condensation of propylene glycol with maleic anhydride is the initial step in the synthesis of both poly(propylene fumarate-co-ethylene glycol) and poly(propylene fumarate-co-sebacate-co-ethylene glycol) comacromers. However, the ratio of propylene glycol to maleic anhydride is 1:2 in the former and 1:1 in the latter to ensure availability of suitable functional groups for stoichiometric reactions.

The functional groups of the comacromers were investigated with FT-IR spectral analysis. The FT-IR spectrum of the poly(propylene fumarate-co-ethylene glycol) comacromer (Figure - 5A) gives a peak at 974 cm^{-1} (CH bending of trans –CH=CH-), 1639 cm^{-1} (-C=C- stretching of –CH=CH- bond), 1730 cm^{-1} (C=O stretching in ester bond), 1079 cm^{-1} (C-O-H stretching), 3451 cm^{-1} (O-H stretch of hydrogen bonded alcohols), 1404 cm^{-1} (C-H bending) and 2199 cm^{-1} (C-H stretching). The spectral response of poly(propylene fumarate-co-sebacate-co-ethylene glycol) comacromer (Figure - 5B) revealed peaks at 1730 cm^{-1} (C=O stretching in ester bond), 1639 cm^{-1} (C=C stretching of –CH=CH–), 935 cm^{-1} (C–H bending of trans CH=CH), 1457 cm^{-1} (C-H bending) and 1110 cm^{-1} (C-O-H stretching). The absorption at 3440 cm^{-1} and 2901 cm^{-1}

corresponds to the stretching vibration of hydrogen bonded alcohols group and C-H group in sebacic acid respectively.

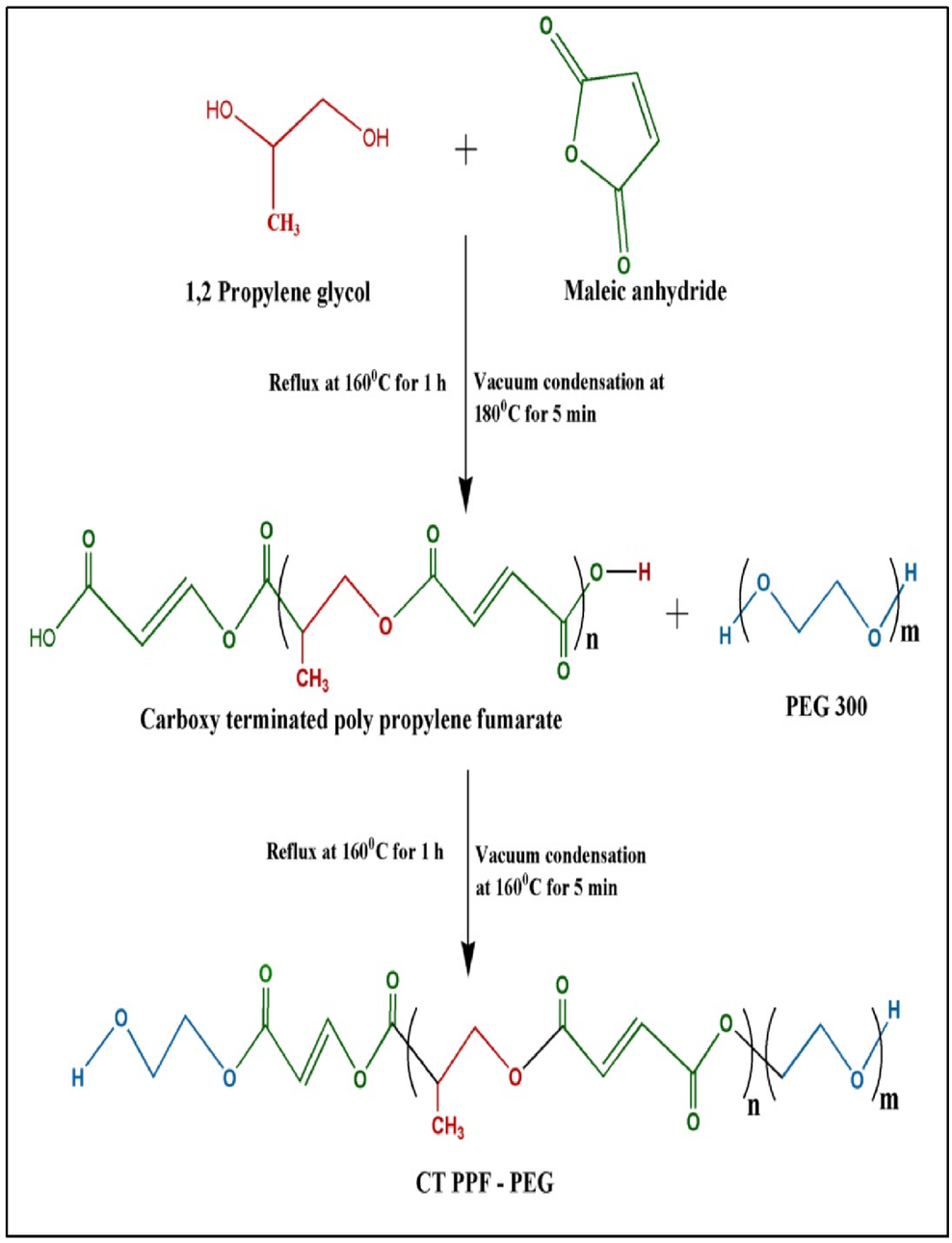

Figure - 3: Synthesis of poly(propylene fumarate-co-ethylene glycol) comacromer

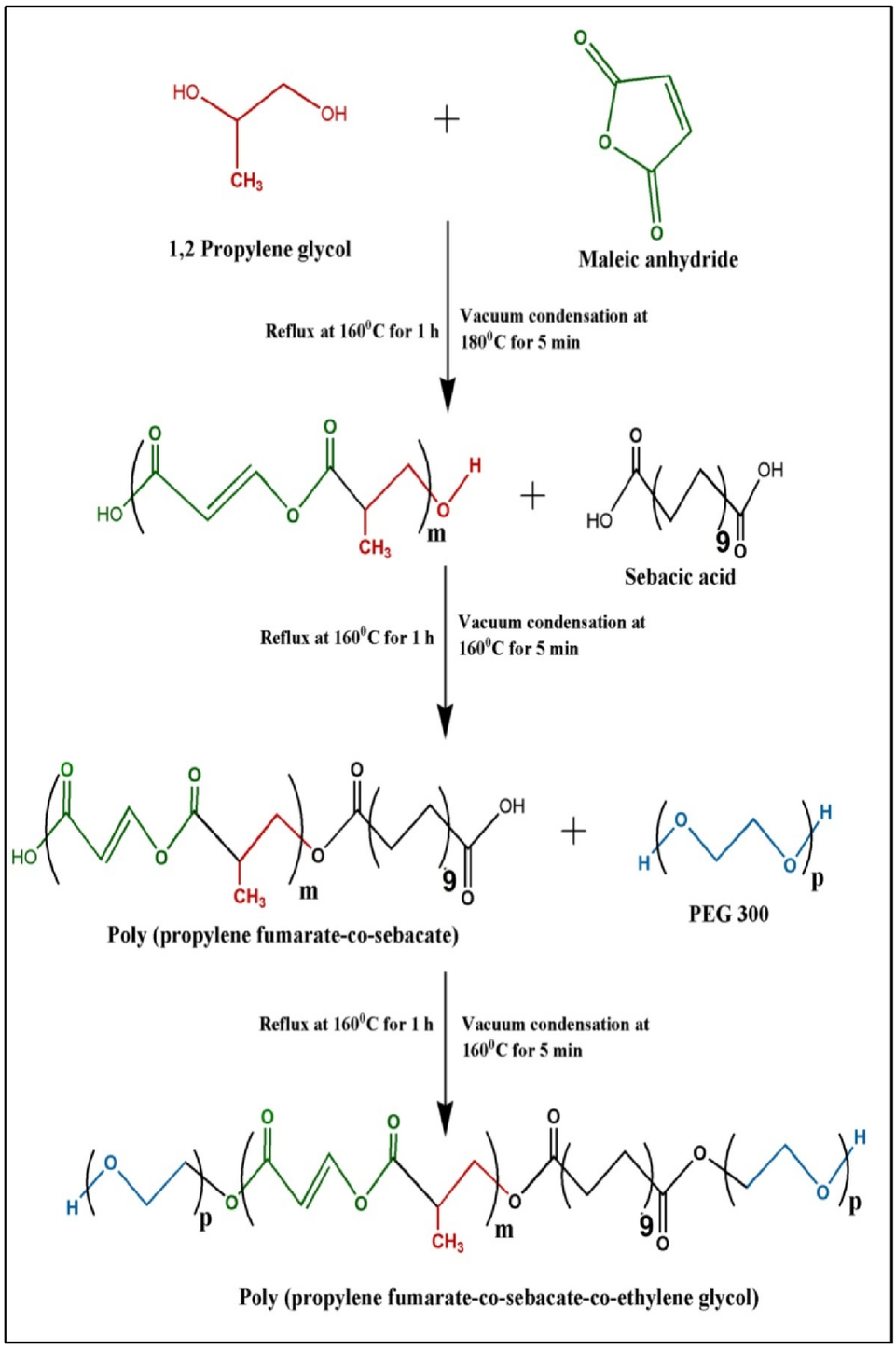

Figure - 4: Synthesis of poly(propylene fumarate-co-sebacate-co-ethylene glycol)

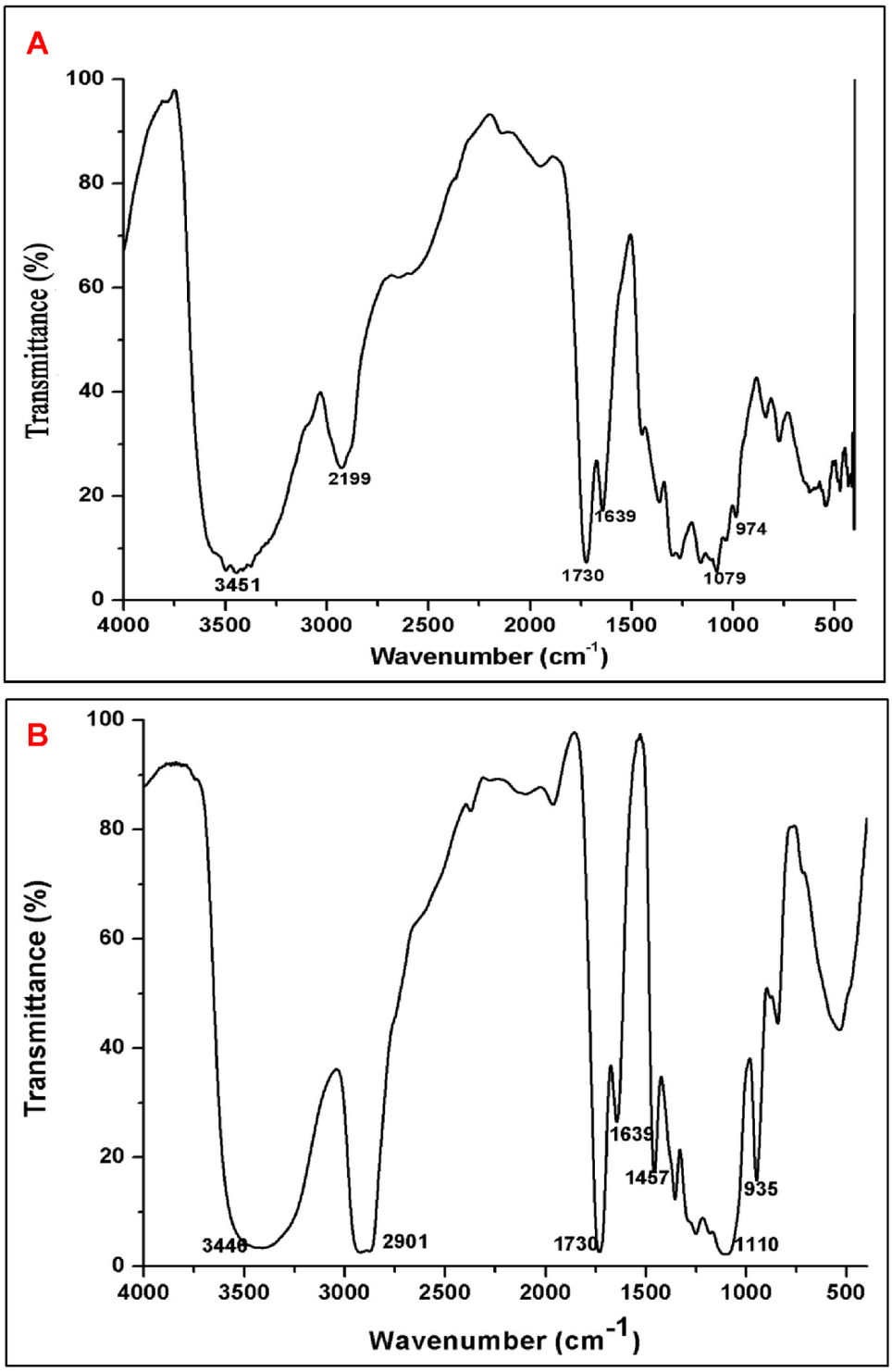

Figure - 5: FT-IR spectra of comacromers. Poly(propylene fumarate-co-ethylene glycol) (A) and poly(propylene fumarate-co-sebacate-co-ethylene glycol) (B).

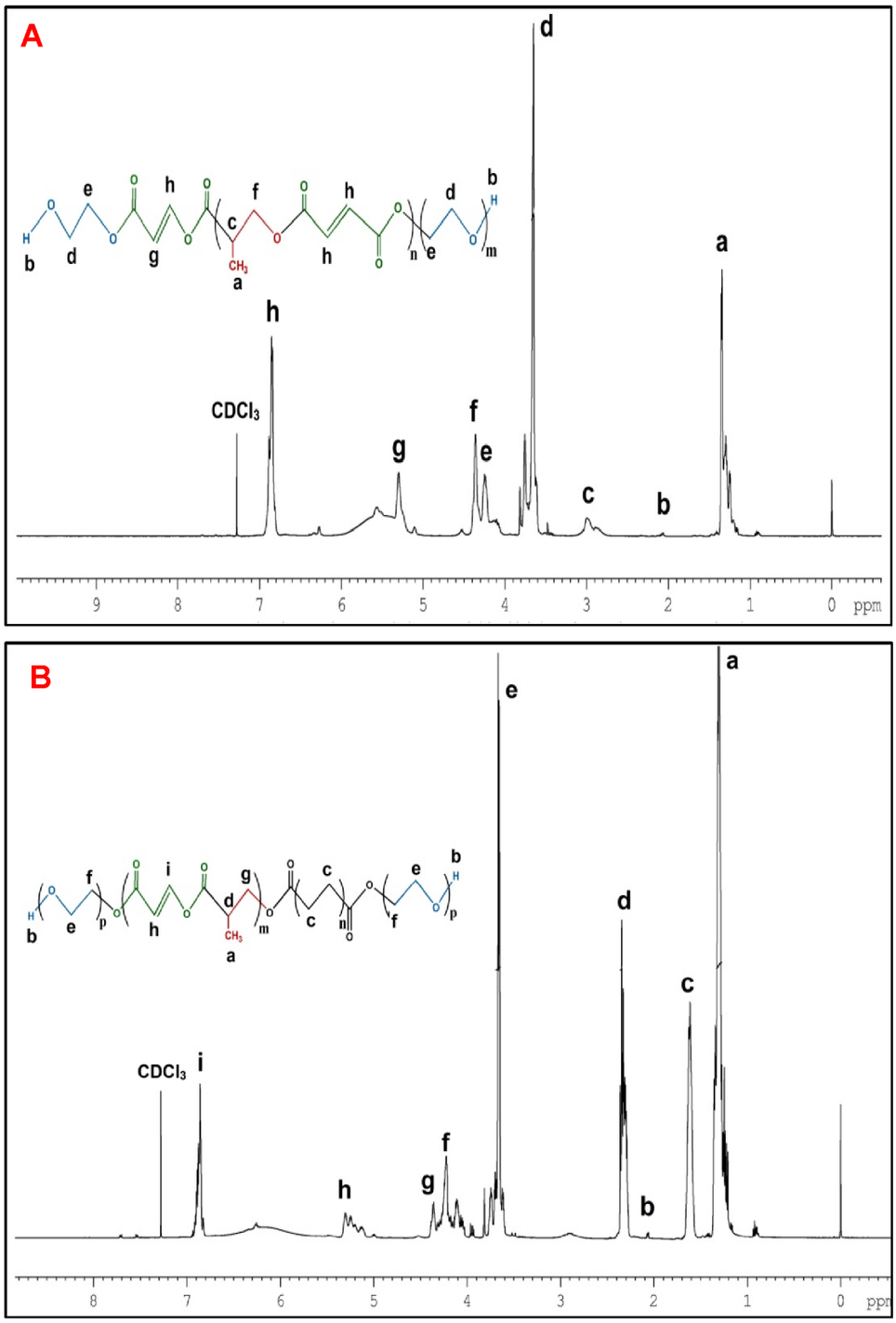

Figure - 6: ^{1}H-NMR spectra of comacromers. Poly(propylene fumarate-co-ethylene glycol) (A) and poly(propylene fumarate-co-sebacate-co-ethylene glycol) (B).

The structural analysis of the comacromers was carried out with ^{1}H-NMR spectroscopy. The ^{1}H-NMR spectra of poly(propylene fumarate-co-ethylene glycol) comacromer exhibit chemical shifts at 1.3 (CH_3), 2 (-OH), 2.9 (CH), 3.8 (O-CH_2-CH_2), 4.3(O-CH_2-CH), 5.4 (C-CH=CH-) and 6.8 ppm (CH=CH-O-) (Figure - 6A). The chemical shift of proton associated with poly(propylene fumarate-co-sebacate-co-ethylene glycol) is at 1.3 (CH_3), 1.6 (C-CH_2-CH_2), 2.3(-OH), 3.7(O-CH_2-CH_2), 4.3 (O-CH_2-CH), 5.4(C-CH=CH-) and 6.8 ppm (CH=CH-O-) (Figure - 6B).

4.1.2. Synthesis and characterization of sugar alcohol based comacromers

The xylitol-fumarate-poly(ethylene adipate)-fumarate-PEG (coded as PEAX) and mannitol-fumarate-poly(ethylene adipate)-fumarate-PEG (coded as PEAM) comacromers were synthesized for hydrogel preparation. The reaction schemes of PEAX and PEAM comacromers are given in figure 7 and 8 respectively. The synthesis involves both esterification and isomerization reactions. The free hydroxyl groups in mannitol and xylitol are used for condensation reactions. The reaction was carried out at high temperature for the proper melting of sugar alcohols and cis-trans isomerization of maleic acid (at 160-180 ^{0}C). The ring opening reaction of maleic anhydride at a temperature above 160 ^{0}C results in an unsaturated dicarboxylic fumaric acid. The double bonds in fumaric acid facilitate *in situ* crosslinking with vinyl crosslinkers.

The FT-IR spectrum of PEAX and PEAM comacromers gives spectral responses at 1730 cm^{-1} and 1640 cm^{-1}(Figure - 9A, 9B). Broad peaks at 3424 cm^{-1} and 3438 cm^{-1} in the FT-IR spectra of PEAX and PEAM corresponds to the

stretching vibration of hydrogen bonded alcohols. The responses at 2939 and 2947 cm^{-1} correspond to the alcohol groups associated with carboxylic acid. The peaks are also observed at 974, 913 cm^{-1} (CH bending of trans –CH=CH-), 1640, 1639 cm^{-1} (-C=C- stretching of –CH=CH- bond), 1110 and 1026 cm^{-1} (C-O-H stretching) for PEAX and PEAM comacromers. The peak at 1730 cm^{-1} in both PEAX and PEAM corresponds to the C=O stretching in ester bond.

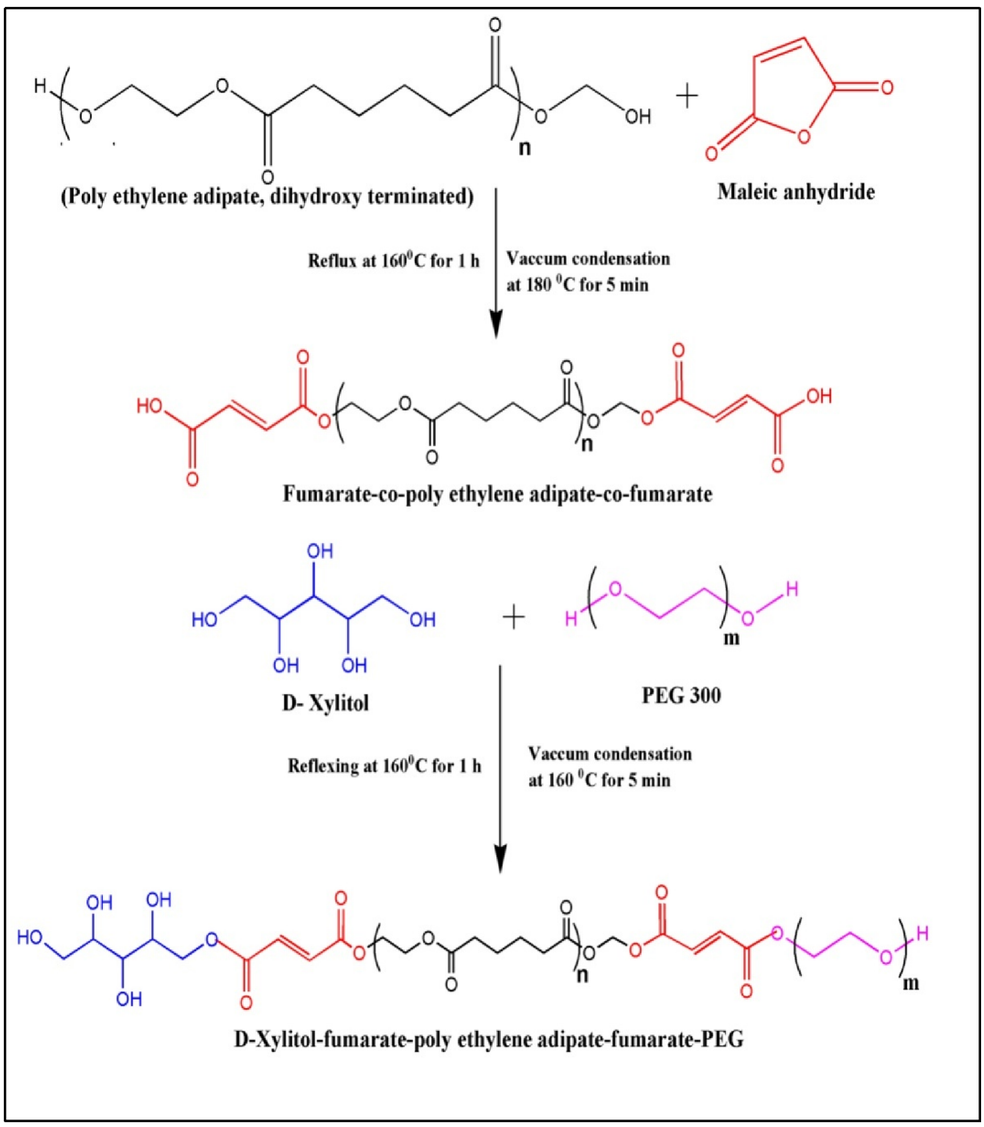

Figure-7: Synthesis of xylitol-fumarate-poly(ethylene adipate)-fumarate-PEG comacromer.

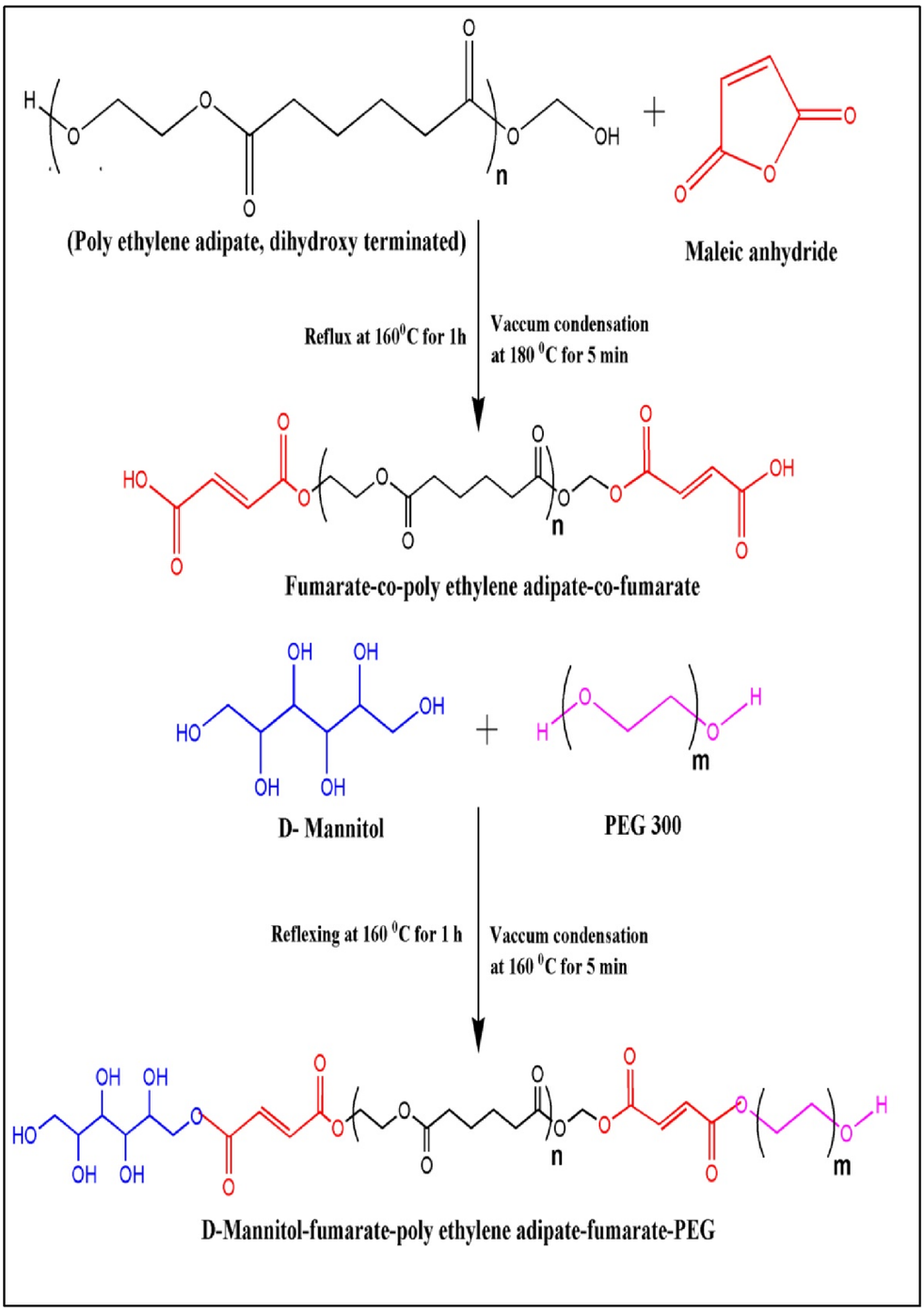

Figure - 8: Synthesis of mannitol-fumarate-poly(ethylene adipate)-fumarate-PEG comacromer.

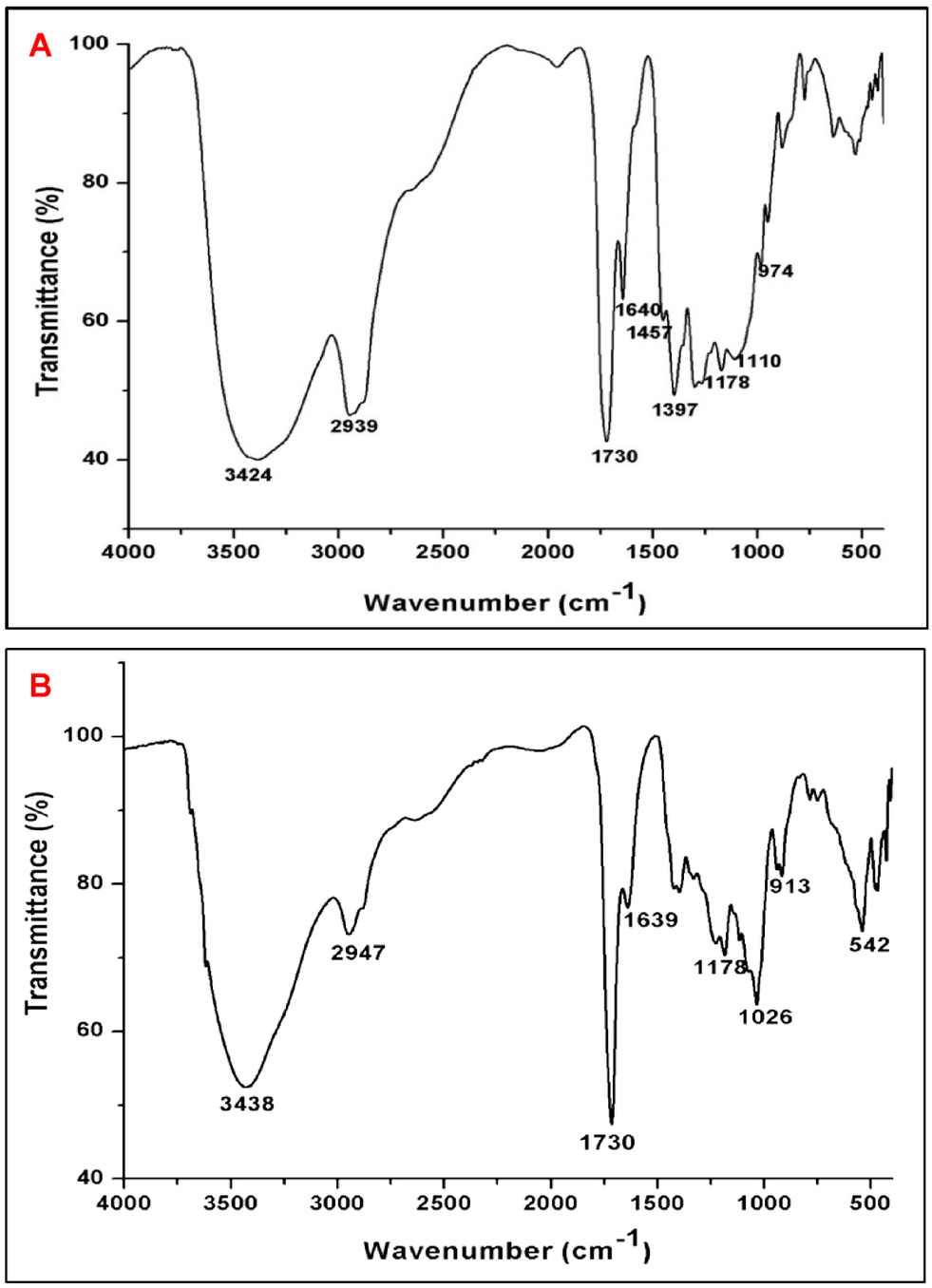

Figure - 9: FT-IR spectra of comacromers. Xylitol-fumarate-poly(ethylene adipate)-fumarate-PEG (A) and mannitol-fumarate-poly(ethylene adipate)-fumarate-PEG (B).

^{1}H-NMR spectrum of PEAX comacromer exhibits chemical shifts at 1.5 (CH_2-CH_2), 2.2 (-OH), 2.5 (C-CH_2), 3.6 (O-CH_2-CH_2), 4.2 (O-CH_2-) and 6.8

(CH=CH) ppm (Figure - 10A). The ^{1}H-NMR spectrum of PEAM comacromer gives peaks at 1.5(CH_2-CH_2), 2.2(-OH), 3.5(O-CH_2-CH_2), 4.1(O-CH_2-) and 6.8(CH=CH) ppm (Figure - 10B).

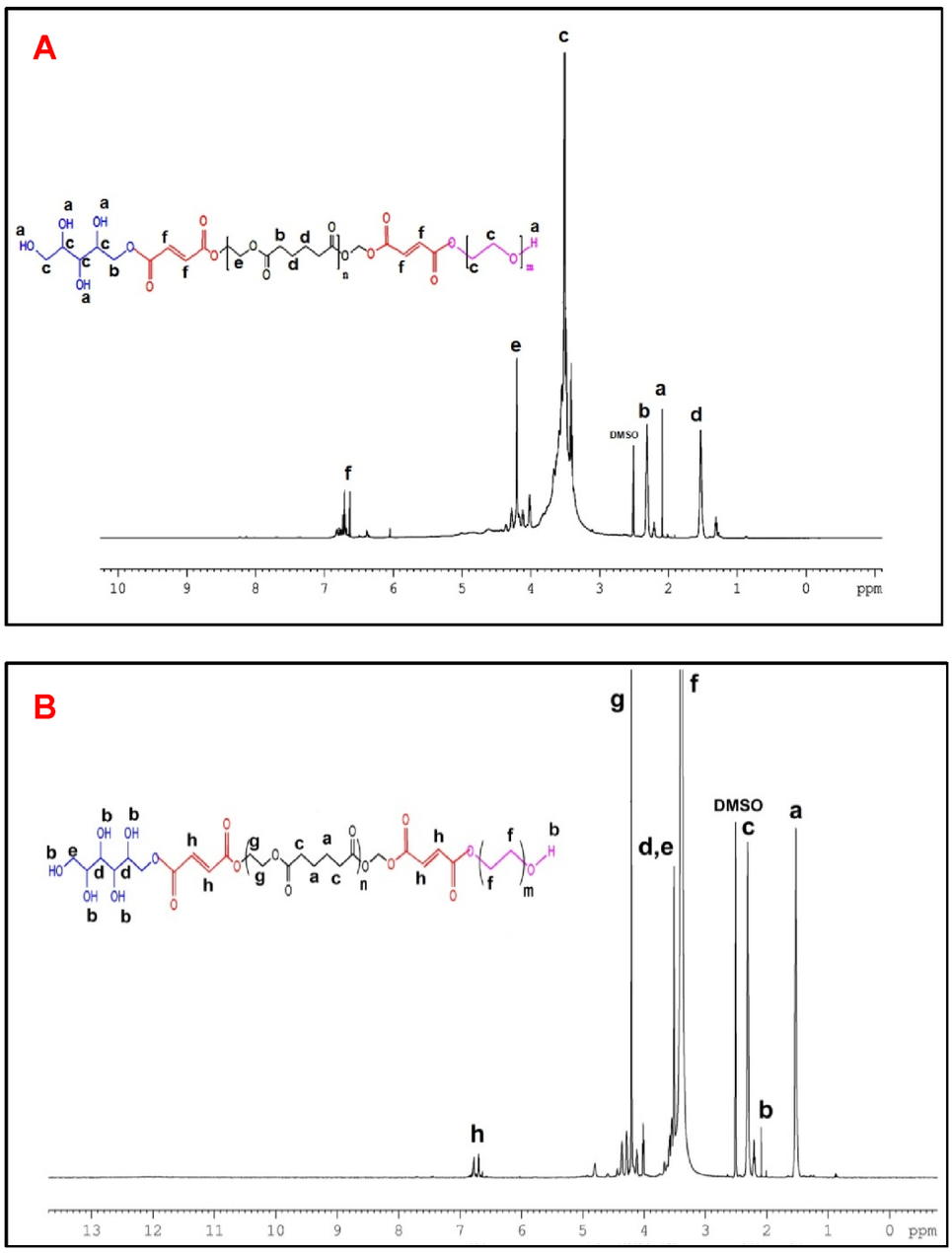

Figure - 10: ^{1}H-NMR spectra of comacromers. Xylitol-fumarate-poly(ethylene adipate)-fumarate-PEG (A) and mannitol-fumarate-poly(ethylene adipate)-fumarate-PEG (B)

4.1.3. Synthesis and characterization of polyaniline based comacromers.

The polyaniline based *in situ* crosslinking comacromers were synthesized to prepare electrically conducting injectable hydrogels. Initially, the emeraldine salt of polyaniline (PANI) was synthesized by solution polymerization of anilinium hydrochloride in the presence of the oxidizing agent, ammonium persulfate (Figure - 11). Polymerization was monitored by the gradual appearance of dark green polyaniline in light brown anilinium hydrochloride solution.

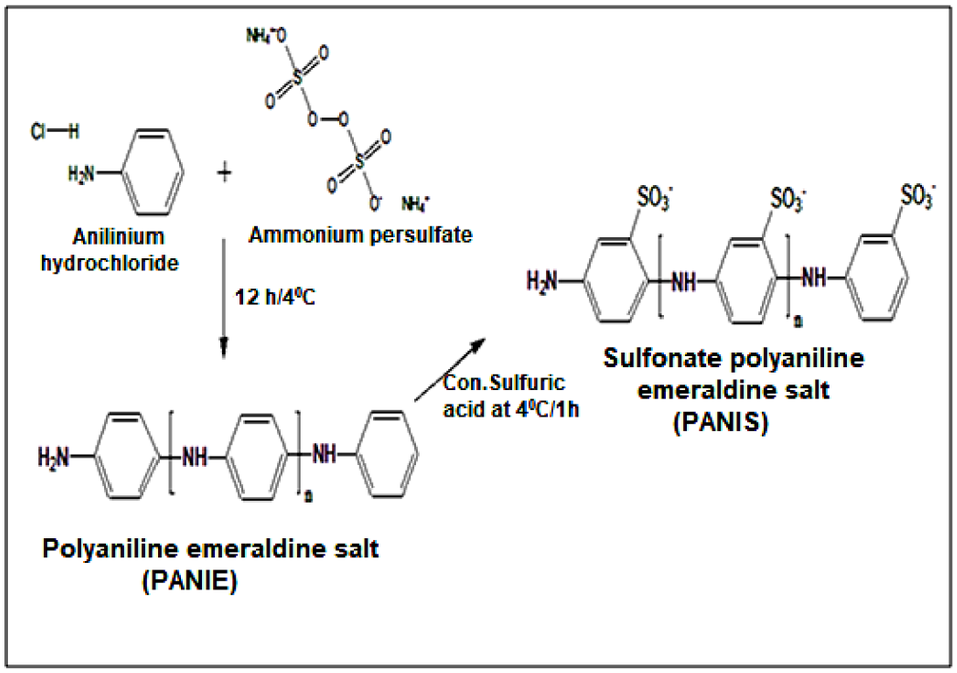

Figure - 11: Synthesis of polyaniline emeraldine salt and sulfonated polyaniline

The polymerization was exothermic; however, the temperature was maintained at 4 ^{0}C throughout the reaction. The benzene ring of polyaniline undergoes sulfonation on treating with fuming sulfuric acid at 4 ^{0}C.

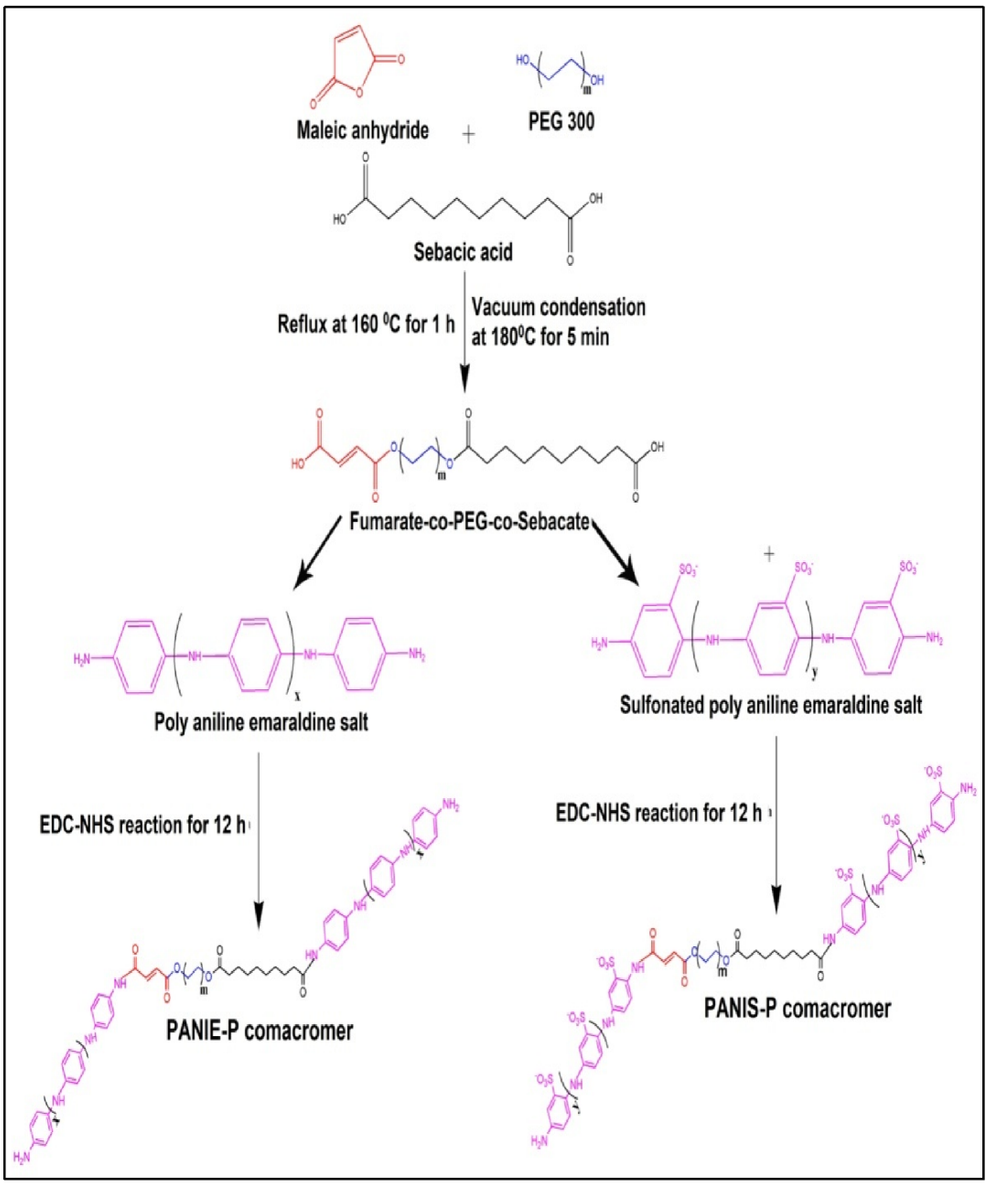

Figure - 12: Synthesis of polyaniline conjugated *in situ* crosslinkable comacromers.

The conducting *in situ* crosslinkable comacromer was prepared by coupling carboxyl group of fumarate-co-PEG-co-sebacate to the amino group of polyaniline by EDC-NHS reaction (Figure - 12).

EDC reacts with carboxyl groups of fumarate-co-PEG-co-sebacate to form an active intermediate, which is stabilized by NHS at physiological pH. The intermediate compound with an activated carboxyl group is highly reactive to the primary amine, which facilitates conjugation of comacromer with polyaniline.

The structural analysis was done with FT-IR and ^{1}H-NMR spectroscopy. The FT-IR spectrum of fumarate-co-PEG-co-sebacate comacromer exhibit responses at 1722 cm^{-1} (C=O stretching in ester bond) and 1631 cm^{-1} (C=C stretching of –CH=CH–). The PANIE-P comacromer exhibit spectral responses at 1714 cm^{-1} (C=O stretching), 1647 cm^{-1} (C=C stretching of –CH=CH–), 1556 cm^{-1} (N-H bending vibration), 1320 cm^{-1} (N–H stretching) and 1095 cm^{-1}(C-O-H stretching). The FT-IR spectrum of PANIS-P gives the absorbance at 1730 cm^{-1} (C=O stretching), 1647 cm^{-1} (C=C stretching of –CH=CH–), 1556 cm^{-1} (N-H bending vibration), 1389 cm^{-1} (N–H stretching) and 1095 cm^{-1}(C-O-H stretching) (Figure - 13).

The ^{1}H-NMR spectrum of fumarate-co-PEG-co-sebacate comacromer exhibit chemical shifts at 1.1 (CH_2-CH_2), 2.1 (-CH_2-C-), 3.4 (O-CH_2-CH_2) and 6.7 (CH=CH) ppm (Figure - 14A). The protons in PANIE-P comacromer gives peaks at 1.1, 1.5, 1.7, 2.4, 3.1, 3.6, 4.3, 6.8 (CH=CH) and 7.0 (CO-NH) ppm (Figure - 14B), whereas PANIS-P exhibits ^{1}H-NMR peaks at 1.2, 1.6, 2.3, 3.6, 4.2, 6.8(CH=CH) and 7.0 (CO-NH) ppm (Figure - 14C).

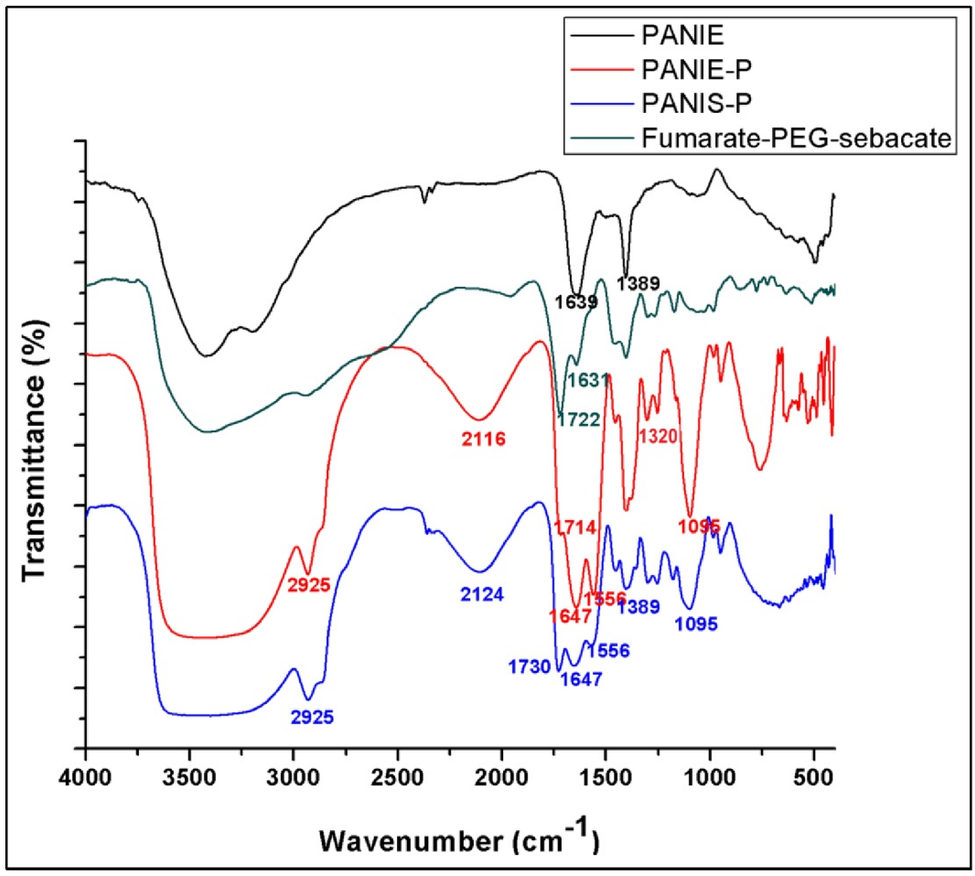

Figure - 13: FT-IR spectra of fumarate-PEG-sebacate, PANIE, PANIE-P and PANIS-P comacromers.

The structural groups in PANIE, PANIS, PANIE-P and PANIS-P comacromers were analyzed by UV-Visible spectroscopy to determine the presence of free electrons responsible for electrical conductivity of PANI. The PANIE and PANIS exhibit characteristic absorbance at 300-450 nm and 800 nm (Figure - 15). The PANIE-P and PANIS-P comacromers exhibit sharp absorbance at 200-300 nm. PANIE-P retains the absorbance at 800 nm; however, PANIS-P shifts the absorbance from 800 to 685 nm.

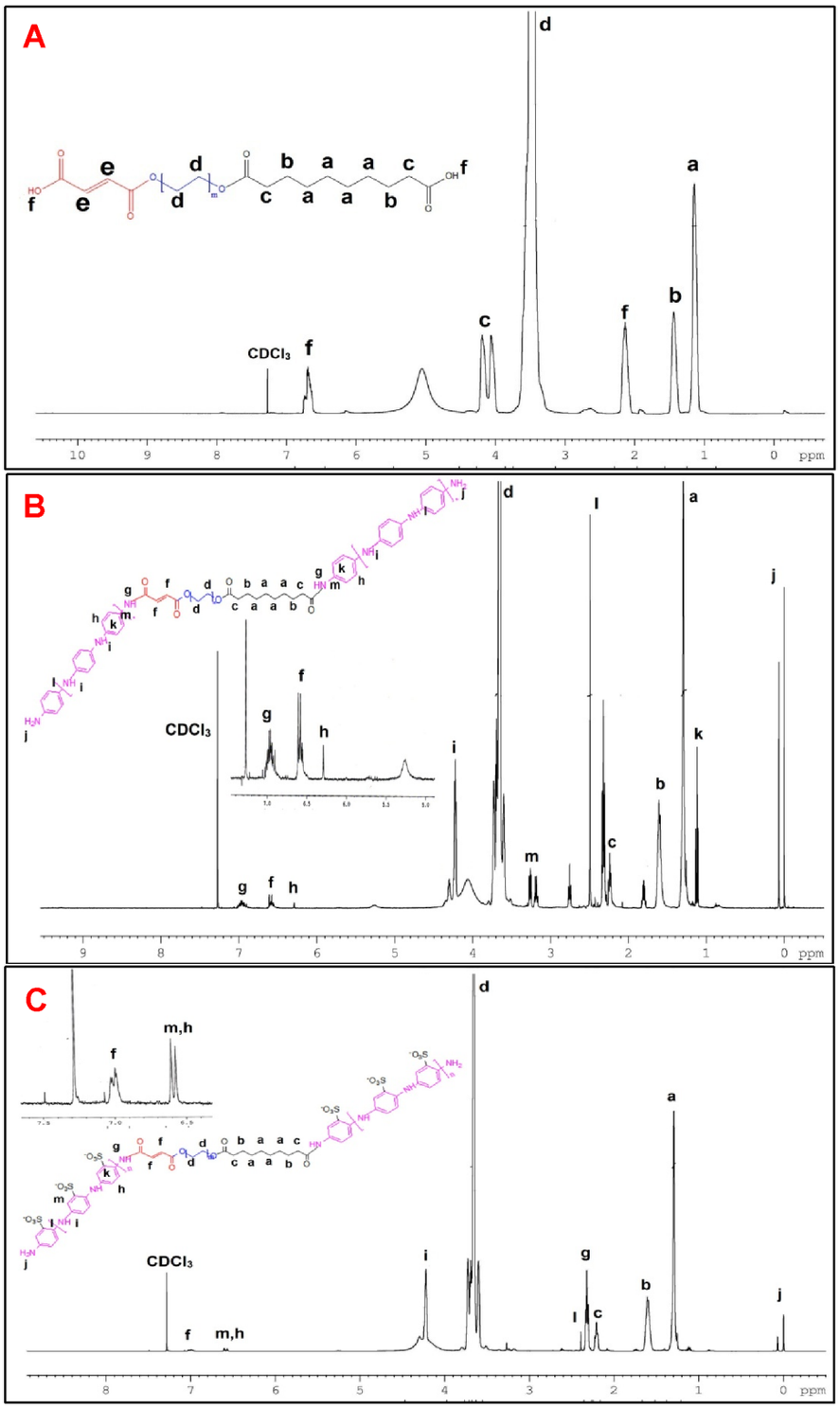

Figure - 14: ^{1}H-NMR spectra of comacromers. Fumarate-co-PEG-co-sebacate (A), PANIE-P (B) and PANIS-P (C).

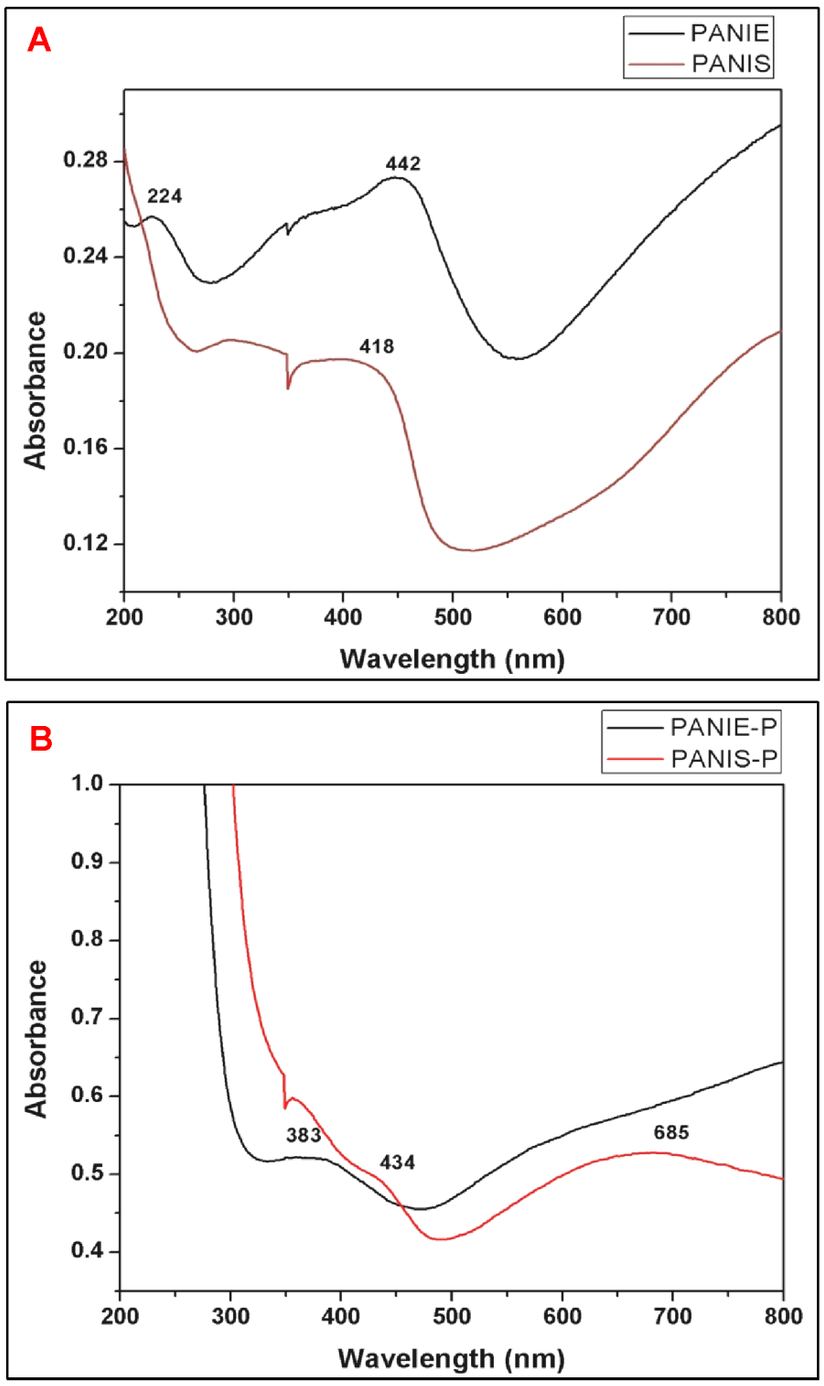

Figure - 15: UV-Visible spectra of comacromers. PANIE and PANIS (A), PANIE-P and PANIS-P (B)

4.2. Molecular weight distribution of comacromers

The Molecular weight data of PP, SP, PEAM and PEAX comacromers are given in table - 4.

Table-4: Molecular weight distribution of comacromers

Comacromers	Number average mol.weight	Weight average mol.weight	Polydispersity
Poly(propylene fumarate) based comacromers			
PP	2524	3056	1.21
SP	2057	2262	1.10
Sugar alcohol based comacromers			
PEAM	3479	4292	1.23
PEAX	2028	2684	1.32

4.3. Preparation of injectable hydrogels

Initially, the comacromers are neutralized with sodium bicarbonate to the physiological pH 7.3 and dialyzed against PBS (1X) to ensure the osmolarity of injectable formulation comparable to the physiological fluids. The hydrogels were prepared by free radical polymerization initiated by two-component APS/TEMED system. Poly(ethylene glycol) diacrylate is a vinyl crosslinker, which forms crosslink junctions at trans double bonds of the comacromer. The concentration of

crosslinker and initiators were standardized to obtain the gelation characteristics favorable for injectable applications.

4.3.1. Preparation of hydrogels from poly(propylene fumarate) based comacromers

The PP and SP comacromers undergo sol-gel transition with PEGDA. The gelation completes within 10 and 8 min for PP6 and SP 17 hydrogels respectively. The gelation is exothermic with 2 ^{0}C and 3 ^{0}C rise in temperature for PP6 and SP 17 hydrogels respectively (Table - 5). Both PP6 and SP 17 hydrogels are transparent. The structure of crosslinked comacromers in the formation of hydrogels PP6 and SP 17 are shown in Figure - 16.

Table-5: Gelation characteristics of PP6 and SP 17 hydrogels

Hydrogels	**PP 6**	**SP 17**
Concentration of resin (g/ml)	0.25	0.1
Neutralized Resin(µl)	200	200
PEGDA(mg)	14	17
0.4 M, APS(µl)	10	10
6 M, TEMED(µl)	1	1
Setting temperature(^{0}C)	33.5	32
Rise in temperature during setting (^{0}C)	2	3
Setting time (min)	10	8
Transparency of hydrogel	Transparent	Transparent

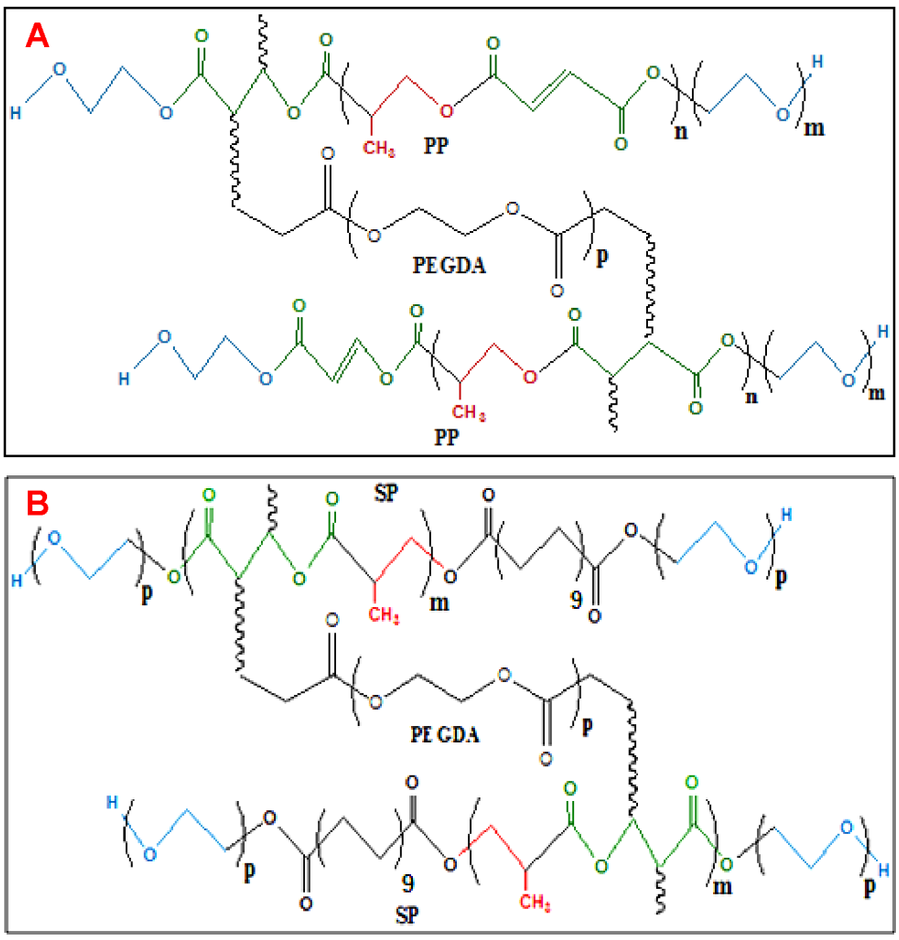

Figure - 16: Structure of crosslinked comacromers with PEGDA. Crosslinked PP comacromer to PP6 hydrogel (A), crosslinked SP comacromer to SP 17 hydrogel (B)

4.3.2. Preparation of hydrogels from sugar alcohol based comacromers

The PEAX and PEAM comacromers undergo sol-gel transition with 20 mg of PEGDA. The gelation completes within 5 and 8 min for PEAX-P and PEAM-P hydrogels respectively. The gelation is exothermic with 2 ^{0}C rise in temperature for PEAX-P and PEAM-P hydrogels (Table - 6). While, PEAX-P hydrogel is opaque and PEAM-P hydrogel is translucent. The structure of the crosslinked comacromer with PEGDA in the formation of PEAX-P and PEAM-P hydrogels are shown in Figure - 17.

Table-6: Gelation characteristics of PEAX-P and PEAM-P hydrogels

Hydrogels	PEAX-P	PEAM-P
Concentration of resin (g/ml)	0.025	0.025
Neutralized Resin(µl)	200	200
PEGDA(mg)	20	20
0.4 M, APS(µl)	10	10
6 M, TEMED(µl)	1	1
Setting temperature(^{0}C)	33	31
Rise in temperature during setting (^{0}C)	2	2
Setting time (min)	5	8
Transparency of hydrogel	Opaque	Translucent

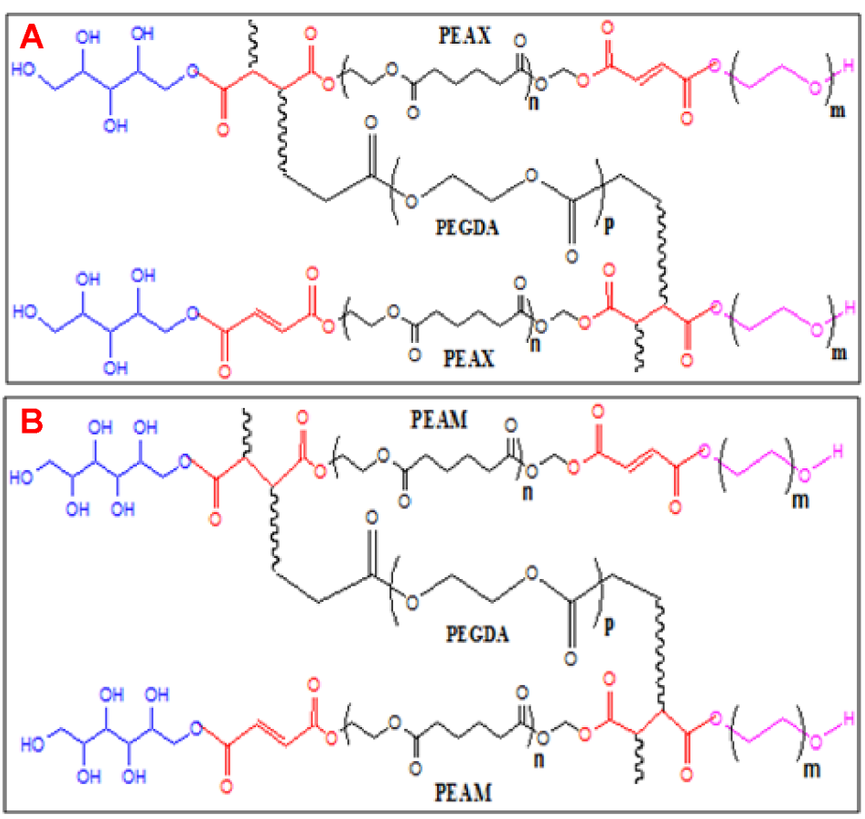

Figure - 17: Structure of crosslinked comacromers with PEGDA. Crosslinked PEAX comacromer to PEAX-P hydrogel (A) and crosslinked PEAM comacromer to PEAM-P hydrogel (B).

4.3.3. Preparation of hydrogels from polyaniline based comacromers

The PANIE-P and PANIS-P comacromers undergo sol-gel transition with 20 mg of PEGDA to PE50P and PS50P hydrogels respectively.

Table-7: Gelation characteristics of PE50P and PS50P hydrogels

Hydrogels	PE50P	PS50P
Concentration of resin (g/ml)	0.020	0.020
Neutralized resin (µl)	100	100
Distilled water (µl)	100	100
PEGDA(mg)	20	20
0.4 M, APS(µl)	10	10
6 M, TEMED(µl)	1	1
Setting temperature(^{0}C)	32	33
Rise in temperature during setting (^{0}C)	2	2
Setting time (min)	6	4
Transparency of hydrogel	Black, opaque	Black, opaque

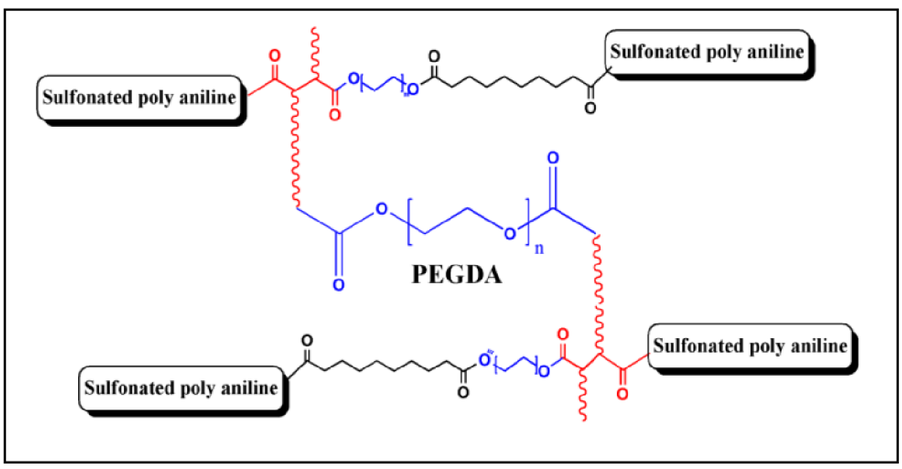

Figure - 18: Structure of crosslinked PANIS-P comacromer with PEGDA to PS50P hydrogel.

The gelation completes within 6 and 4 min for PE50P and PS50P hydrogels respectively. The gelation is exothermic with 2 ^{0}C rise in temperature for PE50P and PS50P hydrogels (Table - 7). Both PE50P and PS50P hydrogels are black in color. The structure of the crosslinked PANIS-P comacromer with PEGDA in the formation of PS50P hydrogel is shown in Figure - 18.

4.4. Physico-chemical characterization of injectable hydrogels

4.4.1. Swelling property and crosslink density of hydrogels

The swelling ratio and equilibrium water content of hydrogels were determined in PBS. PP6 hydrogel retains 84.4% water at equilibrium swelling, which is reduced to 70.5% in SP 17 hydrogel. The PEAX-P and PEAM-P hydrogels swell with the similar swelling ratio. The PE50P hydrogel holds 82.48% water at equilibrium swelling, which is slightly lesser than the PS50P hydrogel with 84.08% (Table - 8). The crosslink density and molecular weight between crosslinks of each hydrogel are given in table 8.

Table-8: Swelling characteristics and crosslink density of hydrogels

Hydrogels	**Weight swelling ratio**	**Equilibrium water content (%)**	**Crosslink density (mol/cm^3)**	**Molecular weight between crosslinks (g/mol)**
Poly(propylene fumarate) based hydrogels				
PP6	6.4 ± 0.3	84.4 ± 0.80	0.024 ± 0.003	38 ± 6.94
SP 17	2.4 ± 0.2	70.5 ± 3.08	0.016 ± 0.003	62 ± 11.33
Sugar alcohol based hydrogels				
PEAX-P	4.9 ± 0.4	79.61 ± 2.14	0.016 ± 0.0002	62 ± 17.59
PEAM-P	4.8 ± 0.3	79.28 ± 2.08	0.045 ± 0.005	22 ± 3.02
Polyaniline based hydrogels				
PE50P	5.7 ± 0.4	82.48 ± 1.35	0.015 ± 0.002	66 ± 10.42
PS50P	6.3 ± 0.6	84.08 ± 1.78	0.030 ± 0.0009	32 ± 1.03

4.4.2. State of water inside the hydrogels

Water can exist in bound or free state inside the hydrogels. The state of water inside the hydrogel was identified by DSC analysis of swollen hydrogels.

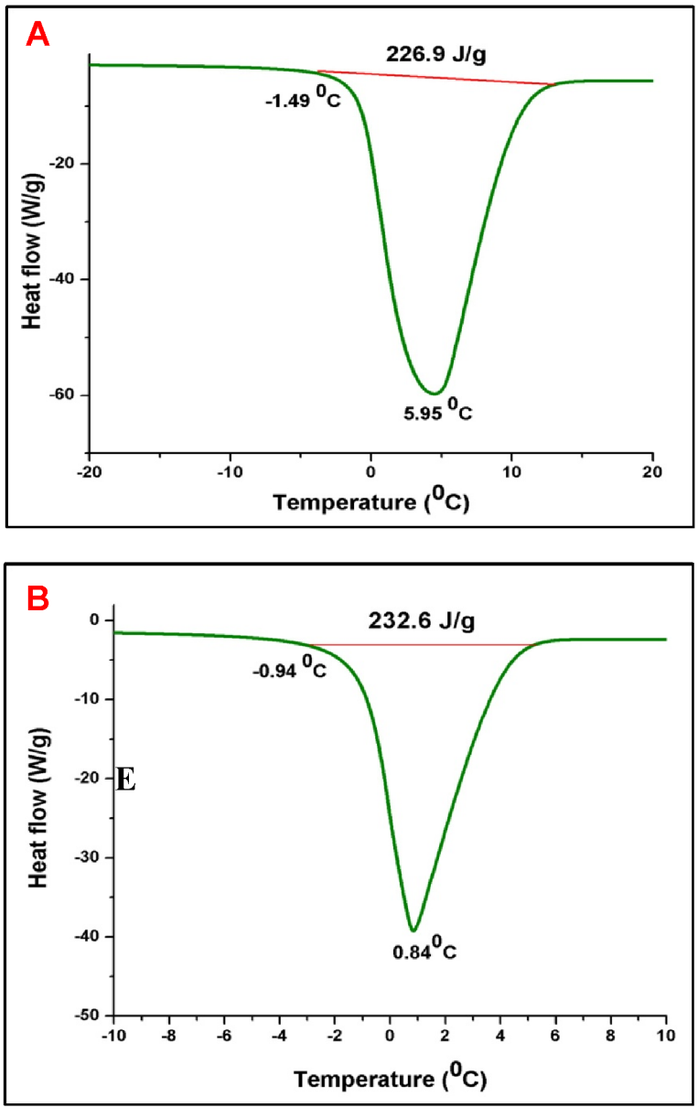

Figure - 19: DSC thermogram of hydrogels.
PP6 (A) and SP 17 (B).

The heating curves of PP6 and SP 17 hydrogels are given in Figure - 19. The water inside the PP6 and SP 17 hydrogels melts at 5.95 and 0.84 ^{0}C respectively. The enthalpy of melting is 226.9 and 232.6 J/g in PP6 and SP 17 hydrogels respectively.

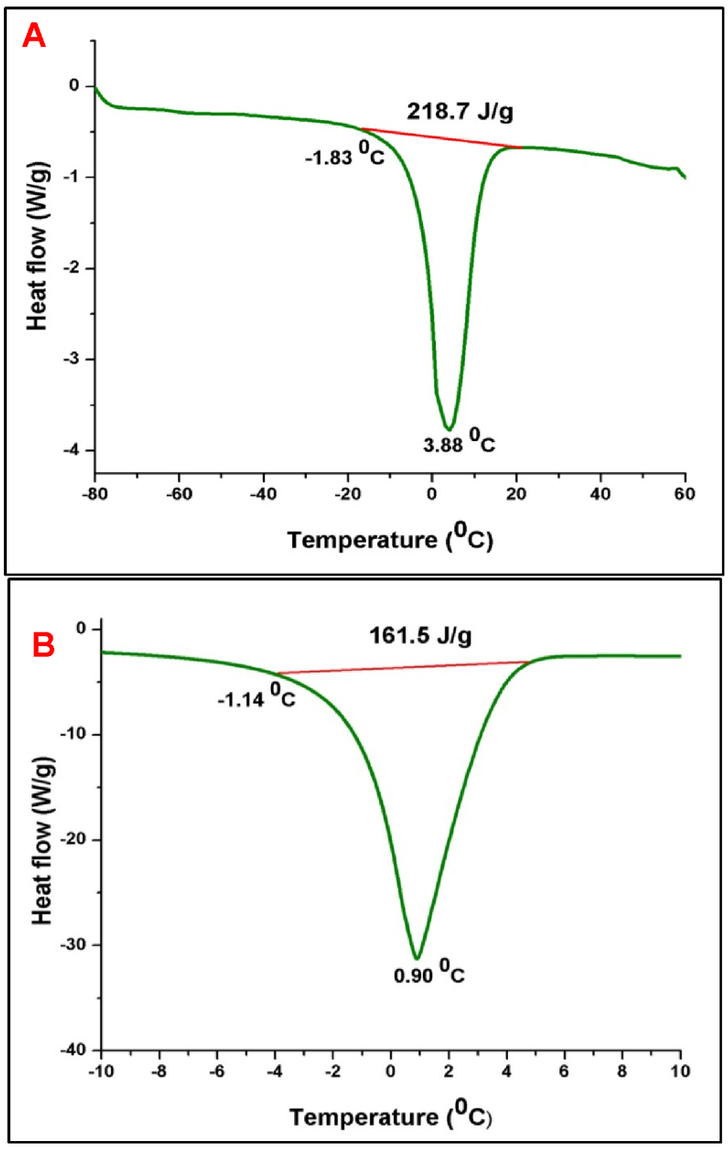

Figure - 20: DSC thermogram of hydrogels.
PEAX-P (A) and PEAM-P (B) hydrogels

With PEAX-P and PEAM-P hydrogels, the water inside the hydrogels melts at 3.88 and 0.90 ^{0}C respectively. The enthalpy of melting is 218.7 and 161.5 J/g in PEAX-P and PEAM-P hydrogels respectively (Figure - 20).

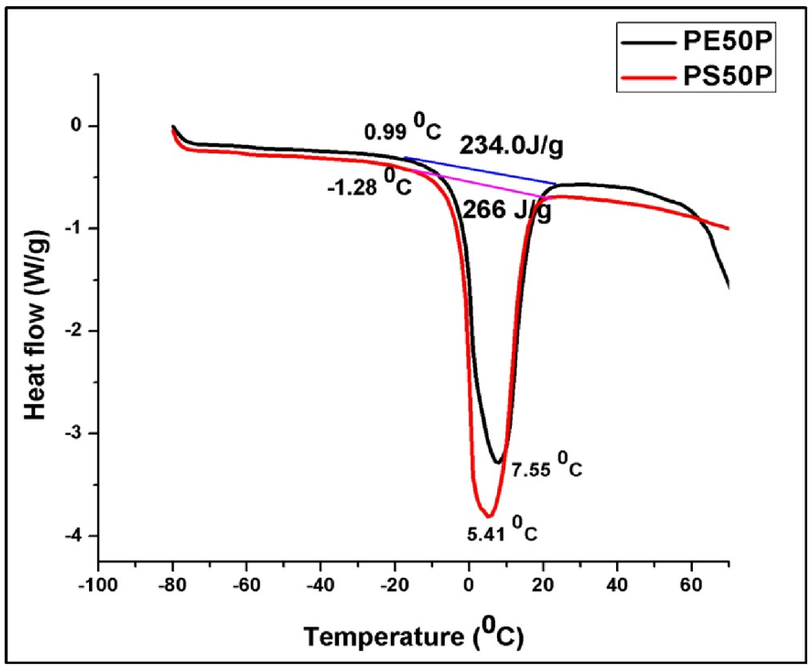

Figure - 21: DSC thermogram of hydrogels.
PE50P and PS50P hydrogels.

With PE50P and PS50P hydrogels, the water inside the hydrogels melts at 7.55 and 5.41 ^{0}C respectively. The enthalpy of melting is 234 and 266 J/g in PE50P and PS50P hydrogels respectively (Figure - 21).

The fraction of freezable free water was calculated based on the enthalpy of endothermic peaks corresponding to each hydrogel. The bound water in PP6 hydrogel is 16.52%, which is significantly higher compared to SP 17 hydrogel (0.941%). The bound water fraction in PEAM-P hydrogel is 30.92%, which is higher compared to other hydrogels. The fraction of free water in PS50P hydrogel

is 79.73%, is comparatively higher than PE50P hydrogel (Table - 9). The major fraction of water inside all hydrogels is freezable free water (Figure - 22).

Table-9: Freezable free water and bound water inside the hydrogels

Hydrogels	Onset of T_{endo} (^{0}C)	Melting temperature (^{0}C)	Enthalpy of melting (J/g)	Free water content (FW+FBW) (%)	Bound water content (NBW) (%)
Poly(propylene fumarate) based hydrogels					
PP6	-1.49	5.95	226.9	67.93	16.52
SP 17	-0.94	0.84	232.6	69.64	0.941
Sugar alcohol based hydrogels					
PEAX-P	-1.83	3.88	218.7	65.47	14.13
PEAM-P	-1.14	0.90	161.5	48.35	30.92
Polyaniline based hydrogels					
PE50P	0.99	7.55	234	70.05	12.42
PS50P	-1.28	5.41	266	79.73	4.35

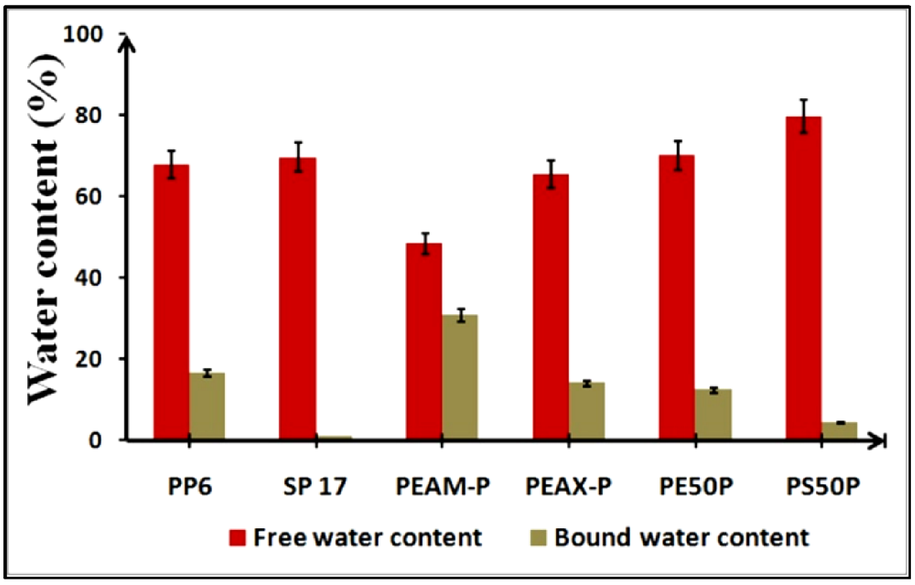

Figure - 22: Diagrammatic representation of freezable free water and bound water inside the hydrogels

4.4.3. Surface and internal morphology of hydrogels

The morphology of the present hydrogels was assessed using ESEM analysis to identify the pore distribution on the surface and bulk of hydrogels.

The PP6 hydrogel has porous structure both in surface and in bulk of the hydrogel. The pores are interconnected inside the hydrogel. The pores with a diameter of 15-40 µm are observed on the surface of PP6 hydrogel, with maximum pores with 25 µm in diameter (Figure - 23).

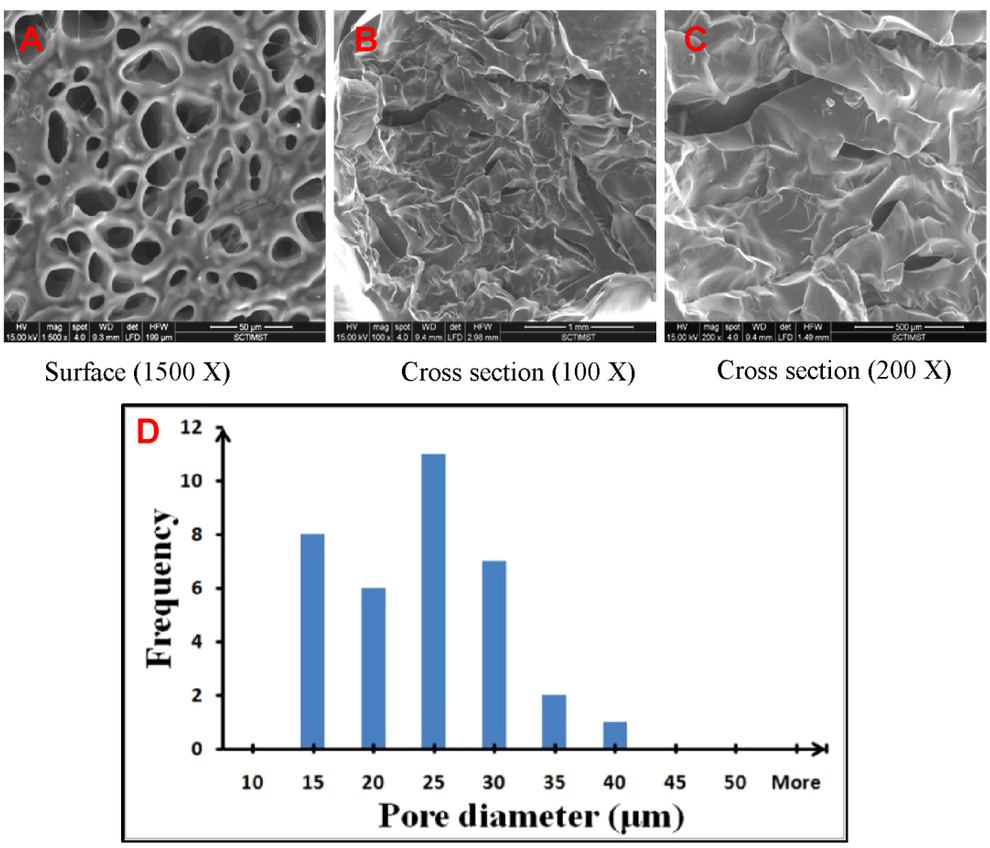

Surface (1500 X) Cross section (100 X) Cross section (200 X)

Figure - 23: Surface and cross-sectional morphology of PP6 hydrogel (A, B, C) and histogram for the pore diameter on the surface of PP6 hydrogel (D)

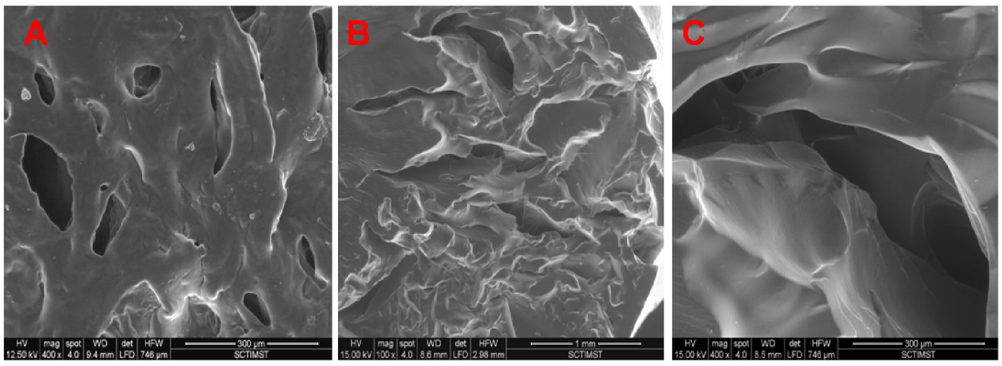

Surface (400 X) Cross section (100 X) Cross section (400 X)

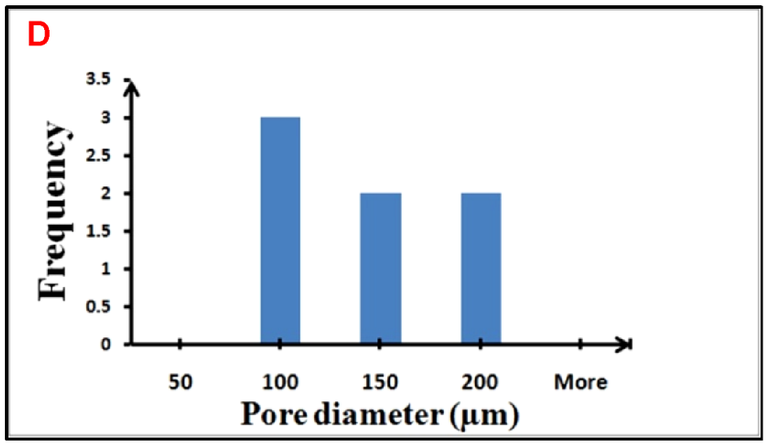

Figure - 24: Surface and cross-sectional morphology of SP 17 hydrogel (A, B, C) and histogram for the pore diameter on the surface of SP 17 hydrogel (D)

The SP 17 hydrogel has porous structure both in surface and in bulk of the hydrogel. The pores are interconnected inside the hydrogel. The pores with a diameter of 100-200 µm are observed on the surface of SP 17 hydrogel, with maximum pores of 100 µm in diameter (Figure - 24).

The PEAX-P hydrogel has highly porous structure both in surface and internal structure. The pores are interconnected inside the hydrogel. The pores with a diameter of 15-30 µm are observed on the surface of PEAX-P hydrogel,

with maximum pores with 20 µm in diameter. The pores with the diameter of 75 µm are mostly observed inside the PEAX-P hydrogel (Figure - 25).

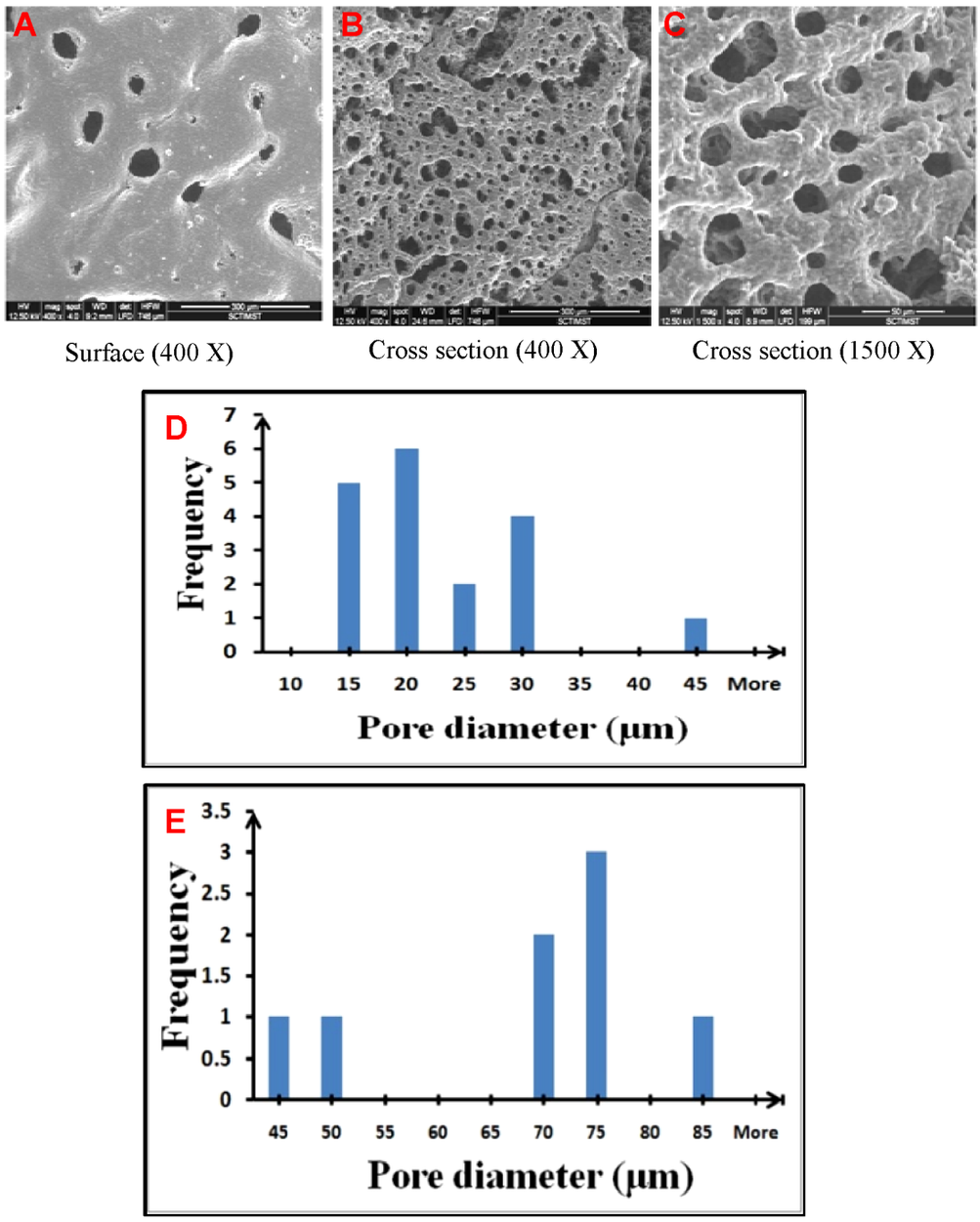

Figure - 25: Surface and cross-sectional morphology of PEAX-P hydrogel (A, B, C). Pore distribution on the surface (D) and cross section of PEAX-P hydrogel (E).

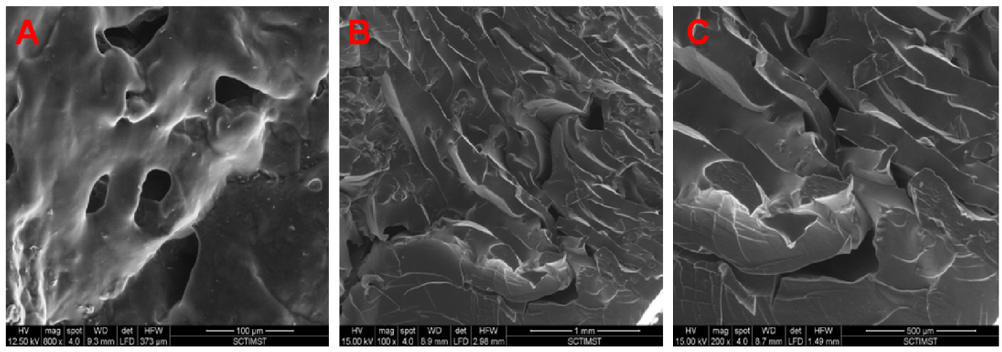

Surface (800 X) Cross section (100 X) Cross section (200 X)

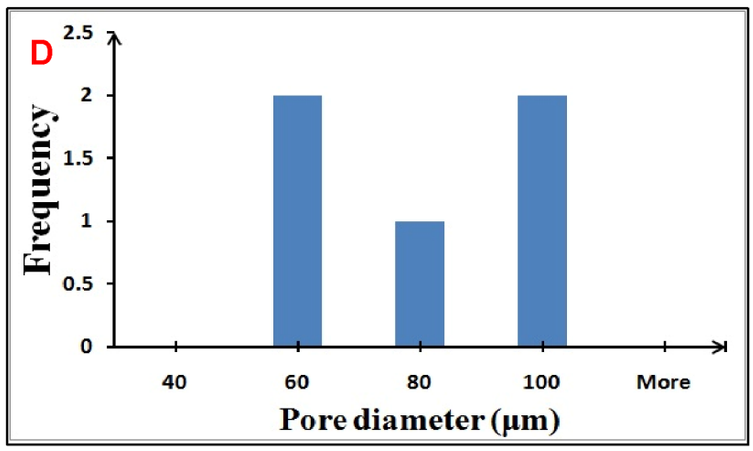

Figure - 26: Surface and cross-sectional morphology of PEAM-P hydrogel (A, B, C). Pore distribution on the surface of PEAM-P hydrogel (D).

The PEAM-P hydrogel has a porous surface and internal morphology. The internal structure of PEAM-P hydrogel has aligned and interconnected morphology. The pores with a diameter of 60-100 µm are observed on the surface of PEAM-P hydrogel (Figure - 26).

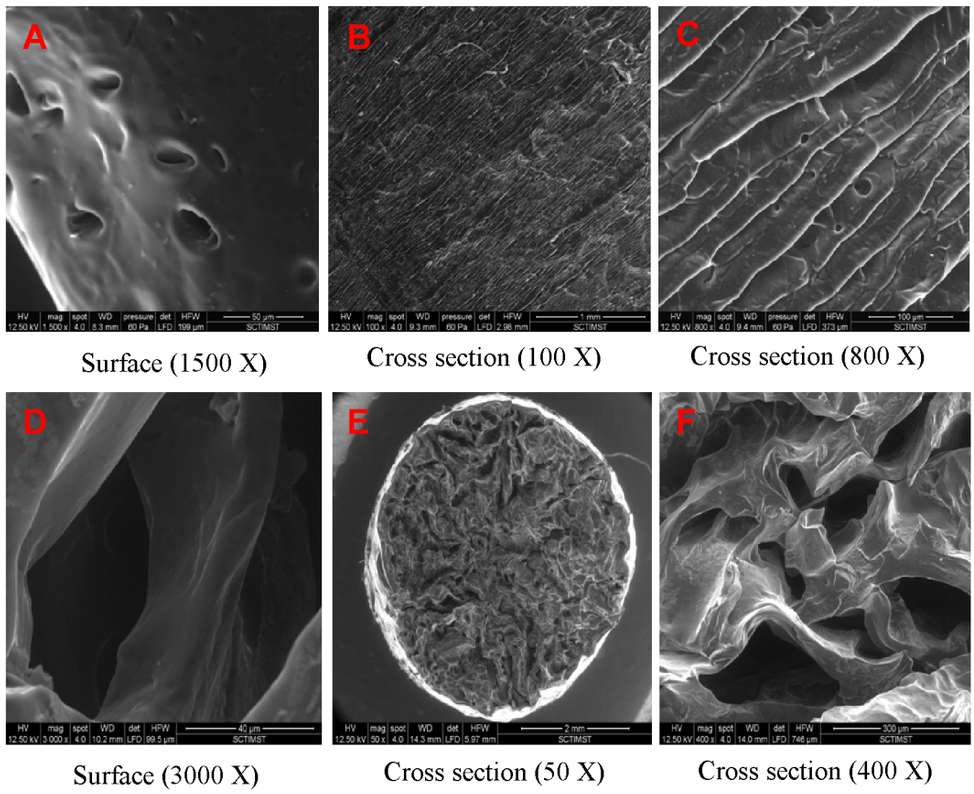

Figure - 27: Surface and cross-sectional morphology of hydrogels.
PE50P (A, B, C) and PS50P (D, E, F) hydrogels.

The PE50P hydrogel has a porous surface. The internal structure of PE50P hydrogel has aligned and interconnected morphology. The PS50P hydrogel has a porous surface. The internal structure of PS50P hydrogel is highly porous with large interconnected pores (Figure - 27).

4.4.4. *In vitro* ageing and biomechanical analysis

The variation of a compressive mechanical property of the present hydrogels with ageing was studied to determine the biomechanical stability. The compressive Young modulus, maximum load at break and compressive stress at maximum load of the present hydrogels are given in Table - 10. The PP6 hydrogel breaks at 1.76 N, whereas, SP 17 hydrogel breaks at 1.36 N. The Young modulus

of PP6 hydrogel (212 kPa) is greater than the SP 17 hydrogel with 142 kPa. The Young modulus of PEAX-P hydrogel is 100 kPa, which collapse at 8 kPa stress, whereas, PEAM-P hydrogel has a Young modulus of 370 kPa and collapse at 18 kPa stress. The PS50P hydrogel has a Young modulus of 442 kPa, which is significantly higher compared to PE50P hydrogel.

Table-10: Compressive mechanical property of hydrogels

Hydrogels	**Maximum load(N) at break**	**Young modulus (kPa)**	**Compressive stress (kPa)**
Poly(propylene fumarate) based hydrogels			
PP6	1.76 ± 0.17	212 ± 10.1	24 ± 0.03
SP 17	1.36 ± 0.48	142 ± 5.01	19 ± 0.07
Sugar alcohol based hydrogels			
PEAX-P	0.516 ± 0.01	100 ± 8.6	8 ± 0.02
PEAM-P	3.30 ± 1.33	370 ± 13.1	18 ± 0.06
Polyaniline based hydrogels			
PE50P	0.195 ± 0.08	117 ± 10.8	2 ± 0.02
PS50P	2.86 ± 0.80	442 ± 16.4	10 ± 0.07

The variation in mechanical property of the present hydrogels on *in vitro* ageing in the physiological medium was determined to evaluate the biomechanical stability. The stress-strain behavior of the present hydrogels was studied for 0-60% compression to understand the elastic behavior of hydrogels with ageing.

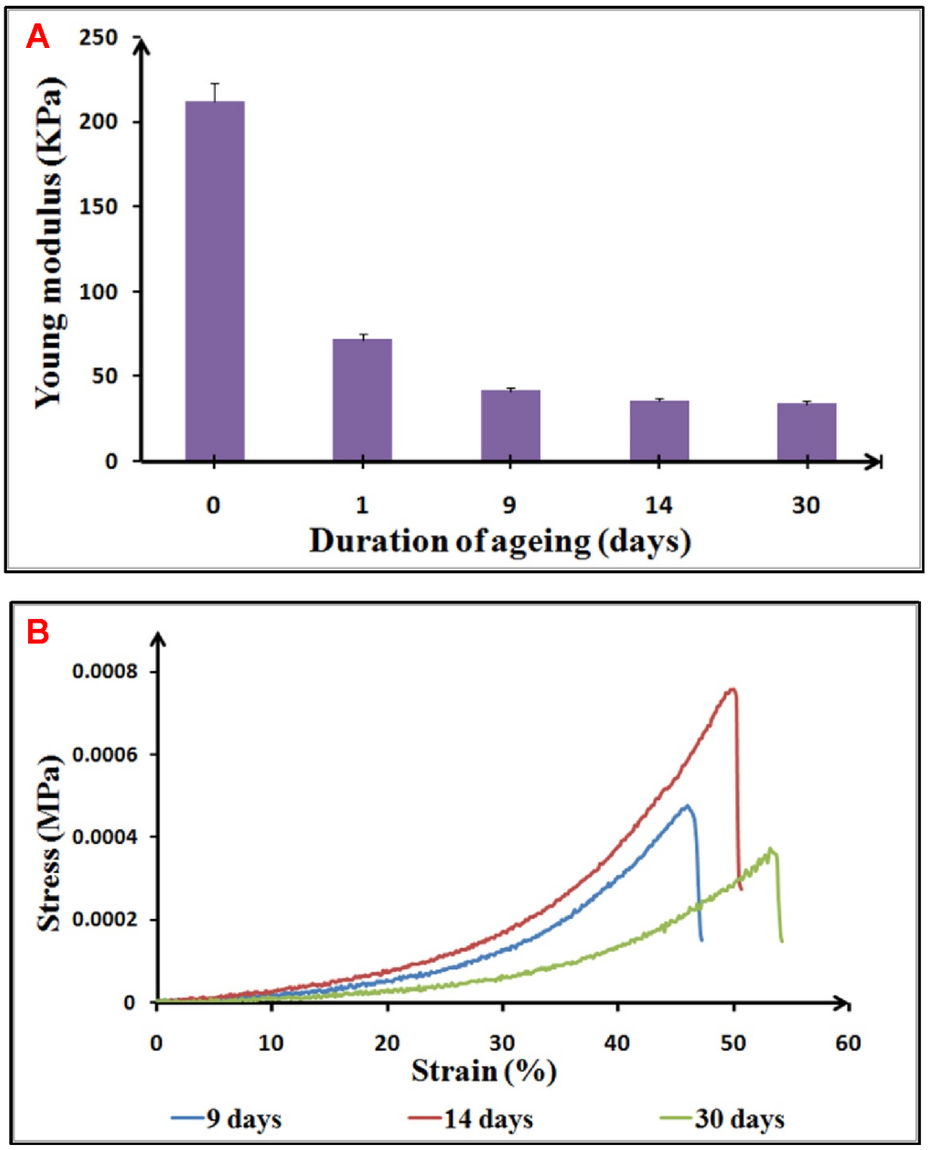

Figure - 28: Variation of Young modulus with the ageing of PP6 hydrogel (A). Stress-strain behavior of PP6 hydrogel with ageing (B).

The compressive modulus of PP6 hydrogel is reduced from 212 kPa to 34 kPa after 30 days of *in vitro* ageing. The PP6 hydrogel collapsed at 45%, 50% and 55% strain after 9, 14 and 30 days of *in vitro* ageing in PBS respectively (Figure - 28).

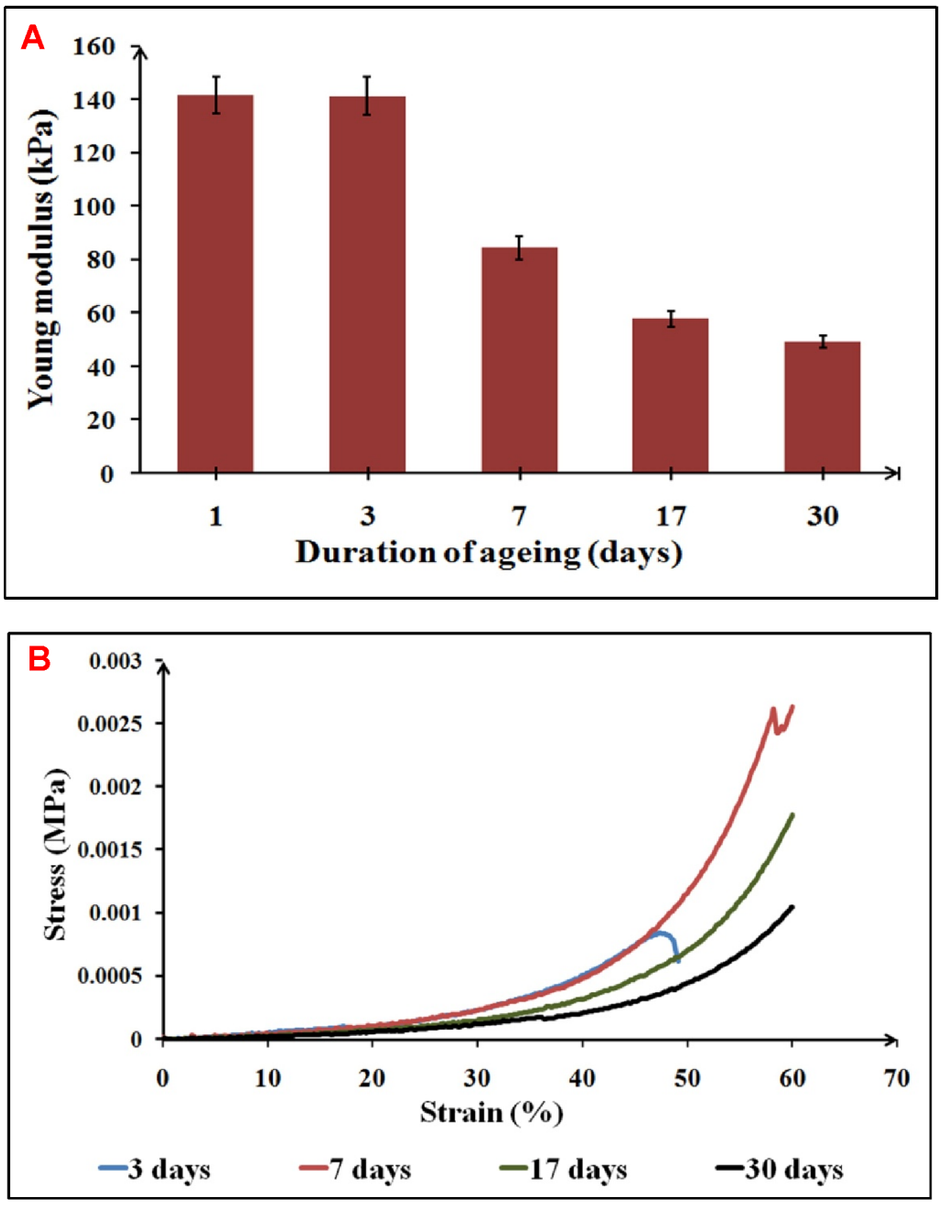

Figure - 29: Variation of Young modulus with the ageing of SP 17 hydrogel (A). Stress-strain behavior of SP 17 hydrogel with ageing (B)

Similarly, the Young modulus of SP 17 hydrogel is reduced from 142 kPa to 49 kPa after 30 days. The SP 17 hydrogel exhibits maximum extensibility without collapsing at 60% compression after 17 and 30 days of *in vitro* ageing (Figure - 29).

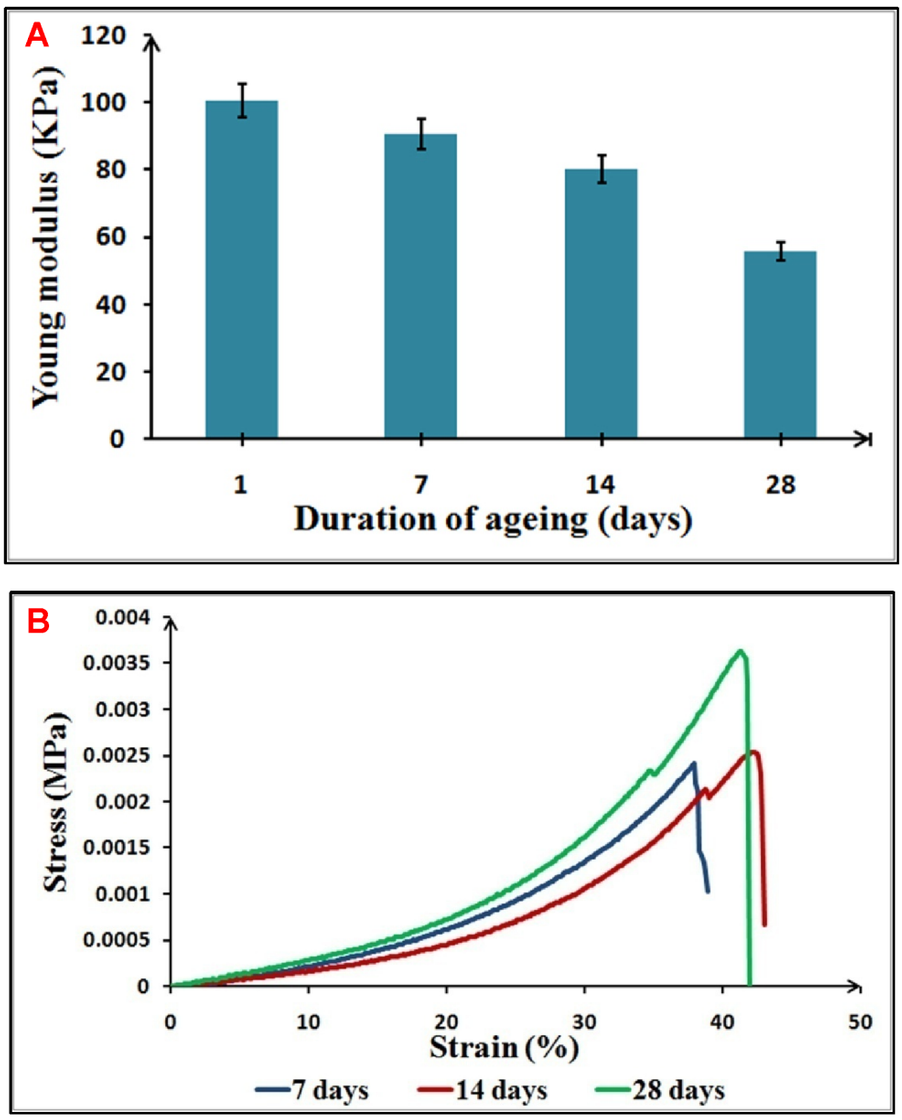

Figure - 30: Variation of Young modulus with the ageing of PEAX-P hydrogel (A). Stress-strain behavior of PEAX-P hydrogel with ageing (B)

The Young modulus of PEAX-P hydrogel is decreased from 100 kPa to 56 kPa after 28 days of *in vitro* ageing in PBS. The PEAX-P hydrogel exhibit J-shaped stress-strain graph with the maximum extensibility of 37%, 43% and 40% after 7, 14 and 28 days of *in vitro* ageing respectively (Figure - 30).

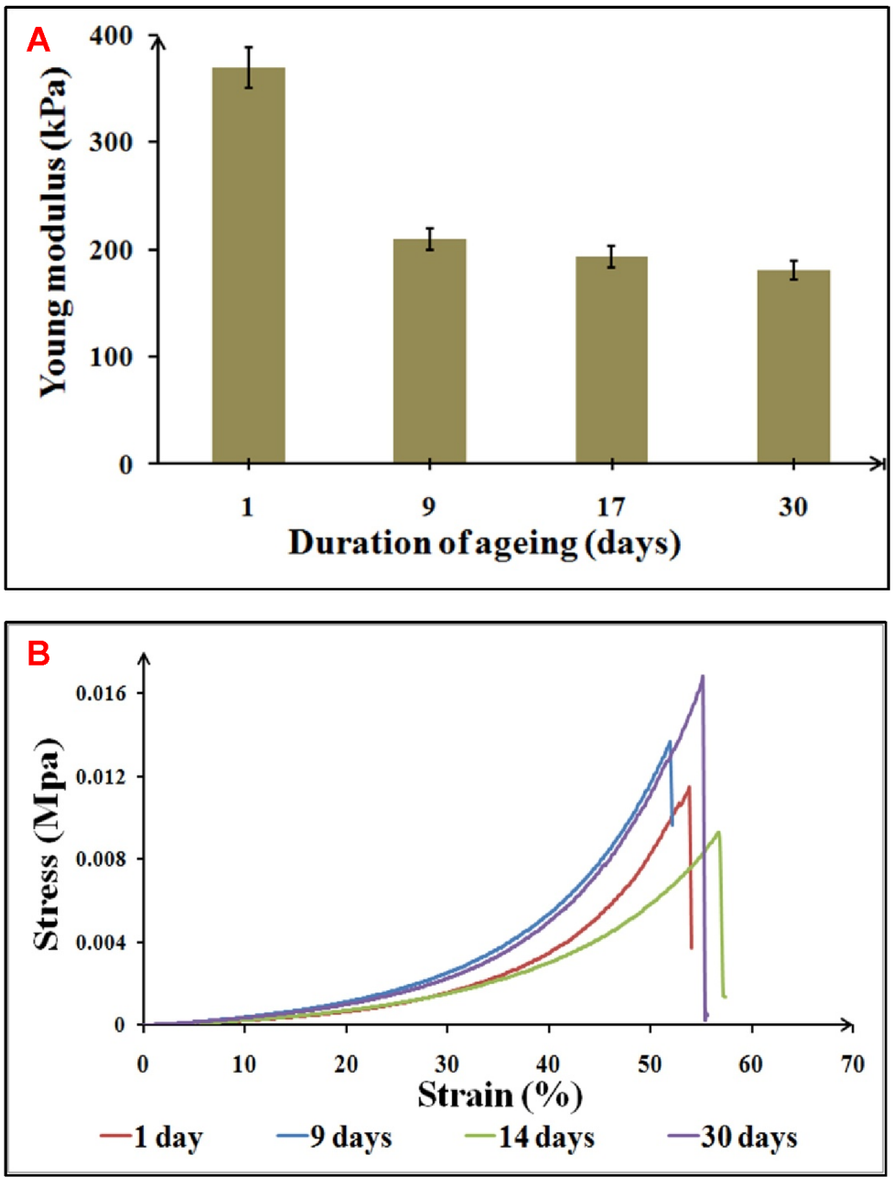

Figure - 31: Variation of Young modulus with the ageing of PEAM-P hydrogel (A). Stress-strain behavior of PEAM-P hydrogel with ageing (B)

The Young modulus of PEAM-P hydrogel is reduced from 370 kPa to 200 kPa in one month of *in vitro* ageing in PBS. The PEAM-P hydrogel collapses at 50-60% strain after 30 days of *in vitro* ageing (Figure - 31).

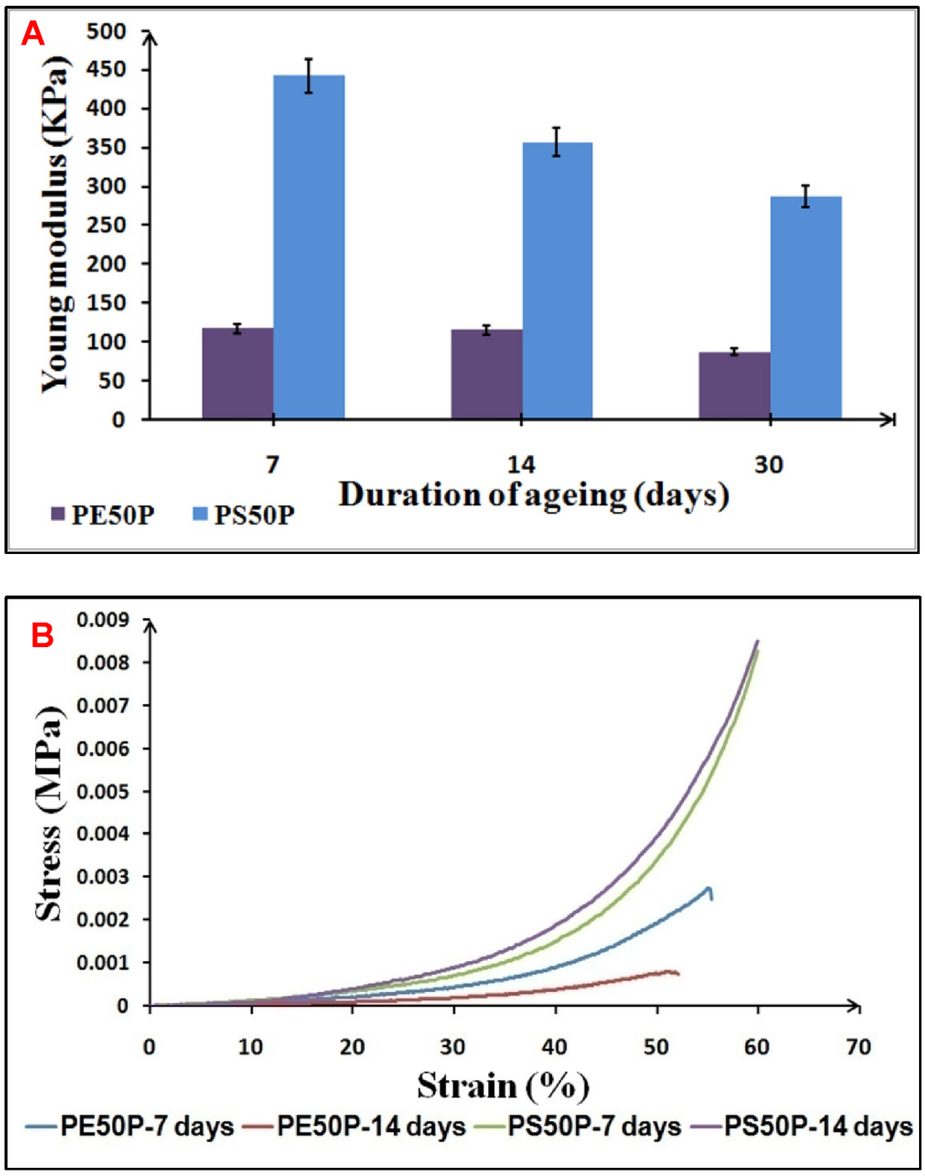

Figure - 32: Variation of Young modulus with the ageing of PE50P and PS50P hydrogels (A). Stress-strain behavior of PE50P and PS50P hydrogels with ageing (B).

The PE50P hydrogel has a Young modulus of 117 kPa, which is reduced to 87% after 30 days of *in vitro* ageing in PBS. Whereas, the Young modulus of PS50P hydrogel is decreased from 442 kPa to 288 kPa after 30 days of *in vitro* ageing under similar conditions. Both PE50P and PS50P hydrogels after 7 and 14 days of *in vitro* ageing are not collapsing at 60% strain (Figure - 32).

4.4.5. Electrical conductivity of polyaniline based hydrogels

The electrical conductivity of PANIE-P/PEGDA and PANIS-P/PEGDA based hydrogels is given in table -11. The present PE100P and PS100P hydrogels have the highest electrical conductivity of 3.51± 0.043 x 10^{-4} S cm^{-1} and 5.50 ± 0.016 x 10^{-4} S cm^{-1} at 100% comacromer concentration.

Table-11: Electrical conductivity of polyaniline based hydrogels

Hydrogels	Comacromer concentration (%)	Electrical conductivity of hydrogels (S/cm) (x 10^{-4})
PANIE-P comacromer based hydrogel		
PE20P	20	3.31± 0.029
PE50P	50	3.46 ± 0.019
PE100P	100	3.51± 0.043
PANIS-P comacromer based hydrogel		
PS20P	20	3.64 ± 0.020
PS50P	50	3.78 ± 0.030
PS100P	100	5.50 ± 0.016

4.5. Cytocompatibility of hydrogels

The cytocompatibility of hydrogels with L929 cells was evaluated by MTT assay, direct contact assay and live dead assay. The viability of L929 cells with extracts of the present hydrogels was identified by MTT assay as per ISO10993-5, annexure C. The direct contact assay and live dead assay are the

qualitative assays to identify the morphology and viability of the L929 cells on direct incubation with the hydrogels.

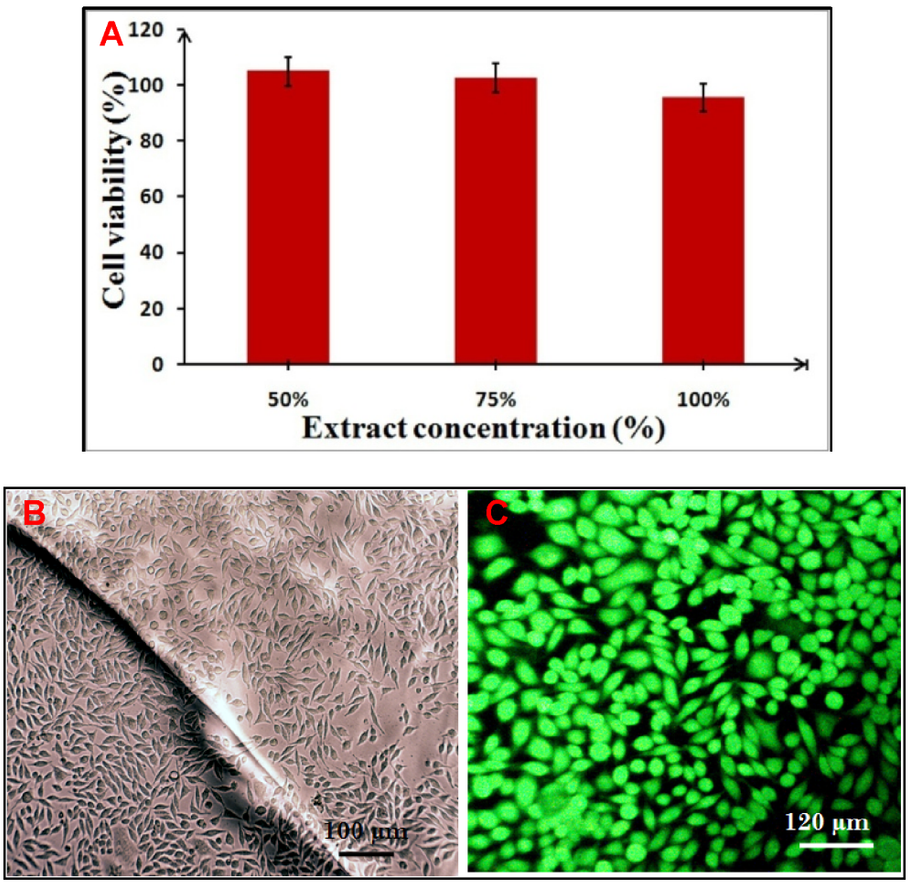

Figure - 33: Cytocompatibility of PP6 hydrogel. MTT assay of L929 cells with hydrogel extract (A), direct contact of hydrogel with L929 cells (B) and live dead assay of L929 cells with hydrogel for 24 h (C).

With poly(propylene fumarate) based hydrogels, the L929 monolayer exhibit 100% viability when incubated with 50% concentration of PP6 hydrogel extract. The viability of cells decreased to 90% when treated with the extract of PP6 hydrogel without dilution (Figure - 33A). The direct contact assay of PP6 hydrogel with L929 monolayer does not change the spindle bipolarity of cells (Figure - 33B). The green fluorescing L929 cells with more than 80% confluence

are observed in live dead assay after direct contact test with PP6 hydrogel (Figure - 33C).

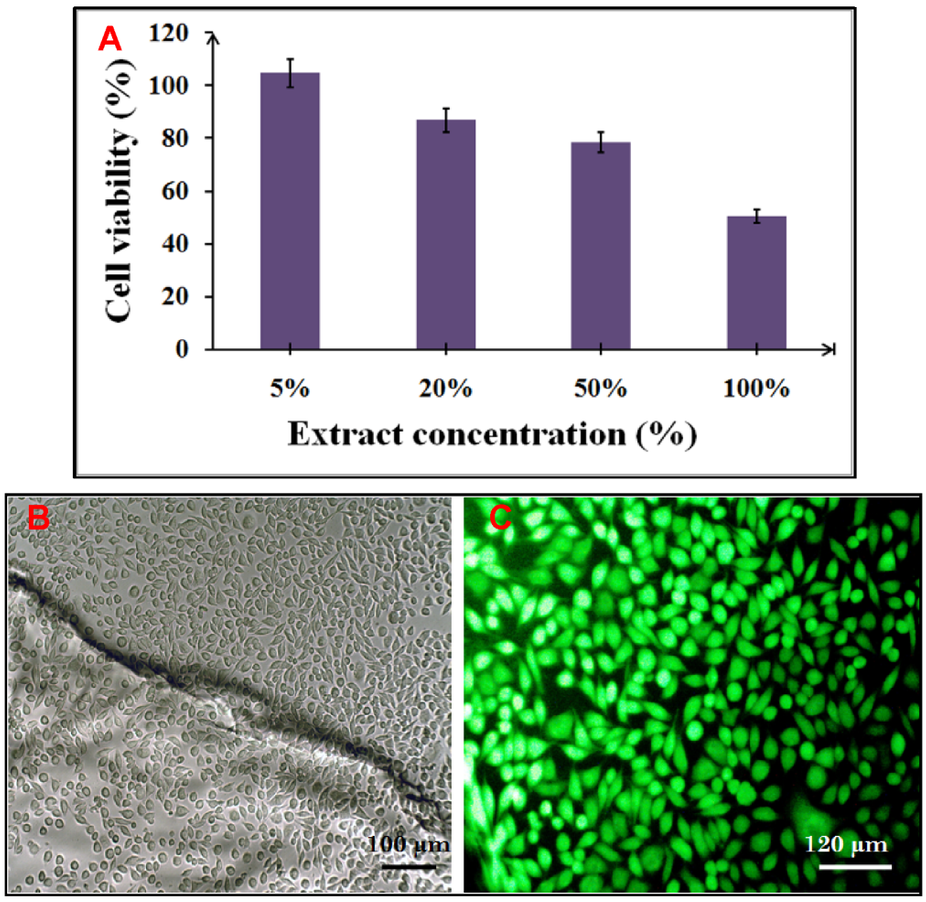

Figure - 34: Cytocompatibility of SP 17 hydrogel. MTT assay of L929 cells with hydrogel extract (A), direct contact of hydrogel with L929 cells (B) and live dead assay of L929 cells with hydrogel for 24 h (C).

With poly(propylene fumarate) based hydrogels, the L929 monolayer exhibits 80% viability when incubated with 50% concentration of SP 17 hydrogel extract. The viability of cells has decreased to 50% when treated with the extract of SP 17 hydrogel without dilution (Figure - 34A). The direct contact assay of SP 17 hydrogel with L929 monolayer retains the morphology of cells (Figure - 34B).

The green fluorescing L929 cells with more than 80% confluence are observed in live dead assay after direct contact test with SP 17 hydrogel (Figure - 34C).

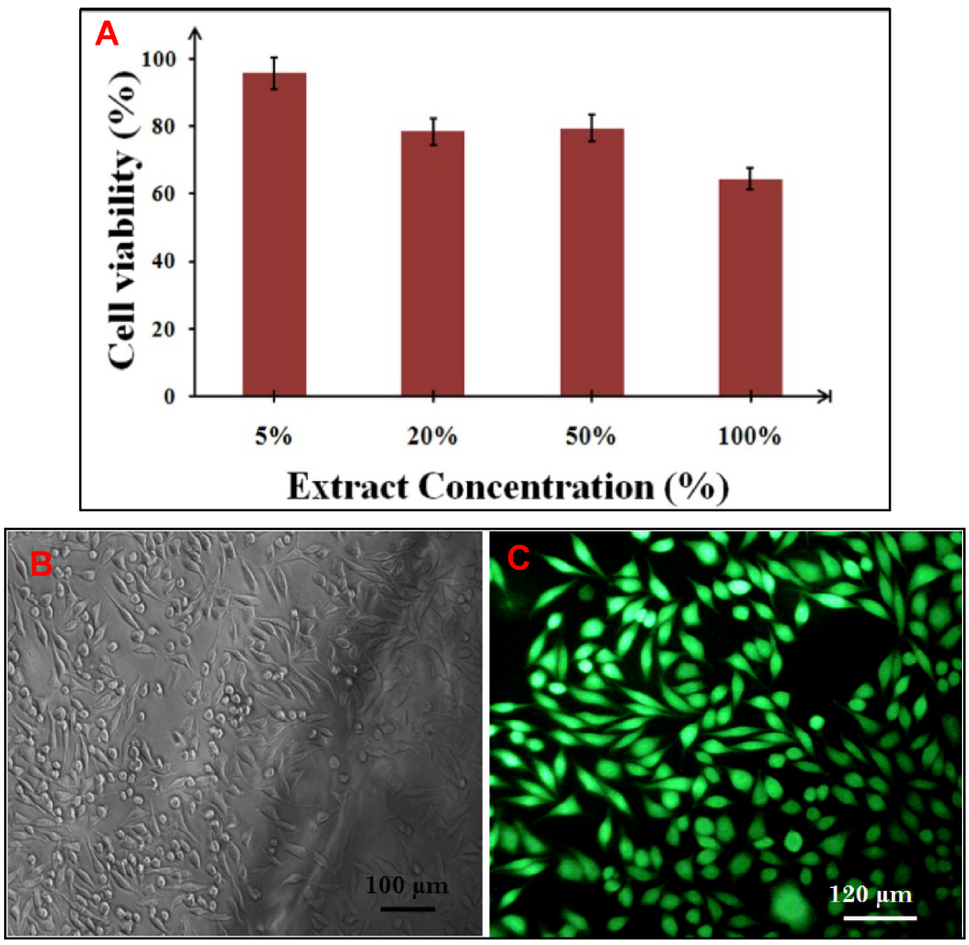

Figure - 35: Cytocompatibility of PEAX-P hydrogel. MTT assay of L929 cells with hydrogel extract (A), direct contact of hydrogel with L929 cells (B) and live dead assay of L929 cells with hydrogel for 24 h (C).

With sugar alcohol based hydrogels, the L929 monolayer exhibits 80% viability when incubated with 50% concentration of PEAX-P hydrogel extract. The viability of cells remained at 65% when treated with the extract of PEAX-P hydrogel without dilution (Figure - 35A). The direct contact assay of PEAX-P hydrogel with L929 monolayer does not change the spindle bipolarity of cells

(Figure - 35B). The green fluorescing L929 cells with more than 70% confluence are observed in live dead assay after direct contact test with PEAX-P hydrogel (Figure - 35C).

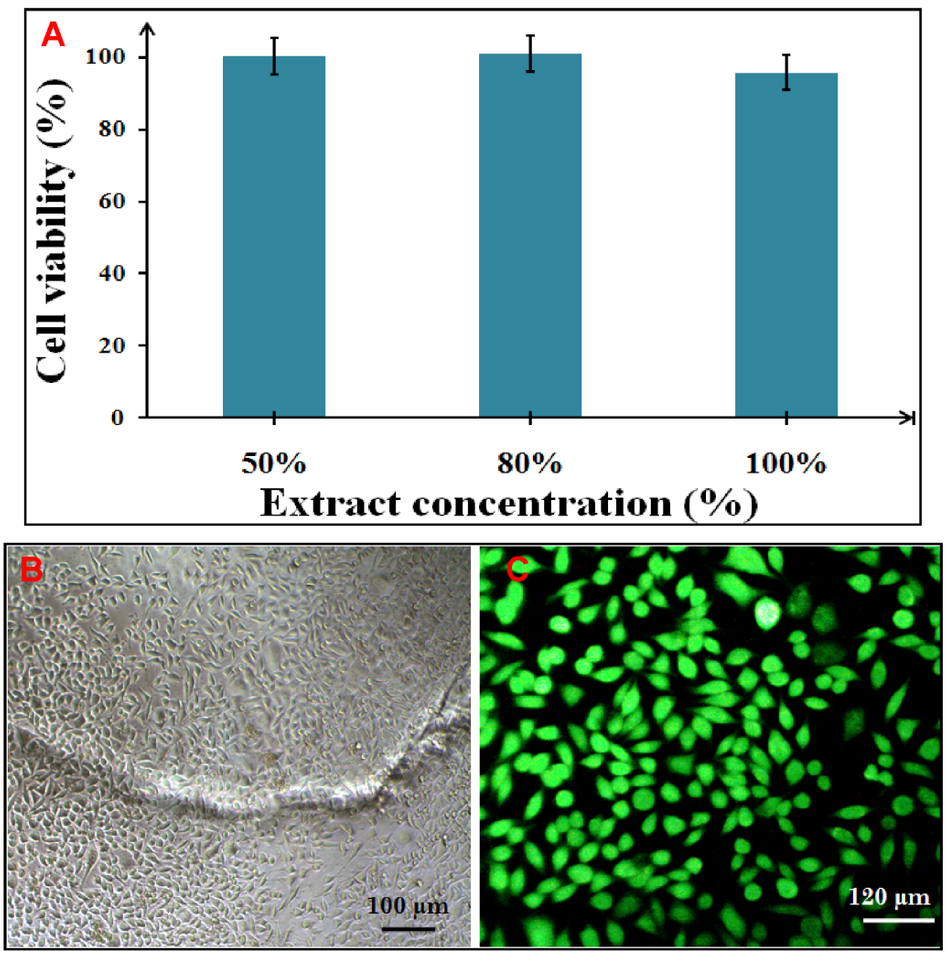

Figure - 36: Cytocompatibility of PEAM-P hydrogel. MTT assay of L929 cells with hydrogel extract (A), direct contact of hydrogel with L929 cells (B) and live dead assay of L929 cells with hydrogel for 24 h (C).

With the sugar alcohol based hydrogels, the L929 monolayer exhibits 100% viability when incubated with 50% concentration of PEAM-P hydrogel extract. The viability of cells has decreased to 95% when treated with the extract of PEAM-P hydrogel without dilution (Figure - 36A). The direct contact assay of

PEAM-P hydrogel with L929 monolayer does not change the spindle bipolarity of cells (Figure - 36B). The green fluorescing L929 cells with more than 80% confluence are observed in live dead assay after direct contact test with PEAM-P hydrogel (Figure - 36C).

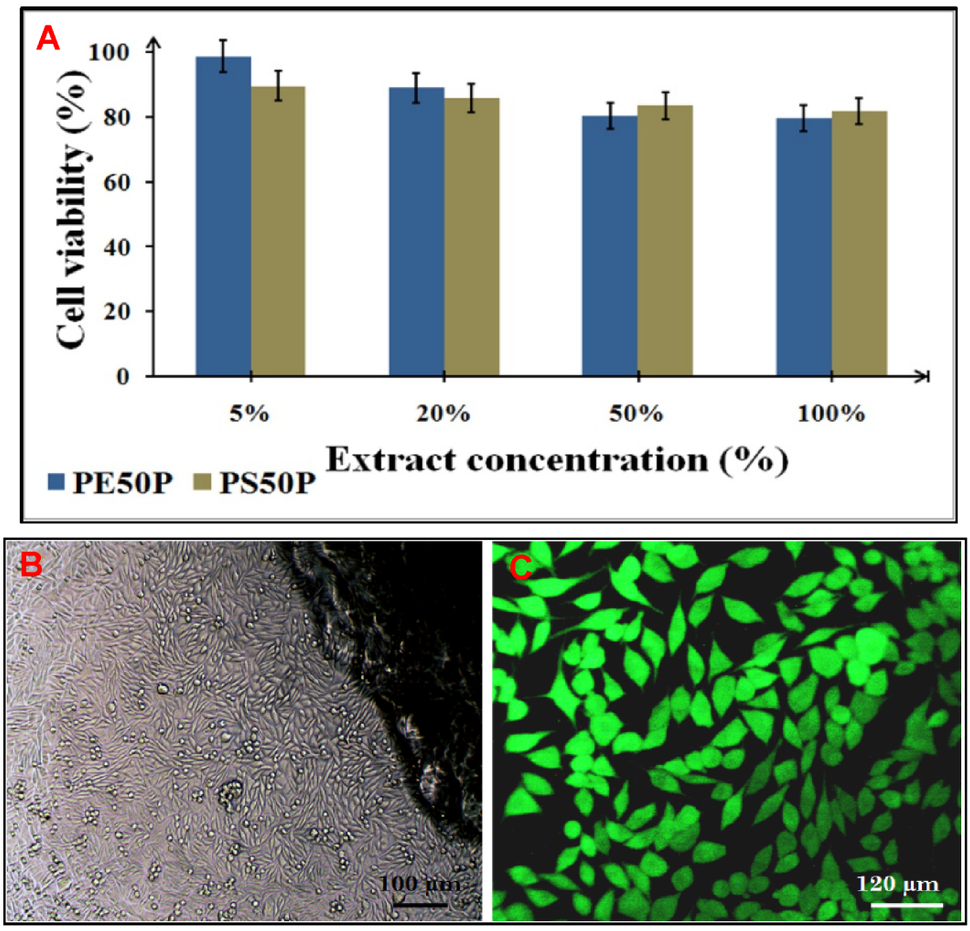

Figure - 37: Cytocompatibility of PS50P and PE50P hydrogels. MTT assay of L929 cells with hydrogel extract (A), direct contact of PS50P hydrogen with L929 cells (B) and live dead assay of L929 cells with PS50P hydrogel for 24 h (C).

With polyaniline-based hydrogels, the L929 monolayer exhibits 80% and 85% viability when incubated with 50% concentration of PE50P and PS50P hydrogel extracts respectively. The MTT assay gives more or less similar values for the viability of cells when treated with 100% concentration of extract

compared to 50% concentration (Figure - 37A). The direct contact assay of PS50P hydrogel with L929 monolayer does not change the spindle bipolarity of cells (Figure - 37B). The green fluorescing L929 cells are observed in live dead assay after direct contact test with PS50P hydrogel (Figure - 37C).

4.6. Hemolysis

The compatibility of the selected PEAM-P and PS50P hydrogels with red blood cells was evaluated by hemolysis assay.

Table-12: Hemolysis of PEAM-P and PS50P hydrogels.

Hydrogels	Hemolysis (%)
PEAM-P	0.06
PS50P	0.04
Control (Well plate alone)	0.01

The hemolysis (%) data of selected PEAM-P and PS50P hydrogels are given in table - 12.

4.7. Studies on free radical scavenging characteristics of hydrogels

4.7.1. Biochemical assays

The scavenging effect of the present hydrogels over a wide range of free radicals was studied by the following biochemical assays.

4.7.1.1. DPPH radical scavenging property of hydrogels

The PP6 and SP 17 hydrogels scavenge 54% and 48% of DPPH radicals respectively. The PEAM-P and PEAX-P hydrogels scavenge 57% and 51% of

DPPH radicals respectively (Figure - 38). In polyaniline-based hydrogels, the PS50P hydrogel scavenges 63% of DPPH radical, which is comparatively higher than PE50P hydrogel with 33%. The P/PEGDA hydrogel, prepared from fumarate-PEG-sebacate comacromer, exhibits comparatively lower DPPH scavenging effect (27%) than the polyaniline conjugated fumarate-PEG-sebacate hydrogels. The DPPH radical scavenging effect of hydrogels is compared with ascorbic acid at different concentrations. The ascorbic acid with 25 µM concentration exhibits maximum DPPH radical scavenging of 58%.

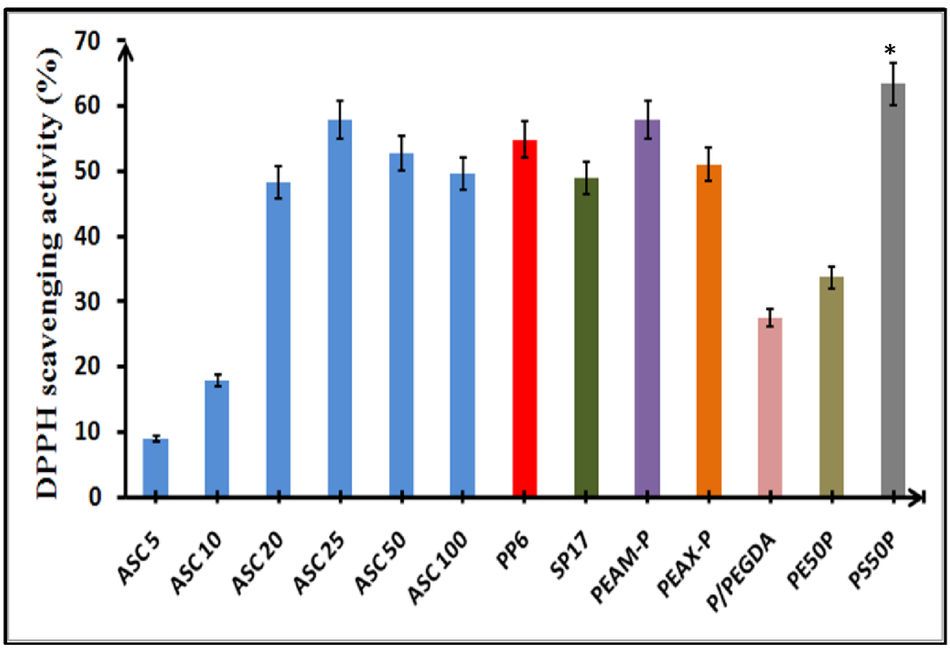

Figure - 38: DPPH radical scavenging percentage of hydrogels

4.7.1.2. Hydroxyl radical scavenging property of hydrogels

The PP6 and SP 17 hydrogels scavenge 10% and 14% of hydroxyl radicals respectively. The PEAM-P hydrogel scavenges 31% of hydroxyl radicals, which is comparatively higher than PEAX-P hydrogel (25%) (Figure - 39). The P/PEGDA hydrogel, prepared from fumarate-PEG-sebacate comacromer, exhibits

comparatively lower hydroxyl scavenging effect (14%) than the PS50P hydrogel (22%). The hydroxyl radical scavenging effect of hydrogels is compared with ascorbic acid at different concentrations. The ascorbic acid at 100 µM exhibits hydroxyl radical scavenging percentage of 8.

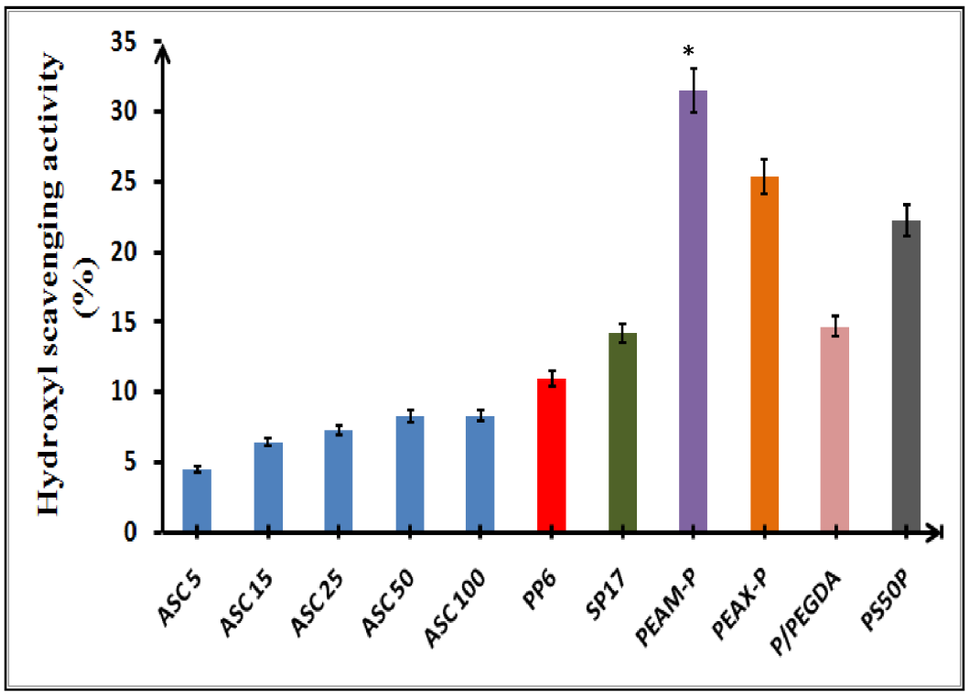

Figure - 39: Hydroxyl radical scavenging percentage of hydrogels

4.7.1.3. Nitric oxide radical scavenging property of hydrogels

The PP6 and SP 17 hydrogels scavenge 12% and 18% of nitric oxide radicals respectively. The PEAM-P hydrogel scavenges 23% of nitric oxide radicals, whereas PEAX-P hydrogel scavenges 30% of radicals (Figure - 40). The P/PEGDA hydrogel, prepared from fumarate-PEG-sebacate comacromer, exhibit comparatively lower nitric oxide scavenging effect (9%) than PS50P hydrogel (11%).

The nitric oxide radical scavenging effect of hydrogels is compared with ascorbic acid at different concentrations. The ascorbic acid at 100 µM exhibits nitric oxide radical scavenging percentage of 57.

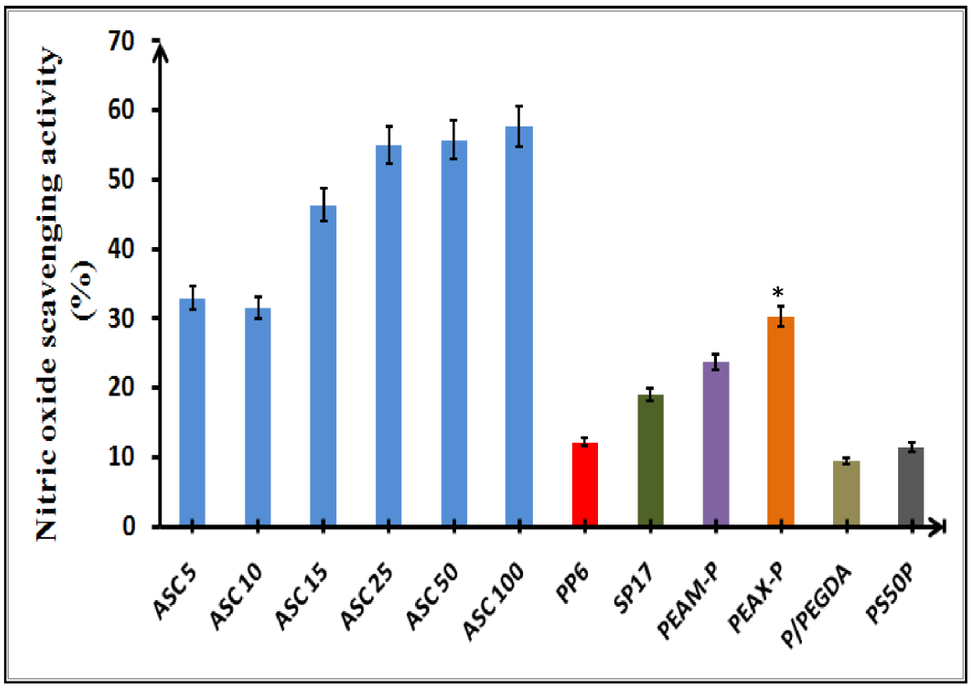

Figure - 40: Nitric oxide radical scavenging percentage of hydrogels

4.7.1.4 . Reducing power of hydrogels

The reducing power of the present hydrogels was determined to ensure the presence of free electrons associated with the comacromers inside the hydrogel. The PP6 and SP 17 hydrogels exhibit 48% and 49% of reducing power respectively. The reducing power of PEAM-P hydrogel is 60%, which is comparatively similar to PEAX-P hydrogel (58%) (Figure - 41).

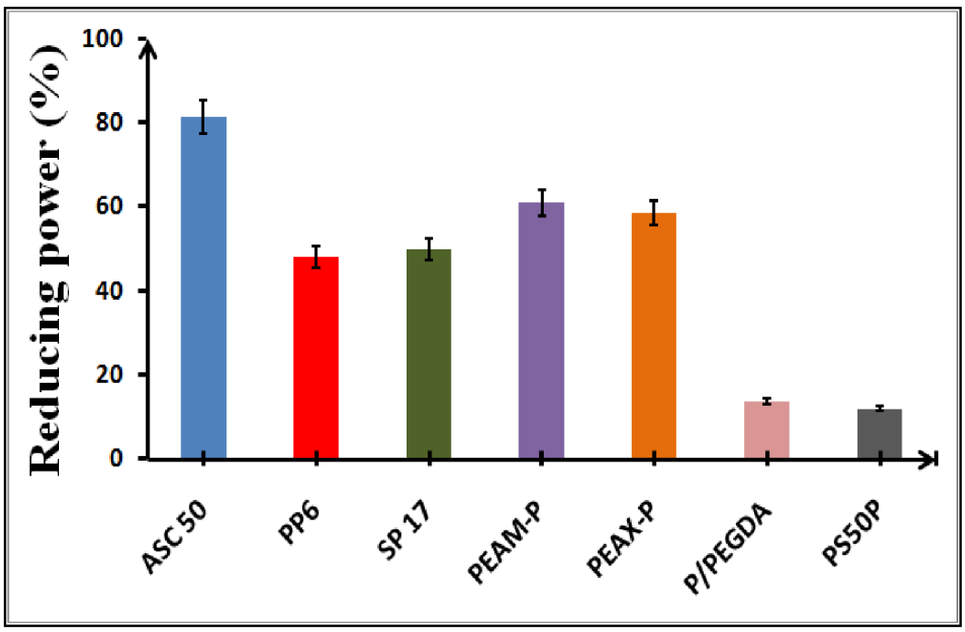

Figure - 41: Reducing power of hydrogels

The P/PEGDA hydrogel, prepared from fumarate-PEG-sebacate comacromer, exhibit 13% reducing power, whereas, the PS50P hydrogel, exhibit 12% reducing power. The reducing power of ascorbic acid at 50 µM concentration is 81%.

4.7.2. *In vitro* studies

In the present studies, the hydroxyl radicals are generated over cardiomyoblast cells through Fenton reaction. The minimum inhibitory concentration of Fenton reactants was identified using MTT assay. The minimum inhibitory concentration of H_2O_2 and $FeCl_3$, capable of killing 50% of H9c2 cells is identified as 70 µM. The H9c2 cells treated with 70 µM H_2O_2 and 70 µM $FeCl_3$ exhibit 50% metabolic activity (Figure - 42).

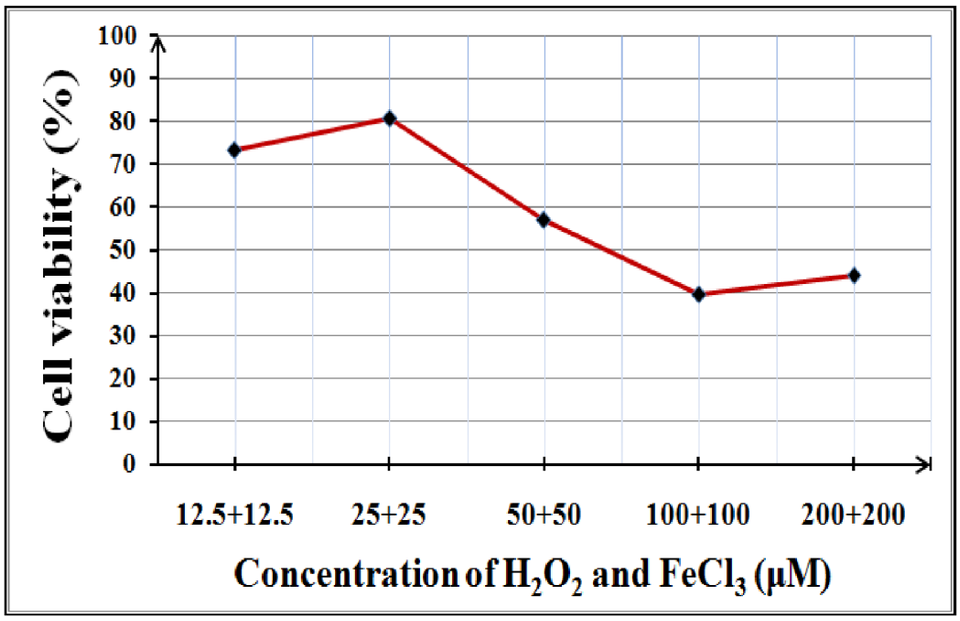

Figure - 42: Viability of cardiomyoblast cells with different concentrations of H_2O_2 and $FeCl_3$ by MTT assay.

4.7.2.1. Effect on cell metabolic activity under oxidative stress

The metabolic activity of the cardiomyoblast cells treated with stress inducing media was studied in the presence of hydrogels to assess the free radical scavenging effect of the present hydrogels. The cardiomyoblast cells treated with stress inducing media in the presence of ascorbic acid exhibit 71% viability. The cardiomyoblast cells treated with stress inducing media in the presence of PP6, PEAX-P, PEAM-P and PS50P hydrogels exhibit 67%, 51%, 75%, and 55% viability. The higher cell viability is observed with SP 17 hydrogel, which protects 86% of cells from oxidative stress (Figure - 43).

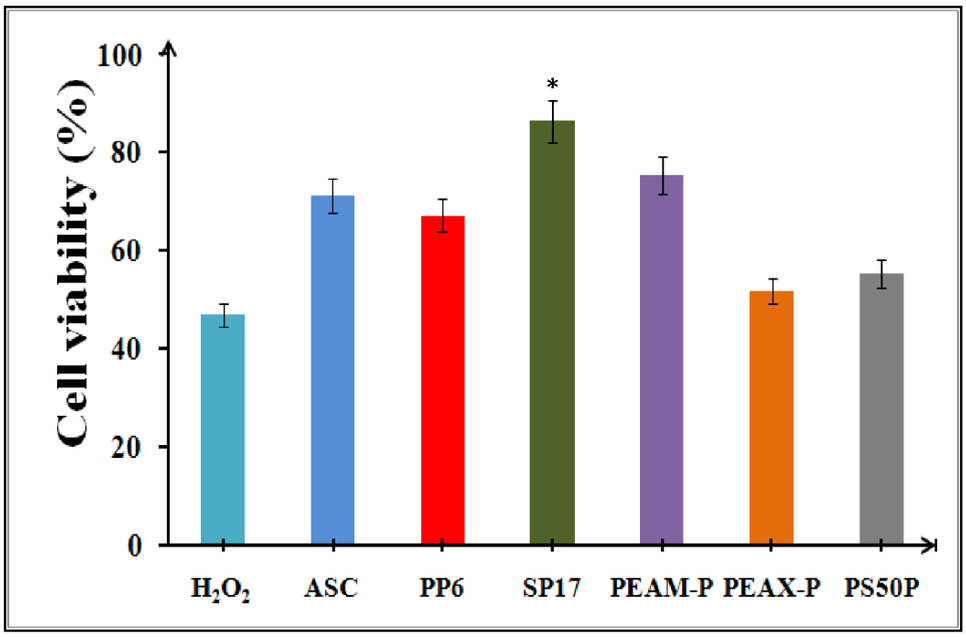

Figure - 43: Viability of cardiomyoblast cells treated with stress inducing media in the presence of hydrogels by MTT assay

4.7.2.2. Effect on cell apoptosis under oxidative stress

The live dead assay of cardiomyoblast cells treated with stress inducing media in the presence of PP6, SP 17, PEAM-P, PEAX-P and PS50P hydrogels was carried out to validate the quantitative results obtained from MTT assay. The tightly packed green fluorescing cells are observed in cardiomyoblast control group; whereas, the majority of cells fluoresces in orange when treated with stress inducing media (Figure - 44).

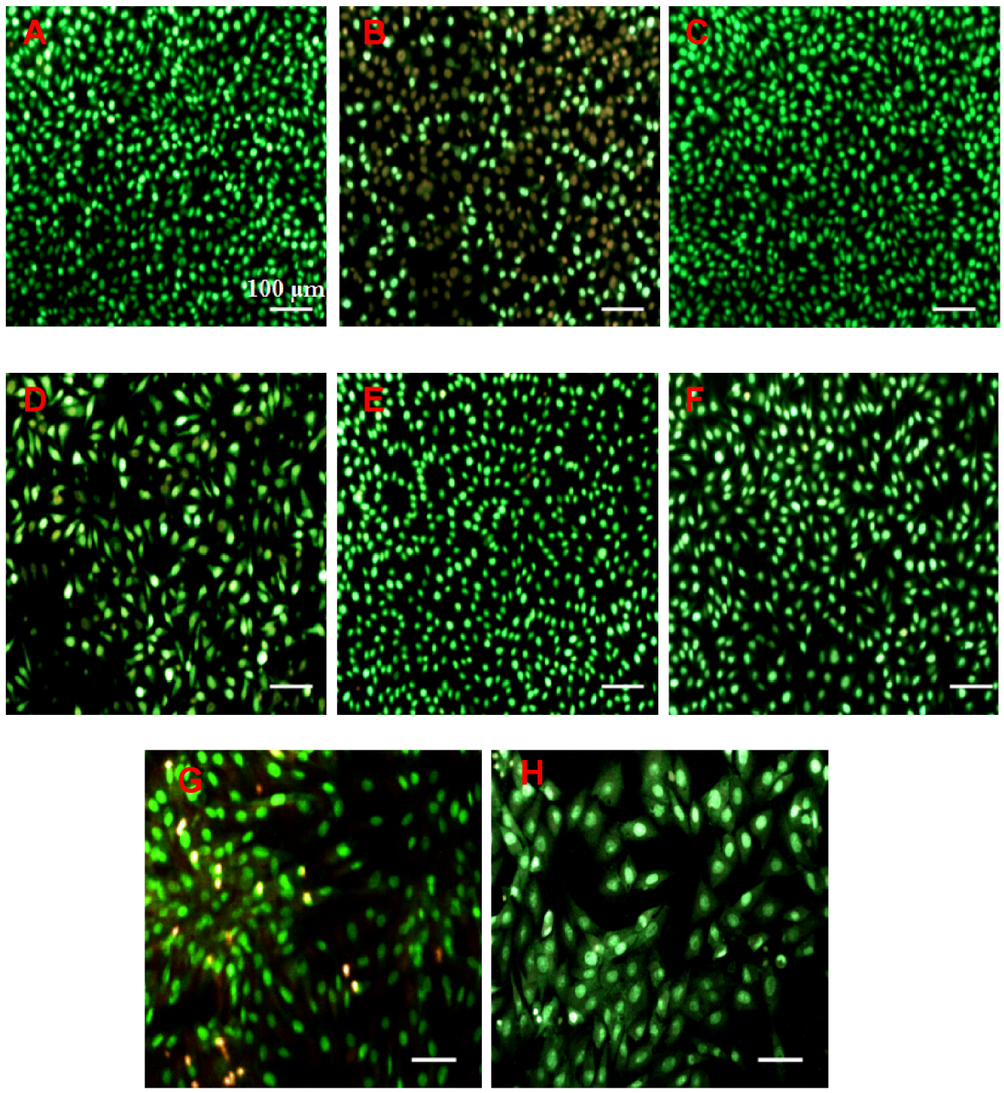

Figure - 44: Live dead assay of cardiomyoblast control cells (A), cells under oxidative stress (B), cells under stress-inducing media and treated with ascorbic acid (C) and cells under stress-inducing media and treated with hydrogels, PP6 (D), SP 17 (E), PEAM-P (F), PEAX-P (G) and PS50P (H).

The density of green fluorescing cells under oxidative stress treated with SP 17 and PEAM-P hydrogels is comparatively higher than other hydrogel treated cells and comparable to ascorbic acid-treated group (Table - 13).

Table-13: Density of cardiomyoblast cells

Cell density/ viability	Control cell	Cells with stress inducing media	Cells with stress-inducing media and test materials			
			Ascorbic acid	PP6	SP17	PEAM-P
No. of cells/70000 square pixels	3952	584	3538	642	3386	2530
Cell viability (%)	100	14.78	89.52	16.24	85.68	64.02

4.7.2.3. Studies on intracellular ROS generation and scavenging by hydrogels

In DCFH-DA study, 2',7' dichloro dihydro fluorescein diacetate (H_2DCFDA-AM) pass through the cell membrane and interacts with esterases to form the non-fluorescent H_2DCFDA, which is retained inside the cell due to the ionic in nature. When the cells are treated with stress inducing media, the H_2O_2 cross the cell membrane and induce the generation of ROS in cardiomyoblast cells. The generated ROS species convert H_2DCFDA to highly fluorescent 2',7' dichloro dihydro fluorescein (DCF).

The fluorescence intensity of 2',7' dichloro dihydro fluorescein (DCF) from the cardiomyoblast cells treated with stress inducing media is 336, which is reduced significantly to 106 when treated with ascorbic acid. The intensity of fluorescence from cardiomyoblast cells treated with stress inducing media in the presence of SP 17 and PEAM-P hydrogels are 59 and 46 respectively (Figure - 45).

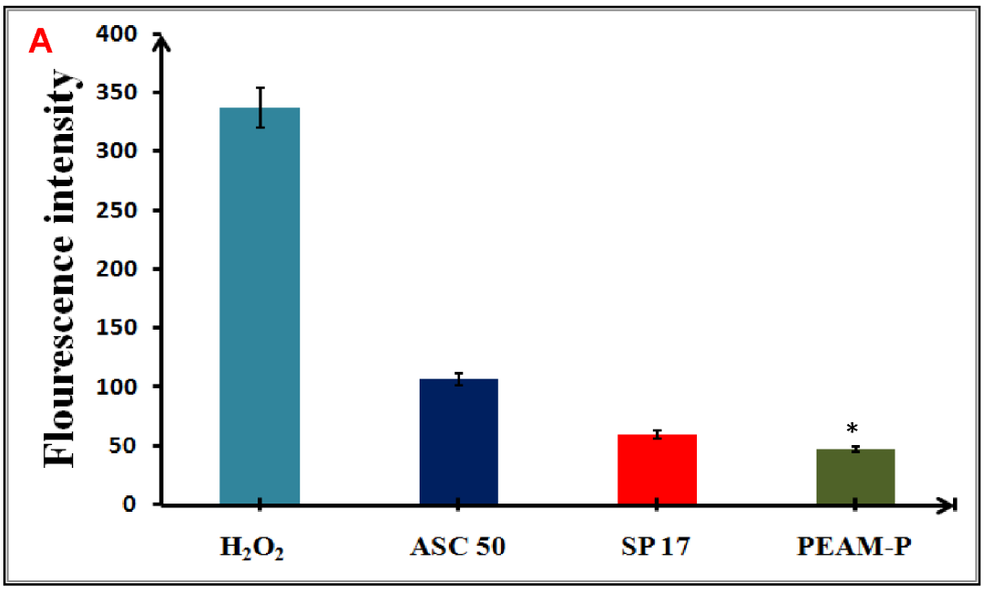

Figure - 45: Intracellular ROS generation in cardiomyoblast cells treated with stress inducing media and in the presence of SP 17 and PEAM-P hydrogels.
* sign indicates statistical significance.

4.8. Encapsulation of cardiomyoblast cells inside the hydrogels

The H9c2 cardiomyoblast cells were encapsulated inside the present hydrogels. The morphology, viability, proliferation and extracellular matrix remodeling by the encapsulated cells inside the hydrogels were studied for a long-term basis to identify the cell encapsulation efficiency.

The encapsulated cardiomyoblast cells appear with different morphology inside the hydrogels compared to the cells in 2D culture (Figure - 46). The cardiomyoblast cells have characteristic morphology under 2D culture, which has changed in the encapsulated hydrogel structure.

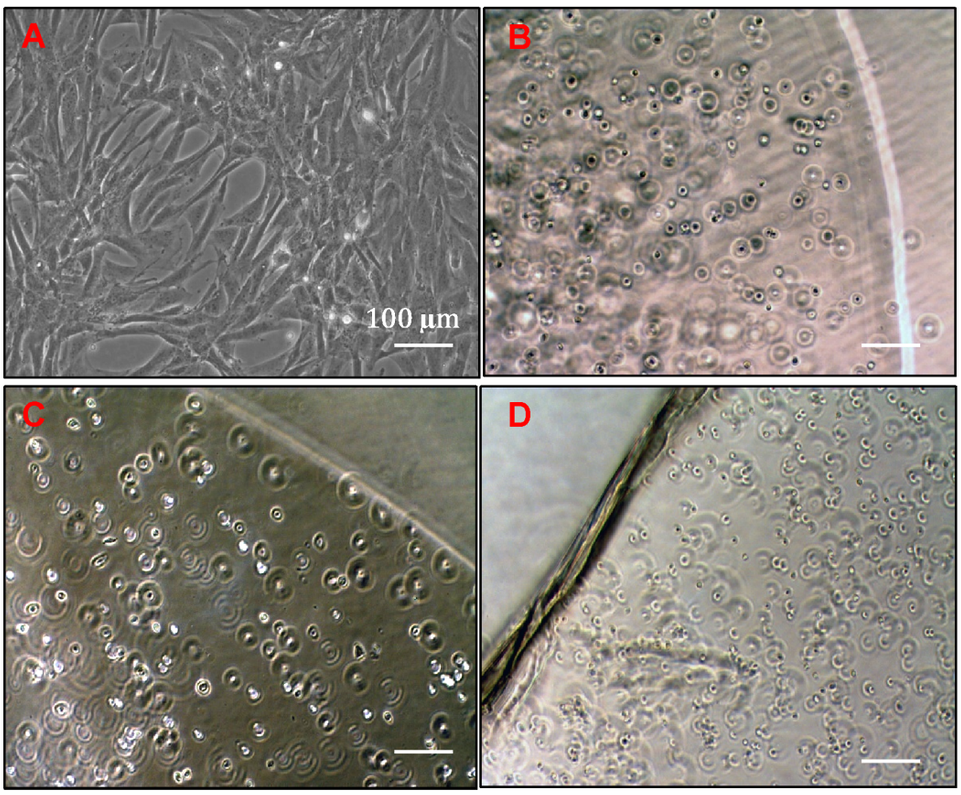

Figure - 46: Phase contrast images of cardiomyoblast cells in 2D culture (A), cardiomyoblast cells inside the PP6 (B), SP 17 (C) and PEAM-P (D) hydrogels.

4.8.1. Proliferation of encapsulated cells

The viability of cardiomyoblast cells cultured inside the hydrogels was identified at different intervals and compared with initial seeding density (1 x 10^6). The PP6 hydrogel retains 3.4 x 10^5 cells when cultured for 10 days after encapsulation, which multiplied to 1.4 x 10^6 at the end of 30 days (Figure - 47A). The density of cells inside SP 17 hydrogel cultured is 7.6 x 10^5 and 1.2 x 10^6 for 10 and 30 days respectively (Figure - 47B).

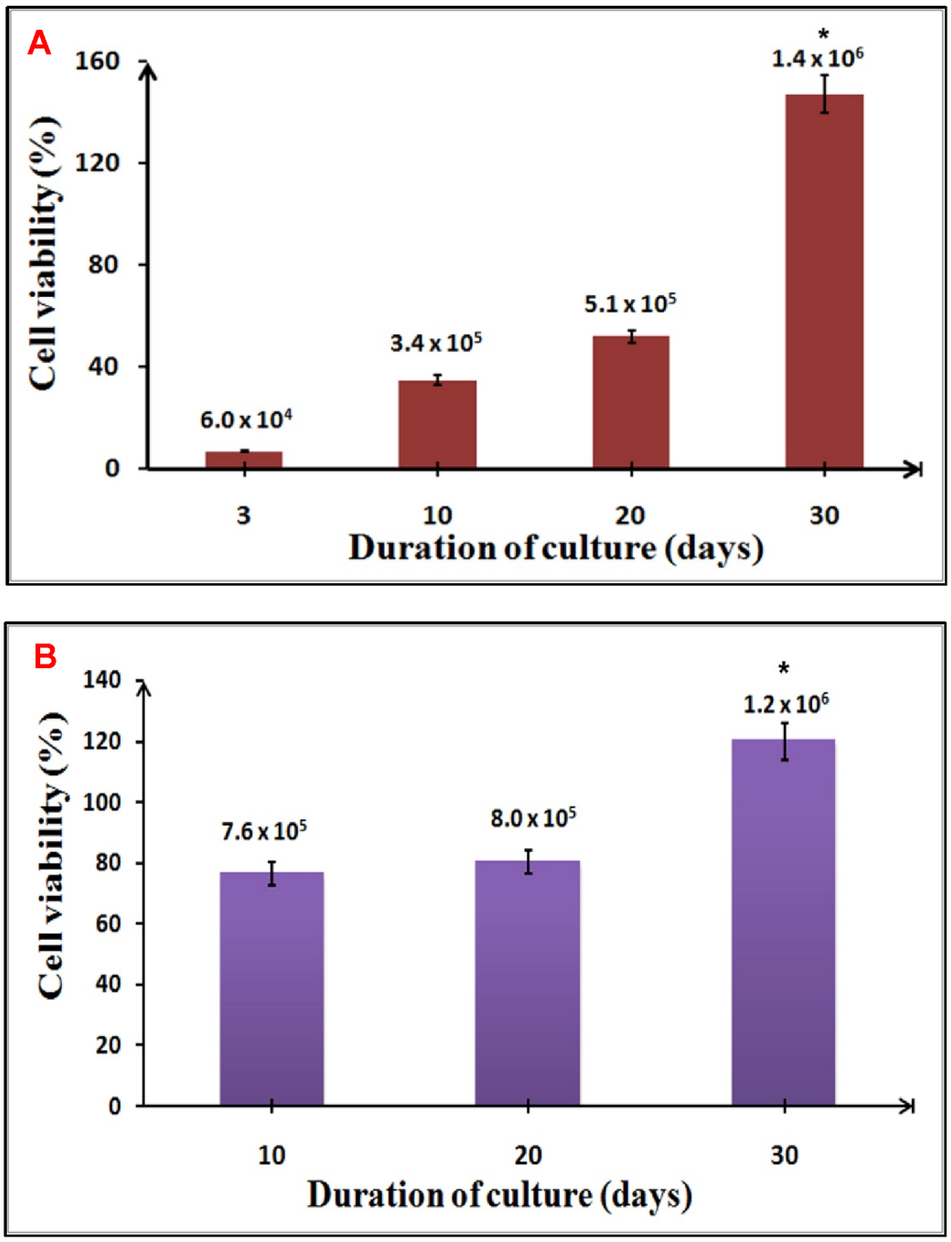

Figure - 47: Proliferation of cardiomyoblast cells inside the hydrogels under *in vitro* culture conditions. PP6 (A) and SP 17 (B). * sign indicate statistical significance.

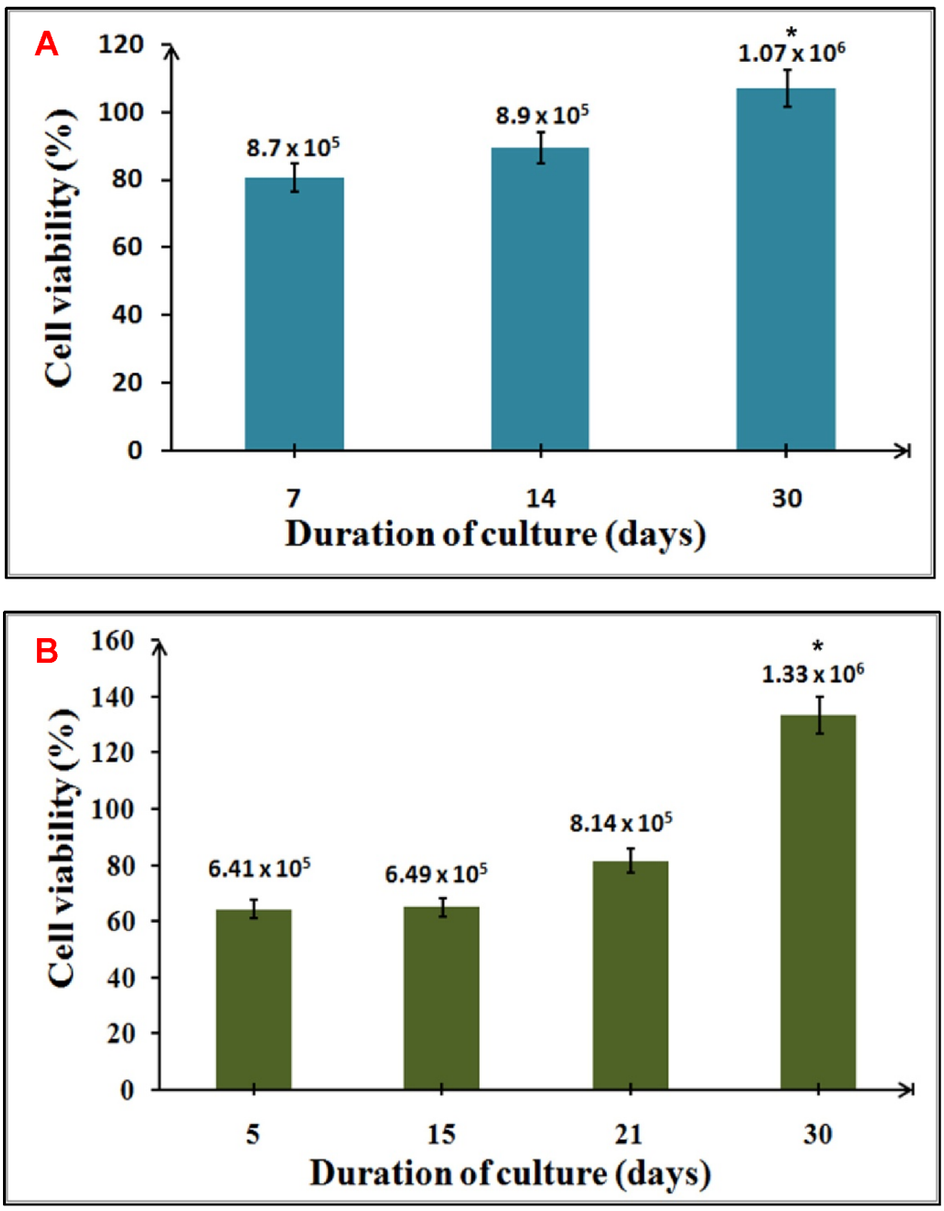

Figure - 48: Proliferation of cardiomyoblast cells inside the hydrogels under *in vitro* culture conditions. PEAX-P (A) and PEAM-P (B).
* sign indicates statistical significance.

The cell encapsulated PEAX-P and PEAM-P hydrogels cultured for 7 days retain 8.7 x 10^5 and 6.4 x 10^5 cells respectively (Figure - 48). In both PEAX-P and PEAM-P hydrogels, the viability and density of encapsulated cells increase on culture to 1.07 x 10^6 and 1.33 x 10^6 respectively at the end of 30 days.

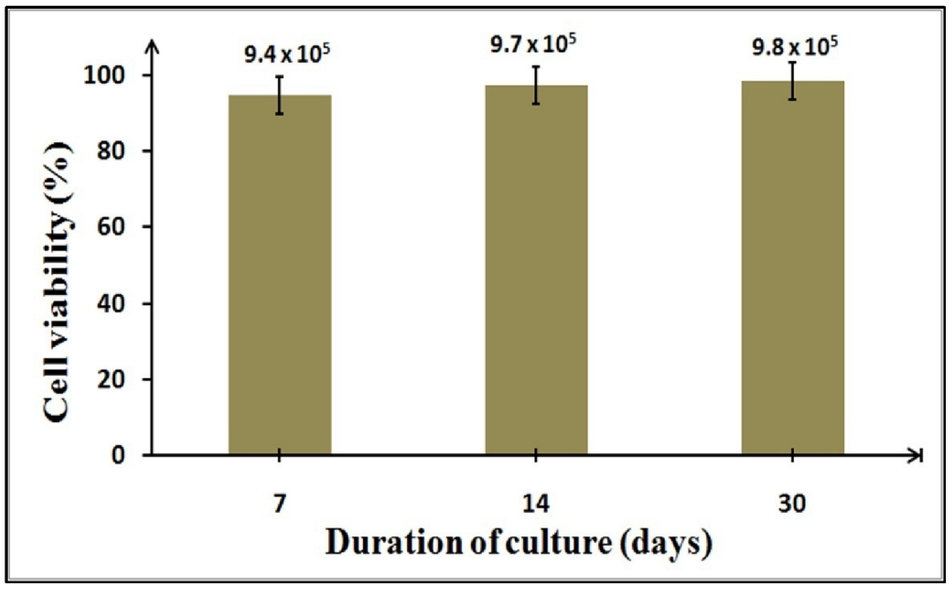

Figure - 49: Proliferation of cardiomyoblast cells inside the PS50P hydrogel under *in vitro* culture conditions.

The density of encapsulated cells inside PS50P hydrogel does not increase appreciably on culture with time. The higher density of cells is observed within 1 week of culture inside the PS50P hydrogel compared to other hydrogels. However, the density of cells after 30 days of culture is comparatively lesser in comparison with the other hydrogels (Figure - 49). The density of cells inside the PP6, SP 17, PEAX-P, PEAM-P and PS50P hydrogels are increased to 1.4 x 10^6, 1.2 x 10^6, 1.07 x10^6, 1.33 x 10^6 and 9.8 x 10^5 cells respectively within 30 days of culture.

4.8.2. Live dead assay

Live dead assay is considered as a qualitative assay to confirm the results obtained from MTT assay. The cell-encapsulated hydrogels cultured for 30 days are subjected to live dead assay. The confocal laser scanning images of cell-encapsulated hydrogels give 3D distribution of viable cells inside the hydrogels.

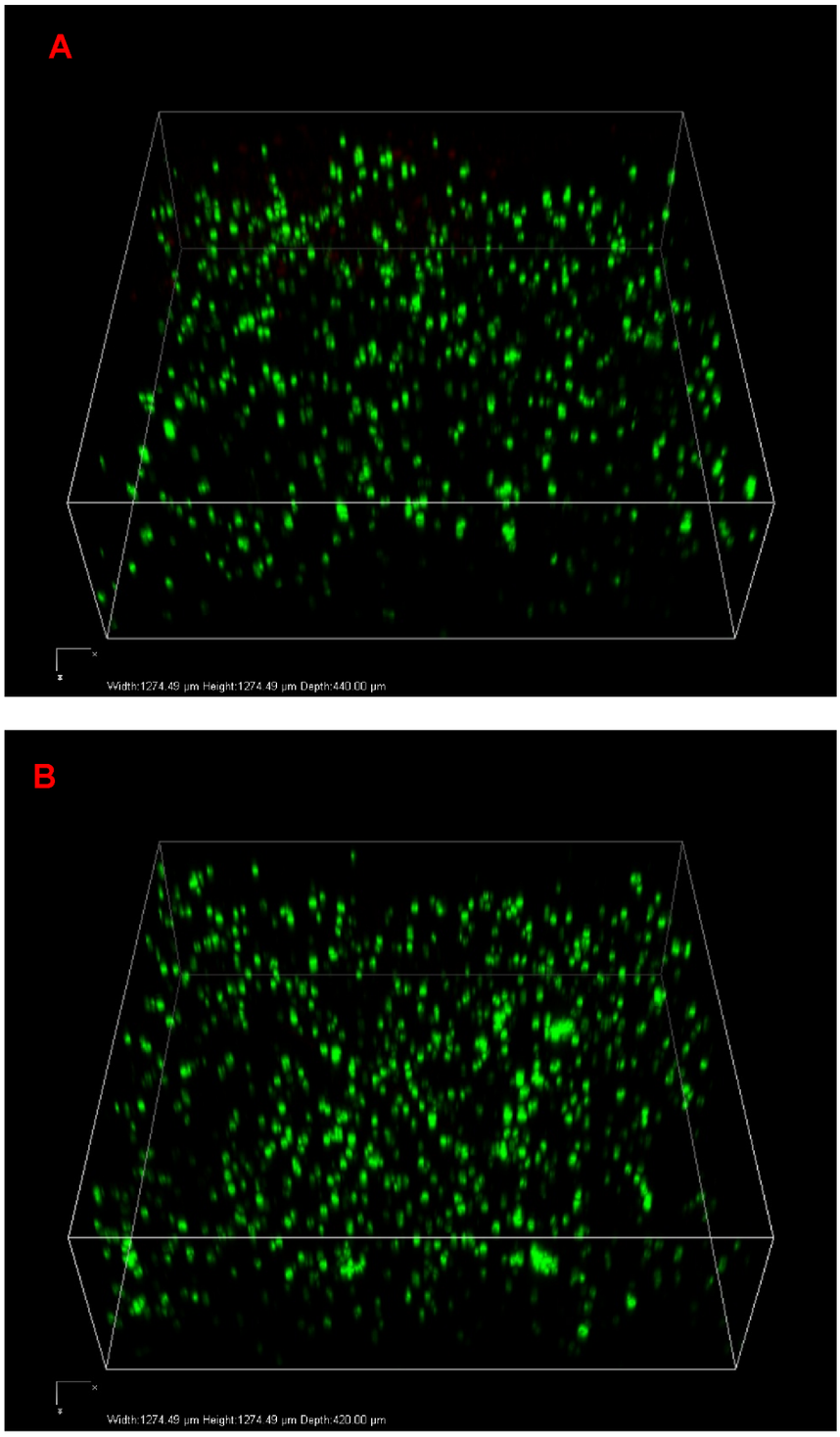

Figure - 50: Confocal laser scanning images of the 3D distribution of cardiomyoblast cells encapsulated inside the hydrogels after live dead staining. PP6 (A) and SP 17(B).

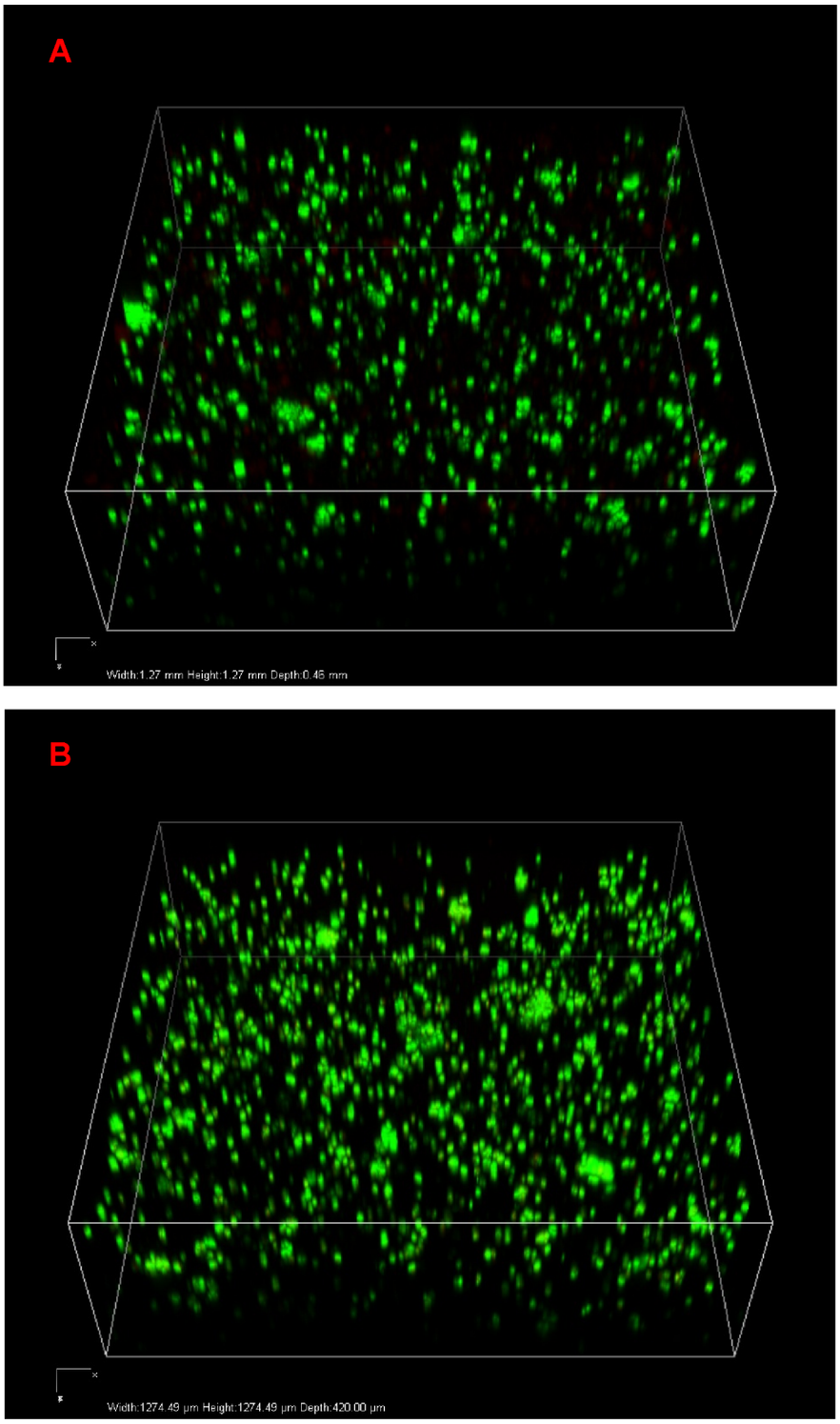

Figure - 51: Confocal laser scanning images of 3D distribution of cardiomyoblast cells encapsulated inside the hydrogels after live dead staining. PEAX-P (A) and PEAM-P (B).

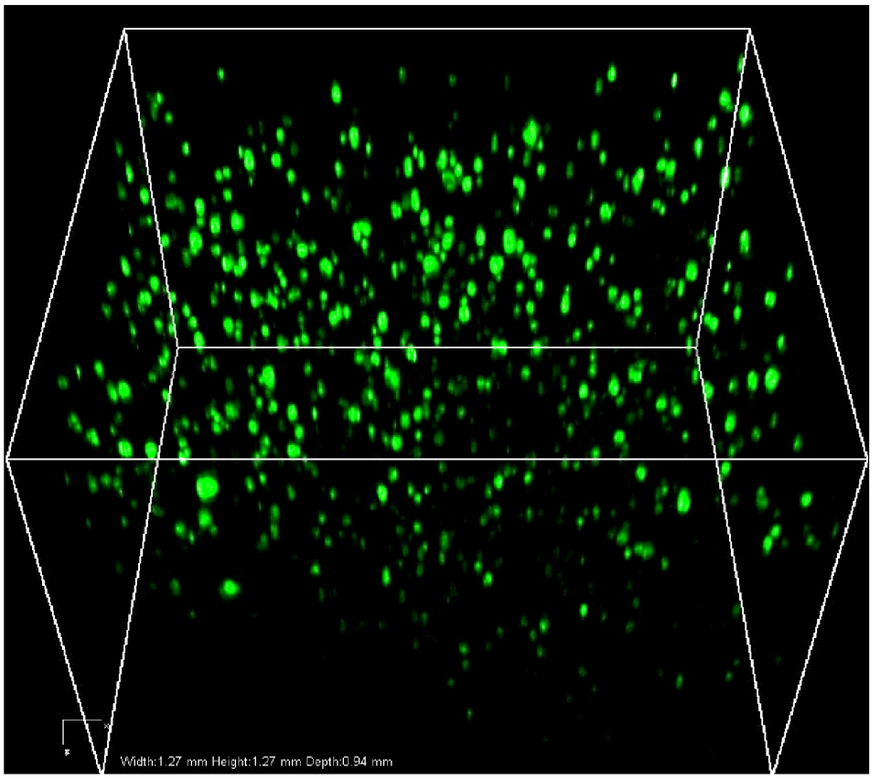

Figure - 52: Confocal laser scanning image of 3D distribution of cardiomyoblast cells encapsulated inside the PS50P hydrogel after live dead staining.

Green fluorescing uniformly distributed cells are observed in PP6 and SP 17 hydrogels up to 440 and 420 µm depth from the surface (Figure - 50). The green fluorescing cells distributed in clusters are observed in PEAX-P and PEAM-P hydrogels after 30 days of culture. Clusters of cells are comparatively more in PEAM-P hydrogel (Figure - 51). The uniformly distributed green fluorescing cells are observed in PS50P hydrogel up to 940 µm depth from the surface. The density of viable cells is observed more towards the surface of hydrogels than at the bottom (Figure - 52).

The density of fluorescing cells at the end of 30 days culture was determined by the image ITCN counting software. The density of cells inside the PEAM-P hydrogel is 1484 cells/mm^2, which is significantly higher than other

hydrogels. The density of cells inside the PP6, SP 17, PEAX-P and PS50P hydrogels are 499, 686, 656 and 292 cells/mm^2 respectively (Table - 14).

Table -14: Density of cardiomyoblast cells inside the hydrogels

Hydrogels	**PP6**	**SP 17**	**PEAX-P**	**PEAM-P**	**PS50P**
Cell number	1121	1470	1534	3168	1397
Area (mm^2)	2.24	2.14	2.34	2.13	4.78
Cell density/mm^2	499	686	656	1484	292

4.8.3. Histological evaluation

The histological staining of cell-encapsulated hydrogels helps to identify the cell distribution and extracellular matrix remodeling inside the hydrogels. The internal sections of cell-encapsulated hydrogels were stained with hematoxylin and eosin. The H&E stained internal section of acellular hydrogel treated with hematoxylin and eosin does not exhibit the purple color as shown in the figure 53A. However, the cell-encapsulated PP6, SP 17, PEAX-P, PEAM-P and PS50P hydrogels are stained in pink color. Clusters of cardiomyoblast cells stained with dark red color are observed in the hydrogels (Figure - 53).

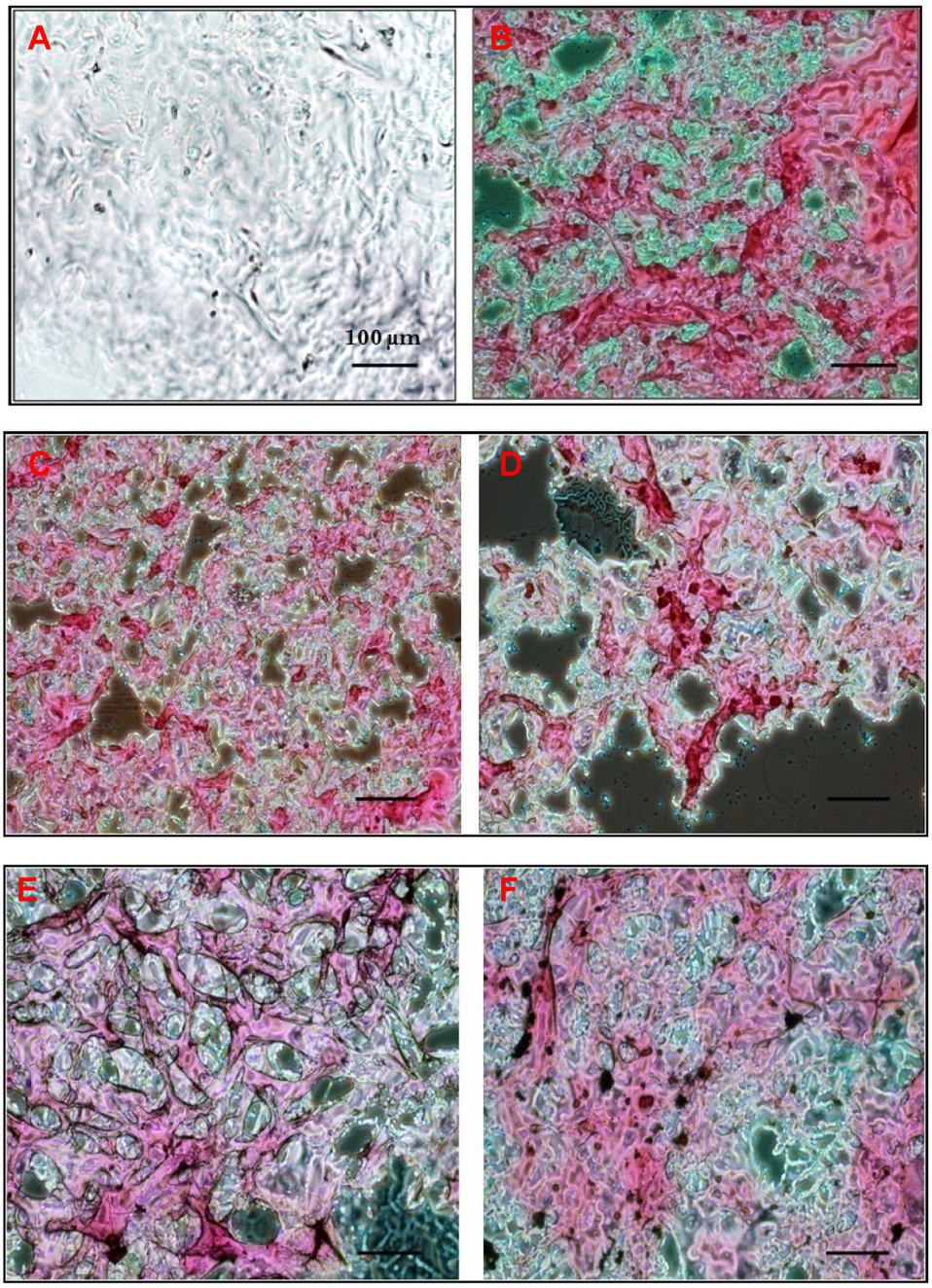

Figure - 53: Hematoxylin and eosin stained sections of cell-encapsulated hydrogels. Acellular hydrogel (A), PP6 (B), SP 17 (C), PEAX-P (D), PEAM-P (E) and PS50P (F).

CHAPTER 5

DISCUSSION

5 Discussion

The synthesis and structural analyses of the present comacromers and gelation characteristics of the injectable hydrogels are discussed. The relevance of swelling of hydrogels in water, surface and cross-sectional morphology, biomechanical stability and state of water inside the hydrogels are presented. The significance of electrical conductivity of polyaniline-based hydrogels is also specified. The cytocompatibility, hemolysis and free radical scavenging property of the present hydrogels are discussed. The cell encapsulation efficiency of the present hydrogels is discussed based on the proliferation, viability and extracellular matrix modeling by the encapsulated cardiomyoblast cells.

5.1. Synthesis and structural characterization of in situ crosslinkable comacromers

The synthesis of present comacromers involves esterification as well as isomerization of maleate to fumarate groups. Generally, esterification happens even at mild temperature conditions [Mamajanov *et al.*, 2014]. However, in the present synthesis of comacromers, high temperature (160-180 ^{0}C) is required to accomplish the isomerization of maleate to fumarate groups. The ring opening reaction of maleic anhydride above 160 ^{0}C yields an unsaturated dicarboxylic

fumaric acid. The double bonds in fumarate facilitate *in situ* crosslinking with vinyl crosslinkers.

5.1.1. Synthesis and characterization of poly(propylene fumarate) based comacromers

Poly(propylene fumarate) (PPF) is an unsaturated linear polyester that degrades into fumaric acid and propylene glycol; fumaric acid undergoes metabolization by Krebs cycle and propylene glycol gets excreted through the excretory organs. PPF contains crosslinkable double bonds which facilitate *in situ* gelation. PPF has promising applications in craniofacial bone implant due to its favorable mechanical strength (Henslee *et al.*, 2014). In the present study, the poly (propylene fumarate- co- ethylene glycol) and poly (propylene fumarate-co-sebacate-co-ethylene glycol) comacromers were synthesized from PPF by co-condensation with PEG 300 and sebacic acid-PEG 300 respectively (Figure - 3, 4). PEG 300 is an FDA approved polyol, which imparts the hydrophilicity and soft nature. Sebacic acid is an FDA approved chemical, which improves the cell adhesion and elastomeric property of hydrogel. The hydrogels with elastic characteristics are desirable for soft tissue applications.

The FT-IR analysis of poly (propylene fumarate- co- ethylene glycol) (PP) and poly (propylene fumarate-co-sebacate-co-ethylene glycol) (SP) comacromers reveal the successful condensation of monomers to comacromers (Figure - 5A,5B). The responses at 974 and 935 cm^{-1} in PP and SP comacromers indicate the cis-trans isomerisation of maleate to fumarate groups. The presence of fumarate double bonds in PP and SP comacromers is confirmed with the

spectral responses at 1639 cm^{-1}. The responses at 1730 cm^{-1} in both PP and SP comacromers substantiate the formation of ester bond during the condensation reaction. The structure of PP and SP comacromers are confirmed with ^{1}H-NMR spectra (Figure - 6A, 6B). The peaks at 5.4 ppm and 6.8 ppm in PP and SP comacromers confirm the presence of fumarate double bond. The SP comacromer has additional peaks at 1.6 ppm compared to PP comacromer, corresponding to the chemical shift or protons associated with the methylene groups of sebacic acid. The FT-IR and ^{1}H-NMR of poly(propylene fumarate-co-ethylene glycol) and poly(propylene fumarate-co-sebacate-co-ethylene glycol) confirm the presence of functional groups originated from the condensation reactions of respective comacromers.

5.1.2. Synthesis and characterization of sugar alcohol based comacromers

The sugar alcohols have inherent oxy-radical scavenging property, which depends upon the number of aliphatic hydroxyl groups (Kang *et al.*, 2016). Mannitol is clinically used in osmotherapy and renal, cardiac protection after surgery. Xylitol is reported for the treatment of dental caries to reduce plaque formation [Mäkinen *et al.*, 2010]. Poly(ethylene adipate) is a biodegradable aliphatic polyester which reduces the hydrophilic nature of comacromer (Hichem *et al.*, 2014). Here, the sugar alcohols, mannitol, and xylitol are condensed with the synthesized poly(ethylene adipate)-fumarate comacromer (Figure - 7,8). The mannitol-fumarate-poly ethylene adipate-fumarate-PEG (PEAM) and xylitol-fumarate-poly ethylene adipate-fumarate-PEG (PEAX) comacromers appears as transparent, homogenous, light yellow resin at room temperature.

The FT-IR analyses reveal peaks at 3424 cm^{-1} and 3438 cm^{-1} for PEAX and PEAM comacromers for the hydrogen bonded alcohol groups in xylitol and mannitol respectively (Figure - 9A, 9B). The alcohol groups associated with carboxylic acid of PEAX and PEAM comacromers exhibit the response at 2939 and 2947 cm^{-1} respectively. FT-IR response for ester group in PEAX and PEAM comacromers substantiate the successful condensation of monomers. The spectral responses of PEAX and PEAM comacromers confirm the presence of crosslinkable trans C=C bonds for *in situ* crosslinking. The presence of PEG in the comacromer exhibit peaks at 1110 and 1026 cm^{-1} in PEAX and PEAM respectively. The ^{1}H-NMR spectra confirm the structure of PEAX and PEAM comacromers (Figure - 10). The chemical shift of hydrogen atoms associated with the alcohol groups of xylitol and mannitol are present in ^{1}H-NMR spectra of PEAX and PEAM comacromers. The presence of fumarate bond in both PEAX and PEAM comacromers is confirmed with ^{1}H-NMR spectra.

5.1.3. Synthesis and characterization of polyaniline based comacromers

The polymeric scaffolds, which are electrically non-conductive, restrict the electrical coupling and alignment of engrafted cells with the surrounding myocardium. Therefore, the conducting polymers like polypyrrole, polyaniline, and polythiophenes are employed for the preparation of electroconductive injectable hydrogels. Electroconductive hydrogels are mostly prepared as a hybrid network with insulating polymers, which provide gelling character. The polymerizable conducting monomers impart electrical conductivity to the hydrogel. However, the diffusion of conducting polymer out of the network in physiological media causes the reduction in conductivity and cytotoxic effects. In

order to overcome the limitations of electroconductive hydrogels from the hybrid system, single component conductive hydrogels are preferred with the conjugated polymer as the main continuous phase. However, this is a rather challenging approach because conjugated polymers lack water solubility, functional side chains, and flexibility. Up to date, there are scarce reports on single component-hydrogels fabricated from covalently conjugated conductive polymers. Here, a single component electroconductive comacromer is synthesized by conjugating the conducting polyaniline with the *in situ* crosslinking fumarate-co-PEG-co-sebacate comacromer. The conductivity of polyaniline varies with pH, which turns into less-conductive at pH >4. Therefore, emeraldine salt of polyaniline is sulfonated using con.sulfuric acid (Figure - 11), which increases the electrical conductivity and improves the solubility of polyaniline in aqueous media. Fumarate-co-PEG-co-sebacate comacromer, is readily soluble in water; it has free carboxyl end groups for conjugation with the amino group of polyaniline. EDC-NHS reaction facilitates the formation of amide bonds to conjugate fumarate-co-PEG-co-sebacate comacromer with polyaniline (Figure - 12). The polyaniline emeraldine salt and sulfonated polyaniline are conjugated with fumarate-co-PEG-co-sebacate comacromer to PANIE-P and PANIS-P comacromers respectively.

The FT-IR analysis of comacromers substantiates the conjugation of polyaniline with the *in situ* crosslinking comacromer (Figure - 13). The sharp spectral responses at 1722 cm^{-1} and 1631 cm^{-1} in the FT-IR spectrum of fumarate-co-PEG-co-sebacate comacromer correspond to the stretching vibrations of C=O group in ester bonds and C=C in fumarate group respectively. The fumarate double bonds are responsible for *in situ* crosslinking with vinyl crosslinkers. The responses of the ester group and fumarate double bonds are also identified in

PANIE-P and PANIS-P comacromers, which substantiate the conjugation of polyaniline with fumarate-co-PEG-co-sebacate. The amide I band associated with C=O stretching vibration of PANIE-P and PANIS-P comacromers is expected to appear in 1600-1700 range in FT-IR spectrum. However, the response is merged with the existing ester and C=C responses. Amide II bands associated with N-H bending vibration in PANIE-P and PANIS-P is present at 1556 cm^{-1}. Amide III bands in FT-IR spectra of PANIE-P and PANIS-P comacromers is observed at 1320 cm^{-1} and 1389 cm^{-1} respectively. Thus, the spectral analyses confirm the formation of an amide bond by the terminal amino group of polyaniline with the free carboxyl end group of fumarate-co-PEG-co-sebacate comacromer.

The ^{1}H-NMR spectra of fumarate-co-PEG-co-sebacate, PANIE-P and PANIS-P comacromers confirm the conjugation of polyaniline with comacromer (Figure - 14). The peaks at 6.7 ppm in ^{1}H-NMR spectra of fumarate-co-PEG-co-sebacate comacromer correspond to the chemical shift of protons associated with fumarate double bonds (Figure - 14A). ^{1}H-NMR spectra of PANIE-P (Figure - 14B) and PANIS-P (Figure - 14C) comacromers includes the chemical shift corresponds to the protons in fumarate-co-PEG-co-sebacate. The sharp and prominent peak at 3.6 ppm in PANIE-P and PANIS-P comacromers is due to the methylene protons of PEG. The peak at 7 ppm in ^{1}H-NMR spectra of PANIE-P and PANIS-P comacromers corresponds to the chemical shift of protons associated with the NH group in amide bond, which conjugates PANI with fumarate-co-PEG-co-sebacate comacromer. The CH_2 protons bonded with amide NH group exhibit chemical shift at 2.2-2.5 ppm in the ^{1}H-NMR spectra of PANIE-P and PANIS-P comacromers, which substantiate the conjugation of the amino group of polyaniline with the carboxyl groups of fumarate-co-PEG-co-

sebacate comacromer. A difference in the nuclear splitting of proton observed in PANIS-P comacromer compared to PANIE-P is due to the effect of the sulfate group. Sulfonation increases the hydrogen-bonding propensity of polyaniline, which results in poorly resolved peaks in PANIS-P. Moreover, the electronegative nature of sulfur attracts sigma electrons associated with benzene ring by the inductive effect, which reduces the intensity of chemical shift by the protons in PANIS-P comacromer.

UV-Visible analysis: Polyaniline exists in various oxidation states with different electrical conductivity. The different states include most reduced leucoemaraldine form, half-oxidized emeraldine salt, and fully oxidized perigraniline. Emeraldine salt of polyaniline is the most useful form with comparatively higher electrical conductivity. PANI emeraldine salt has alternate units of two benzoid and one quinoid group rich in conducting electrons. The transition of PANI between oxidation states can be assessed using UV-Visible spectroscopy. PANIE and PANIS exhibit characteristic absorbance at 300-450 nm and 800 nm, which represents π- π^* transition of the main chain and polaron- π^* transitions respectively (Figure - 15A). Both PANIE and PANIS exhibit sharp absorbance at 800 nm, which indicate the presence of conducting electrons (Cui *et al.*, 2014). Conjugation of polyaniline with fumarate-co-PEG-co-sebacate comacromer is confirmed with the sharp absorbance at 200-300 nm in the UV-visible spectra of PANIE-P and PANIS-P, which corresponds to the ester groups (Figure - 15B). PANIE-P retains the absorbance at 800 nm; however, PANIS-P shifts the absorbance from 800 to 685 nm, which indicates interaction of sulfonated quinoid ring with adjacent imine-phenyl-amine units (Molapo *et al.*, 2012).

5.2. Molecular weight distribution of comacromers

The GPC analysis of poly(propylene fumarate- co- ethylene glycol), poly(propylene fumarate-co-sebacate-co-ethylene glycol), xylitol-fumarate-poly ethylene adipate-fumarate-PEG and mannitol-fumarate-poly ethylene adipate-fumarate-PEG comacromers implies the oligomeric nature (Table - 4). The polydispersity of comacromers is close to unity, which substantiates effective condensation and uniformity in molecular mass.

5.3. Preparation of injectable hydrogels

The present hydrogels are prepared by free radical initiated crosslinking of comacromers with poly(ethylene glycol) diacrylate using conventional two-component APS/TEMED system. The oxidizing peroxide in APS and reducing amine in the TEMED form an active center of initiation [Nicodemus and Bryant., 2008]. PEGDA is a vinyl crosslinker, which forms crosslink junctions at trans double bonds of the comacromers. The free radical initiated crosslinking is favorable for fast gelation with minimum damage to the cells, especially while injecting in deeper tissue regions. Moreover, the radical polymerization can overcome the steric hindrance and ensures the addition reactions between the bulky candidates. Moad and Solomon (2005) have reported that steric hindrance by the adjacent groups in addition reaction on carbon-carbon double bond is a minor issue in radical polymerization. Moreover, only the substituent either at the site of addition or at the radical center influences the reaction. This theory can support the chemical crosslinking of PEGDA with the fumarate double bonds of the present comacromers.

The gelation characteristics of PP6 and SP 17 hydrogels prepared from poly(propylene fumarate- co- ethylene glycol) and poly(propylene fumarate-co-sebacate-co-ethylene glycol) comacromers respectively are favorable for the injectable application (Table - 5). The fumarate double bonds in poly(propylene fumarate- co- ethylene glycol) and poly(propylene fumarate-co-sebacate-co-ethylene glycol) comacromers is the active center for crosslinking as shown in figure 16. PP6 hydrogel takes comparatively more time for gelation than SP 17 hydrogel. In PEAX-P and PEAM-P hydrogels prepared from xylitol-fumarate-poly(ethylene adipate)-fumarate-PEG and mannitol-fumarate-poly(ethylene adipate)-fumarate-PEG, the gelation takes place within 5 and 8 min respectively (Table - 6), which is faster than PP6 and SP 17 hydrogels. The xylitol-fumarate-poly(ethylene adipate)-fumarate-PEG and mannitol-fumarate-poly(ethylene adipate)-fumarate-PEG comacromers have twice the number of double bonds per molecule for crosslinking (Figure - 17) compared to poly(propylene fumarate- co-ethylene glycol) and poly(propylene fumarate-co-sebacate-co-ethylene glycol) comacromers, that can fasten the sol-gel transition. In polyaniline-based hydrogels, the PANIS-P/PEGDA (PS50P) based hydrogel undergoes faster gelation than PANIE-P/PEGDA (PE50P) based hydrogel (Table - 7), which may be due to the better interaction of sulfonated PANI with hydrophilic PEGDA than in the emeraldine form. The fumarate double bonds of fumarate-PEG-sebacate comacromer are the center for crosslinking with PEGDA (Figure - 18). As the free radical crosslinking is not sensitive to physical stimuli, the time taken for sol-gel transition determines the maximum time available for injection. Here, the present hydrogels take reasonable time for sol-gel transition desirable for injectable therapy. The gelation is exothermic, which can increase the temperature

at the injection site. Reissis *et al*, (2013) have reported that the temperature up to 48 ^{0}C for 2.5 min does not affect the metabolism of human cells. Therefore, the rise in temperature during gelation of the present hydrogels is negligible to affect homeostasis of a biological system.

5.4. Physico-chemical characterization of injectable hydrogels

5.4.1. Swelling and crosslink density of hydrogels

The hydrogel absorbs water until the free energy of mixing becomes equals to the elastic free energy of polymer network. The swelling percentage depends on the degree of crosslinking, the hydrophilicity of monomers, degree of neutralization of monomers and solvent interaction. Increasing the dilution and decreasing the crosslink density assist swelling (Fariba Ganji *et al.*, 2010). On neutralization of comacromer with sodium bicarbonate, free sodium ions retained inside the pores increase the osmosis. The ions create repulsive charges with the groups inside the pores and expand the coils to form large pores (Kutty *et al.*, 2007). Higher water retention of the hydrogel is favorable for maturation and proliferation of cells inside the hydrogel. The cell adhesion and proliferation inside the hydrogel explicitly depends on the diffusion of essential nutrients and gasses into the hydrogel matrix.

In poly(propylene fumarate) based hydrogels, the PP6 hydrogel prepared from poly(propylene fumarate- co- ethylene glycol) exhibits higher swelling ratio than SP 17 hydrogel prepared from poly(propylene fumarate-co-sebacate-co-ethylene glycol) (Table - 8). Kim *et al.* (2008) have previously employed sebacic acid to decrease the swelling ratio of PEGDA hydrogels. PEGDA hydrogels are

highly hydrophilic with higher swelling ratio and lower mechanical property. The sebacic acid has decreased the swelling ratio of PEGDA hydrogel and increased the mechanical stiffness. Similarly, the presence of hydrophobic groups of sebacic acid in the present SP 17 hydrogel reduces the water affinity, which is responsible for comparatively lower swelling ratio.

In sugar alcohol based hydrogels, the PEAM-P and PEAX-P hydrogels prepared from mannitol-fumarate-poly ethylene adipate-fumarate-PEG and xylitol-fumarate-poly ethylene adipate-fumarate-PEG comacromers respectively, retain comparatively similar amount of water on equilibrium swelling (Table - 8). This observation underlies the similar effect of xylitol and mannitol on hydrophilicity and swelling property of these hydrogels. The hydroxyl groups in sugar alcohols and PEG moiety enhances water affinity of PEAX-P and PEAM-P hydrogels. The hydrophobic groups in poly (ethylene adipate) prevent super swelling to maintain required mechanical property and porosity.

In polyaniline-based hydrogels, the PS50P hydrogel prepared from sulfonated polyaniline conjugated fumarate-PEG-sebacate has higher swelling ratio compared to PE50P hydrogel prepared from polyaniline emeraldine salt conjugated fumarate-PEG-sebacate (Table - 8). Sulfonated polyaniline contains free sulfate groups, which bind the sodium ions on neutralization of comacromer. Therefore, sodium ion concentration inside the PS50P hydrogel will be higher compared to PE50P hydrogel. The free sodium ions increase the osmotic pressure inside the hydrogel, which enhances the diffusion of water into the hydrogel. Therefore, equilibrium water content of PS50P hydrogel is higher than PE50P hydrogel. PS50P hydrogel has higher crosslink density than PE50P hydrogel. The

presence of hydrophilic sulfonated PANI in PS50P hydrogel increases the interaction of comacromer to the hydrophilic crosslinker PEGDA, which is responsible for higher crosslink density of PS50P than PE50P hydrogel.

Chandy *et al.* (2003) have reported alginate/elastin/PEG hydrogel for cell encapsulation with 61.6% equilibrium water content. Lü *et al.* (2015) have previously reported a self-healing hydrogel based on chondroitin sulfate, multiple aldehyde and N-succinyl-chitosan for cell encapsulation, which retains 60.1% water upon equilibrium swelling. The present PP6, SP 17, PEAX-P, PEAM-P, PE50P and PS50P hydrogels have higher swelling property than the reported hydrogels. The hydrogels for cardiac applications must retain higher mechanical stability. Higher swelling reduces the mechanical stiffness and stress bearing property of hydrogels. Temenoff *et al.* (2002) have reported a hydrogel of oligo poly(ethylene glycol fumarate) (OPF) for the injectable cardiac application. The swelling ratio of OPF hydrogel is comparatively higher (15.7 ± 0.5) than the present hydrogels. However, the higher swelling significantly reduced the mechanical strength of OPF hydrogels to 16.5 ± 4.6 kPa. Here, the PP6, SP 17, PEAX-P, PEAM-P, PE50P and PS50P hydrogels are prepared from the comacromers with amphiphilic nature, which limits super swelling of hydrogels.

5.4.2. State of water inside the hydrogels

The state of water inside the hydrogels is assessed by endothermic curves in DSC thermogram of swollen hydrogels. The water in the hydrogels exist in three forms; free water (FW), freezable bound water (FBW) and non-freezable bound water (NBW). Free water inside the hydrogels undergoes phase transition

on cooling or heating, which melts at a temperature above 0 ^{0}C. Freezable bound water (FBW) is weakly bound to the hydrogel matrix by polymer interaction or capillary effect, which undergoes phase transition along with free water on cooling or heating. However, the freezable bound water melts at a temperature lower than the free water. The FW and FBW inside the hydrogels exhibit endothermic peaks on melting. The strongly bound non-freezable bound water (NBW) does not undergo phase transition on cooling or heating. Therefore, NBW is not detectable in differential scanning calorimetry (Thankam and Muthu., 2013). The major difference between bound water and free water on DSC analysis is the crystallization pattern; the former forms cubic ice and latter forms hexagonal ice upon crystallization (Yoshida et al., 1993). However, the bound water does not show a sharp phase transition on calorimetric analysis. As the water inside the hydrogels crystallizes continuously, it is difficult to distinguish the free water and freezable bound water using the cooling curve of DSC. However, the FW and FBW exhibits melting at different temperatures in the heating curve of DSC thermogram, which is considered for the analysis of water inside the hydrogels (Guan et al., 2011).

The nature of water inside the hydrogel influences the viability of encapsulated cells. The freezable water ensures the uninterrupted cycling of nutrients, metabolites and essential gasses inside the hydrogel matrix, which is favorable to retain the viability of encapsulated cells under slow vascularisation conditions. The bound water inside the hydrogels depends on the hydrophilicity of comacromers. Higher bound water can improve the interaction of cells with hydrogel matrix.

In poly(propylene fumarate) based hydrogels, the PP6 hydrogel prepared from poly (propylene fumarate- co- ethylene glycol) comacromer exhibit endothermic peak with melting temperature of 5.95 ^{0}C. However, the SP 17 hydrogel prepared from poly(propylene fumarate-co-sebacate-co-ethylene glycol) comacromer exhibit sharp endothermic peak with melting temperature at 0.84 ^{0}C, which indicates the presence of a higher fraction of freezable free water (FW) in total freezable water in PP6 hydrogel than that in SP 17 hydrogel (Figure - 19). The onset of melting starts at -1.49 ^{0}C in PP6 hydrogel and -0.94 ^{0}C in SP 17 hydrogel, substantiate higher FW in PP6 hydrogel. The bound water associated with SP 17 hydrogel is lower than PP6 hydrogel, due to the presence of hydrophobic sebacic acid in the former (Table - 9).

In sugar alcohol based hydrogels, the mannitol containing PEAM-P hydrogel exhibit sharp endothermic peak with melting temperature lesser than xylitol based PEAX-P hydrogel, which substantiates higher freezable bound water content in PEAM-P hydrogel (Figure - 20). The PEAM-P hydrogel retains good amount of water in both free and bound state. The alcohol groups associated with mannitol forms hydrogen bonds with water on swelling, which is responsible for a higher fraction of bound water in PEAM-P hydrogel.

In polyaniline-based hydrogels, a slight change is observed in the endothermic peaks of PE50P and PS50P hydrogels (Figure - 21). The free water content of PS50P hydrogel is higher than PE50P hydrogel. However, the less bound water content in PS50P hydrogel substantiates the weak interaction of water molecules with the PS50P polymer. Comparatively, the major fraction of water inside the present hydrogels exists in the freezable free state (Figure - 22).

Previously Thankam and Muthu (2013) have reported hydrogels fabricated from PPF-alginate comacromer crosslinked with n-butyl methacrylate for cardiac applications. The hydrogel exhibits 44.94% free water and 16.35% bound water content. The present hydrogels exhibit higher free water content, with the highest fraction of 79.73% in PS50P hydrogel. Tao Wang (2006) studied the state of water inside the chitosan-poly vinyl alcohol (1:5 molar ratio) hydrogel and observed 17.9% maximum bound water content. Here, the PEAM-P hydrogel exhibits 30.92% bound water fraction, by retaining 48.35% free water, which is favorable for cell survival and cell adhesion.

5.4.3. Surface and internal morphology of hydrogels

The porous nature of hydrogel facilitates the 3D growth of seeded or encapsulated cells to form vascularised tissues. The proper porosity of hydrogels with open interconnected pores is essential for nutrient and oxygen diffusion, homogenous cell distribution and vascularisation (Annabi *et al.*, 2010). Interconnected network inside the hydrogel can form hollow channeled structures, which assist the growth of endothelial cells into matured blood vessels [Muehleder *et al.*, 2014]. The size of the surface pores influences the size of the blood vessels, while the interconnectivity of internal pores influences the blood vessel density [Sarker *et al.*, 2015]. The optimum pore size for neovascularisation and fibroblast ingrowth is 5 μm and 5-15 μm respectively [El-Sherbiny *et al.*, 2013]. Shachar et al. have reported that the pore size of 50-100 μm diameters is adequate for vascularization of scaffolds after implantation (Shachar et al., 2003). However, Radisic and Vunjak-Novakovic have also reported that the pores

with 100-300 μm in diameter are desirable for long-term survival of engineered cardiac tissue (Radisic and Vunjak-Novakovic., 2005). In polyester based hydrogels, surface pores with a smaller diameter are preferred to reduce the water diffusion and rate of hydrolytic degradation. Therefore, the interconnected pores with diameter towards the minimum required size for vascularization are desirable for the present hydrogels.

The PP6, SP 17, PEAX-P, PEAM-P, PE50P and PS50P hydrogels have porous surface morphology. In poly(propylene fumarate) based hydrogels, the PP6 and SP 17 hydrogels have surface pores with 25 μm and 100 μm diameter respectively (Figure - 23, 24). The wide interconnected internal pores in PP6 and SP 17 hydrogels are suitable for vascularization and cell proliferation. The PEAX-P hydrogel prepared from xylitol-fumarate-poly ethylene adipate-fumarate-PEG comacromer has highly porous internal morphology with maximum pores of 75 μm in diameter (Figure - 25). The PEAM-P and PE50P hydrogels have aligned internal pores, which are suitable for the growth and proliferation of cardiomyocytes and endothelial cells (Figure - 26, 27). The aligned internal structure of PE50P may be due to the repulsion of water by the hydrophobic backbone of polyaniline in PANIE-P comacromer (Figure - 27). The sulfonation reduces the hydrophobicity of polyaniline, responsible for large bulk pores in PS50P hydrogel (Figure - 27). Accordingly, the present hydrogels, which may be loaded with the cardiac cells, are suitable for the cell growth and vascularization.

5.4.4. *In vitro* ageing and biomechanical analysis

The mechanical strength of the hydrogel invariably influences the tissue formation by seeded cells. Mechanical stiffness of substratum influences cell adhesion and downstream signaling in cells to shape the tissue. The rigidity of synthetic substrates influences the growth of different cell types. The cell spreading on the substrates by most of the cells increases with increases of rigidity from 10 Pa to 1 Mpa. However, maximum spreading is achieved at an optimum rigidity of between 10 Pa and 1 Mpa (Nemir *et al.*, 2010). Guo *et al.* (2006) have reported poor cell adhesion and proliferation in softer substrates, but better focal adhesion size and cytoskeletal organization on substrates with higher stiffness.

The mechanical stiffness of heart muscles is central to cardiac function throughout its contractile courses. The elastic nature of myocardium supports the rhythmic contraction and relaxation of the heart. Followed by myocardial infarction, the matrix metallo proteinases breaks down the extracellular matrix proteins at the infarct zone, which causes ventricular wall thinning. As the transmural pressure and wall stress are strictly associated with wall thickness, the geometrical changes in ventricular wall signals drastic increase in wall stress. Higher wall stress further induces the stretching of cardiomyocytes especially at infarct border zone, which results in infarct expansion and loss of elastic nature (Tous *et al.*, 2011). Wall *et al.* (2006) have reported that bulking of myocardium attenuate the post-MI remodeling by controlling the wall stress. Kortsmit *et al.* (2013) have studied the effect of hydrogels as a bulking agent in

infarcted myocardial wall. The presence of hydrogel in infarct zone with stiffness more than the surrounding myocardium significantly decreases the wall stress and attenuates the post-MI remodeling. Ifkovits *et al.* (2010) have compared the effect of similarly thickened hyaluronic acid hydrogels prepared with different compressive Young modulus to reduce LV remodeling and observed better bulking effect by the hydrogel with higher Young modulus. However, the higher stiffness of hydrogel shifts the elastomeric property to brittle plastic deformation, which is not suitable to withstand the strong fatigue cycles of heart. Therefore, it is challenging to prepare a hydrogel with higher stiffness and elastic nature.

Nagueh *et al.* (2004) have reported the Young modulus of the myocardium as 10-20 kPa at the beginning and 200-500 kPa at the end of diastole respectively. The Young modulus of the present hydrogels lies in the range of native myocardium (Table - 10). The Young modulus of present hydrogels decreases with ageing (Figure - 28, 29, 30, 31, 32). The PEAM-P and PS50P hydrogels exhibit higher mechanical stiffness even after 30 days of *in vitro* ageing, which is in the range of native myocardium (Figure - 31, 32). Gerecht *et al.* (2007) have previously reported a photocurable elastomeric hydrogel of polyglycerol sebacate (PGSA) with Young modulus of 119 kPa for cell encapsulation. Wu *et al.* (2015) have prepared PEGDA/PANI-based hydrogel by interfacial polymerization of aniline in PEGDA hydrogel with a compressive modulus of 54.4±4 kPa, which decreases with increasing PANI concentration. The present hydrogels, especially PS50P hydrogel has better mechanical stiffness suitable for the cardiac application. The myocardial stress of healthy rat at

end-diastole is 1.33 kPa and at end systole is 13.33 kPa (Kortsmit *et al.*, 2013). The PP6, SP 17 and PEAM-P hydrogels exhibit the maximum compressive stress of 24, 19 and 18 kPa respectively, which is suitable to withstand the stress at end systole (Table - 10).

The stress-strain graphs of the present hydrogels substantiate the elastomeric nature (Figure - 28, 29, 30, 31, 32). The hydrogels undergo higher extension at smaller compressive stress, which substantiates the elastic nature. The J-shaped stress-strain curves indicate the elastomeric nature of the present hydrogels similar to extracellular matrix (Muiznieks and Keeley., 2013). The SP 17, PE50P and PS50P hydrogels, which exhibit maximum extensibility without collapsing at 60% compression, substantiate negligible plastic deformation. The higher extensibility of hydrogels occurs due to the free movement of crosslink junctions. The degradation reduces the number of crosslink junctions and increases the elastomeric property. The higher stiffness with elastic nature of present hydrogels can prevent the collapse of hydrogel even under strong contraction and relaxation dynamics of the myocardium.

5.4.5. Electrical conductivity of polyaniline based hydrogels

The myocardium is composed of electrically excitable cardiomyocytes, which respond to the electrical impulses instantaneously. However, the spontaneous contraction of injected cells not in line with the surrounding cardiac cells ends up in severe arrhythmia. Such situations can be overcome by injecting the cells in electrically conducting, biodegradable

and cytocompatible matrices. The electrically conducting matrices ensure proper orientation and elongation of injected cells with the formation of electrical syncytium with the existing myocardium (You *et al.*, 2011). The electrical conductivity of native myocardium is 1.6 x 10^{-5} S cm^{-1} longitudinally and 5 x 10^{-5} S cm^{-1} transversally (Zhao *et al.*, 2015). The present polyaniline based hydrogels have electrical conductivity higher than the native myocardium, which is suitable for the myocardial applications. The conductivity of PANIE-P/PEGDA and PANIS-P/PEGDA based hydrogels is increasing from lower to a higher concentration of comacromer. PANIS-P/PEGDA based hydrogels exhibit comparatively higher conductivity than PANIE-P/PEGDA based hydrogels at similar comacromer concentration. Fossatti *et al.* (2011) have suggested the structural variation of PANI on sulfonation as a reason for higher conductivity. Sulfonation of PANI causes the conformational transition of PANI backbone from the compact coil to the expanded coil, which increases the charge transfer and electrical conductivity. Guarino *et al.* (2013) have reported electrical conductivity of 1.1 ± 0.5 x 10^{-6} S cm^{-1} for PANI/PEGDA hydrogel even at higher PANI concentration. Li *et al.* (2014) have synthesized a series of gelatin-g-polyaniline conductive hydrogels with the conductivity ranging from 1.21 x 10^{-4} to 4.54 x 10^{-4} S cm^{-1} by varying the PANI concentration. Comparatively, the present hydrogels exhibit higher electrical conductivity than previously reported hydrogels even at lower comacromer concentration containing PANI (Table - 11).

5.5. Cytocompatibility of hydrogels

The cytocompatibility of hydrogels was studied as per ISO10993-5, annexure C, which state that a biomedical material is considered non-toxic when more than 70% cells remain viable with two times dilution of material extract. Under *in vivo* conditions, the leachates from implanted or injected material is expected to be continuously removed or diluted by body fluids to a lesser concentration. Therefore, the viability of cells with diluted hydrogel extract is considered to extrapolate the *in vivo* situation. Here the cell viability with the present hydrogel extracts at 50% concentration is higher than 70%, which substantiate the cytocompatibility (Figure - 33, 34, 35, 36, 37). The direct contact test reveals the cytocompatibility of the candidate hydrogels. The morphology of L929 cells cultured on tissue culture polystyrene plate is retained even after 24 h of incubation with the present hydrogels. The viability of L929 cells after direct contact assay with the present hydrogels is confirmed by live dead assay.

5.6. Hemolysis

The injectable hydrogel formulation with cells is delivered to the myocardium by trans-endocardial or trans-epicardial methods. The chance of leakage of hydrogel particle to the blood in the myocardial cavity is higher when the hydrogel is injected using a catheter by trans-endocardial method (Seif-Naraghi *et al.*, 2013). Therefore, it is essential to analyze the hemolytic potential of the hydrogels. Hemolysis indicates the breakdown of erythrocyte membrane to

release the hemoglobin in plasma. Immunologic abnormalities, antigen-antibody reactions, mechanical injury and some diseases cause hemolysis (Jeswani *et al.*, 2015). The hemolytic potential of leachable from the hydrogels is analyzed as per ISO 10993-4:2002(E). The hemolytic potential of representative hydrogels, PEAM-P and PS50P hydrogels prepared from mannitol-fumarate-poly ethylene adipate-fumarate-PEG and sulfonated polyaniline conjugated fumarate-PEG-sebacate comacromers are given in table 12. Generally, the percentage of hemolysis less than 0.1% is acceptable for implantation. The present PEAM-P and PS50P hydrogels exhibit 0.06% and 0.04%, which is acceptable for *in vivo* application (Table - 12).

5.7. Studies on free radical scavenging characteristics of hydrogels

The reactive oxygen and nitrogen species are generated by the electron leakage or incomplete reduction of molecular oxygen in the mitochondria during oxidative phosphorylation. An endogenous antioxidant system involving enzymatic and non-enzymatic mediators can resolve moderate release of free radicals. The enzymatic system includes superoxide dismutase (SOD), catalase (CAT), glutathione peroxidase (GPx) and glutathione reductase (GRx) which can convert the reactive radicals into neutral excretable or resorbable products. Non-enzymatic antioxidants are divided into metabolic and nutrient type. Lipoic acid, glutathione, melatonin, uric acid, bilirubin, metal-chelating proteins and transferrin are the antioxidants generated through metabolic pathways. However, vitamin E, vitamin C, carotenoids, trace metals, flavonoids, omega-3 and omega-6 fatty acids are nutrient antioxidants procured through food or supplements (Pham-Huy *et al.*, 2008). These antioxidants function either by chain breaking or by

preventive methods. Antioxidants can break the radical chain reaction by stabilizing the secondary radicals or prevent chain reaction by neutralizing the initiating radicals.

Followed by acute MI, the inflammatory cells release superoxides and nitric oxide radicals, which further react to form hydroxyl, peroxynitrile and hydrogen peroxide radicals. An efficient molecule for antioxidant therapy must scavenge a wide range of free radicals to reduce the oxidative stress at infarct zone.

5.7.1. Biochemical assays

The biochemical assays are conducted to identify the scavenging property of the present hydrogels with different types of free radicals. The studies on DPPH, hydroxyl, and nitric oxide radicals are carried out with hydrogels to evaluate the scavenging effect.

5.7.1.1. DPPH radical scavenging property of hydrogels

DPPH scavenging assay is based on the reduction of DPPH radicals to DPPH-H. The free radical scavenging property is observed with the conversion of purple colored DPPH radicals to pale yellow colored DPPH-H. The DPPH scavenging depends on the hydrogen donating groups in antioxidants. The PP6, SP 17, PEAX-P, PEAM-P and PS50P hydrogels exhibit DPPH radical scavenging percentage comparable to ascorbic acid. Comparing the DPPH scavenging capability of the PEAX-P and PEAM-P hydrogels, the scavenging capability of PEAM-P hydrogel prepared from mannitol-fumarate-poly ethylene adipate-fumarate-PEG comacromer (57%) is slightly greater than PEAX-P hydrogel

based on xylitol-fumarate-poly ethylene adipate-fumarate-PEG comacromer (Figure - 38). The presence of more free hydroxyl groups in mannitol compared to xylitol substantiates the higher DPPH reducing power of PEAM-P hydrogel. Comparatively, the hydrogels prepared with polyaniline conjugated comacromer exhibit better scavenging property than P/PEGDA hydrogel, which substantiate the role of aromatic polyaniline units in free radical scavenging. Gizdavic-Nikolaidis *et al.* (2004) have previously reported the antioxidant property of polyaniline beneficial for biomedical applications. The PS50P hydrogel has a higher scavenging effect on DPPH radical compared to PE50P hydrogel. Thankam and Muthu have previously reported a free radical scavenging amphiphilic biosynthetic hydrogel based on alginate-poly ester comacromer (Thankam and Muthu, 2013) and observed the role of free water content in the hydrogel on neutralization and dilution of free radicals. The higher free water content in the present PS50P hydrogel than PE50P hydrogel account for better interaction and reduction of DPPH radical with PS50P hydrogel matrix.

Trombino *et al.* (2009) have reported a cellulose-trans ferulic acid hydrogel (containing a lower concentration of ferulic acid, 5 mg/ml) with 20% DPPH scavenging property. The present hydrogels exhibit better inherent antioxidant property with higher DPPH radical scavenging percentage of 63% for PS50P hydrogel. Li *et al.* (2013) have reported a chitosan-glutathione (CSCl-GSH) hydrogel, which can scavenge 60% DPPH radical; however, it is observed only at higher GSH content. Chitosan alone has a very low scavenging effect (10%). The antioxidant molecules as glutathione have a short time of action, especially in conjugated state. Here the present hydrogels with inherent free

radical scavenging property have a huge number of functional groups and free electrons, which will be sufficient to reduce the oxidative stress in the infarct zone.

5.7.1.2. Hydroxyl radical scavenging property of hydrogels

Hydroxyl radicals have high reactivity and toxicity with damaging effect on DNA, proteins and lipids (Lü *et al.*, 2015). However, short life span of hydroxyl radicals (10^{-9} s) (Pastor *et al.*, 2000) results in localized damage close to the site of formation. Hydroxyl radicals are generated inside the cells by Fenton reaction in which free iron reacts with hydrogen peroxide ($Fe^{2+} + H_2O_2 \rightarrow Fe^{3+} + {}^*OH + OH^-$) (Leonard *et al.*, 2004). Under redox condition, the superoxides inside the cells interact with iron-sulfur containing enzymes and releases free iron into the cytoplasm, which initiates the Fenton reaction. Moreover, superoxides itself form hydroxyl radicals through Haber-Weiss reaction (${}^*O^{2-} + H_2O_2 \rightarrow {}^*OH + OH^- + O_2$) (Liochev and Fridovich, 2002).

In deoxyribose assay, the hydroxyl radicals are generated by the reaction of Fe^{2+}- EDTA with H_2O_2. The released hydroxyl radicals interact with deoxyribose and form pink chromogen on heating with thiobarbituric acid at low pH (Gutteridge and Halliwell, 1988). In the present study, the significant reduction of intensity of pink color was observed with PEAX-P, PEAM-P and PS50P hydrogels prepared from xylitol-fumarate-poly ethylene adipate-fumarate-PEG, mannitol-fumarate-poly ethylene adipate-fumarate-PEG and sulfonated polyaniline conjugated fumarate-PEG-sebacate comacromers respectively, which indicate hydroxyl radical scavenging. The sugar alcohol based PEAX-P and

PEAM-P hydrogels scavenge 25% and 31% of hydroxyl radicals respectively, which is significantly higher than the scavenging effect of ascorbic acid even at 100 μM concentration (Figure - 39). The free π electrons associated with uncrosslinked fumarate double bonds may be responsible for the neutralization of hydroxyl radicals, which is comparable with the radical scavenging mechanism of anthocyanidin (Nimse and Pal, 2015).

5.7.1.3. Nitric oxide radical scavenging property of hydrogels

Nitric oxide (NO) is a free radical generated by nitric oxide synthase involved in the conversion of L-arginine to L-citrulline. NO has high diffusion rate, lipophilicity, and reactivity with 2-30 s half-life. NO reacts with molecules containing unpaired electrons (Habib and Ali, 2011). As most of the biomolecules are stable, these biomolecules remain unaffected even at 2-200 μM concentration of nitric oxide radicals. At this concentration, NO plays a cardioprotective role including regulation of blood pressure, endothelial function and vascular tone, inhibition of platelet aggregation and prevention of smooth muscle cell proliferation (Naseem, 2005). However, in hypoxic conditions, NO react with other reactive oxygen species to form highly toxic peroxynitrile and S-nitrosothiols, which can induce extensive apoptosis and mitochondrial dysfunctions in cells. The peroxynitrile radicals inactivate even antioxidant enzymes by the nitration of aromatic amino acids (Ayala *et al.*, 2014). In the present studies, the hydrogels exhibit a scavenging effect on nitric oxide radicals, which is lower than ascorbic acid. The PEAX-P hydrogel exhibit highest nitric oxide scavenging percentage compared to other hydrogels (Figure - 40). The moderate scavenging effect is beneficial to control the transition of nitric oxide

radical concentration from physiological to pathological level at inflamed or infarcted tissues. The free electrons associated with uncrosslinked double bonds in hydrogels offer the scavenging effect.

5.7.1.4. Reducing power of hydrogels

Reducing power of hydrogel is one of the measures of antioxidant property of hydrogels. Reducing agent donates its electrons to another chemical species. In this assay, the reducing power is evaluated as the ability of the hydrogel to convert the oxidized form of iron (Fe^{3+}) in ferric chloride to ferrous (Fe^{2+}). In poly(propylene fumarate) based hydrogels, the PP6 and SP 17 hydrogels exhibit similar reducing power. Mannitol containing PEAM-P hydrogel has higher reducing power, which is more or less similar to the xylitol-containing PEAX-P hydrogel (Figure - 41). The free electrons associated with fumarate double bonds are responsible for reducing effect.

5.7.2. *In vitro* studies

In the present study, the oxidative stress is induced on the cardiomyoblast cells using H_2O_2 and $FeCl_3$. The H_2O_2 can cross the cell membrane and form hydroxyl radicals in the presence of ferric ion. The cell viability decreases with increasing concentration of Fenton reagents. The minimum inhibitory concentration of H_2O_2 and $FeCl_3$ capable of killing 50% of H9c2 cells is identified as 70 µM (Figure - 42). However, 5% increase in cell viability is observed at 200 µM concentration of H_2O_2 and $FeCl_3$ compared to 100 µM. Higher concentration of H_2O_2 depletes •OH radicals and forms less reactive HO_2•

radicals responsible for comparatively higher cell viability (Nakamura *et al*, 2003).

5.7.2.1. Effect on cell metabolic activity under oxidative stress

The hydroxyl radicals are toxic with damaging effect on DNA, proteins, and lipids (Lü *et al*., 2015). In this study, the scavenging effect of ascorbic acid on hydroxyl radicals is evident with 71% cell viability. Still, the cells treated with PEAM-P and SP 17 hydrogels exhibit 75% and 86% cell viability respectively, which is comparatively higher than ascorbic acid (Figure - 43). These results substantiate the protective effect of the PEAM-P and SP 17 hydrogels on cells under oxidative stress. Dash *et al*. (2008) have studied the antioxidant property of silk protein sercin on skin fibroblast under oxidative stress. The sercin protein from *Bombyx mori* protects 60% cells from oxidative stress at 100 ng/ml concentration, which is comparatively lower than the present PEAM-P and SP 17 hydrogels. The cerium oxide nanoparticles reported by Weaver and Stabler (2015) protects over 70% of cells from superoxide stress at 1mM concentration. However, cerium oxide is highly toxic at a concentration higher than 1 mM. Moreover, cerium oxide deposits inside the cells without degradation. Relatively, the present PEAM-P and SP 17 hydrogels have better free radical scavenging property and protective effect on cardiomyoblast cells.

5.7.2.2. Effect on cell apoptosis under oxidative stress

The live dead assay of hydrogel-cell exposed to free radical confirms the free radical scavenging capability of the hydrogels. Acridine orange/ethidium bromide stain differentiates the live cells (green), early apoptotic cells (yellow)

and dead cells (orange). The viable green fluorescing cells are observed in control group; few viable cells are present in the stress-induced group, which is 14.78% compared to control cells (Table - 13). The free radicals exposure induced apoptosis in cells treated with stress inducing media (Figure - 44). At this point, the cells treated with stress inducing medium in the presence of SP 17 and PEAM-P hydrogels prepared from poly (propylene fumarate-co-sebacate-co-ethylene glycol) and mannitol-fumarate-poly ethylene adipate-fumarate-PEG comacromers respectively, retain appreciable cell viability. However, higher viable cell density is observed with SP 17 hydrogel compared to PEAM-P hydrogel (Table - 13). Thankam and Muthu, (2013) have reported poly(propylene fumarate)- alginate based hydrogels with the inherent antioxidant property, which protects cells from oxidative stress. The present SP 17 and PEAM-P hydrogels protect comparatively more cells from oxidative stress than PA-PEGDA hydrogel.

5.7.2.3. Studies on intracellular ROS generation

When the cells are treated with stress inducing media, the H_2O_2 cross the cell membrane and induce the generation of ROS in cardiomyoblast cells. Under that condition, the H_2DCFDA-AM migrated into the cell membrane gets converted to non-fluorescent H_2DCFDA by esterases, which is further converted to highly fluorescent by the ROS species.

The fluorescence intensity from the cells treated with stress inducing media in the presence of SP 17 and PEAM-P hydrogels prepared from poly (propylene fumarate-co-sebacate-co-ethylene glycol) and mannitol-fumarate-poly ethylene adipate-fumarate-PEG comacromers, has significantly reduced, which

substantiate the scavenging effect of hydrogels on active free radicals generated from Fenton reaction (Figure - 45). The intracellular ROS from cells treated with hydrogels is less compared to ascorbic acid-treated cells. The hydrogel has crosslinked network with potential groups, which can trap and neutralize the free radicals. However, ascorbic acid is a soluble compound, which can only neutralize the radicals but cannot trap or delay the exposure of free radicals with cells.

5.7.2.4. Mechanism of free radical scavenging

So far, the antioxidant property in cellulose, chitosan or alginate hydrogels is attained by mixing or reacting with small antioxidant molecules like trans-ferulic acid, glutathione or metal oxides. The dosage issue and chances of burst release of small molecules in that system may cause a systemic radical imbalance, which can affect essential signal transduction pathways. As various free radical species from different sources contributes to the oxidative stress at the infarct zone, the antioxidant molecules with scavenging effect over a wide range of free radicals is required to mitigate the issue. Here, the cytocompatible and injectable hydrogels are reported with inherent free radical scavenging property for localized antioxidant therapy. The scavenging mechanism is proposed as 1) neutralization of free radicals through free π electrons associated with uncrosslinked fumarate double bonds in comacromer. The studies on the reducing power of hydrogel substantiate the presence of free electrons. 2) The sugar alcohols have inherent oxy-radical scavenging property, which increases with increase in the number of aliphatic hydroxyl groups (Kang *et al*, 2016). The mannitol and xylitol groups present in comacromer contributes to the radical scavenging property of hydrogels

as given in the scheme. Mannitol has more number of free hydroxyl groups available for free radical neutralization compared to xylitol. 3) The free water associated with hydrogels possess a significant role in free radical dilution. The higher equilibrium water content of hydrogel is favorable for radical dilution. The figure - 54 narrates the mechanism of free radical scavenging by PEAM-P hydrogel prepared from mannitol-fumarate-poly ethylene adipate-fumarate-PEG comacromer.

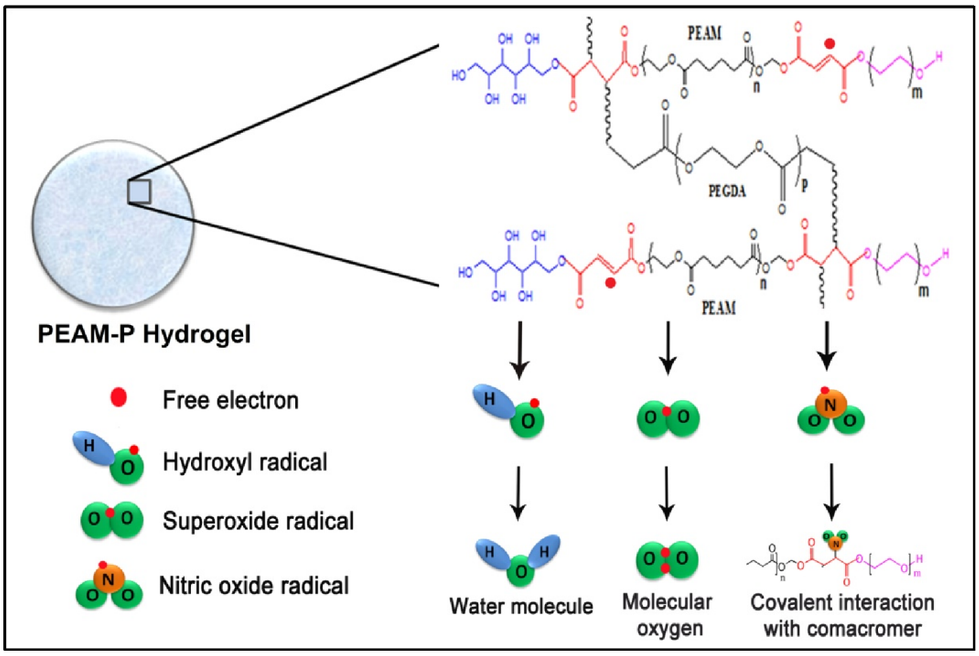

Figure - 54: Mechanism of free radical scavenging by PEAM-P hydrogel.

Grill *et al*., 1992 have identified the concentration of oxygen-centered free radicals in rabbit heart during reperfusion after myocardial ischemic injury. During normal perfusion, the maximum concentration of radical is 1.8 ± 0.8 µM that has increased to 13.0 ± 2.5 µM after 30 min of ischemic injury followed by reperfusion. In the present study, the cells are treated with 70 µM of stress inducing media, which is effectively scavenged or neutralized by the hydrogels,

especially SP 17 and PEAM-P hydrogels. The hydrogels are crosslinked structures with a huge number of reactive centers available for reducing even higher concentration of different type of free radicals. Therefore, the present hydrogels can easily mitigate the oxidative stress at the infarct zone followed by ischemic injury.

5.8. Encapsulation of cardiomyoblast cells inside the hydrogels

The viability and proliferation of injected cells are detrimental for regenerative therapy, especially when mixed with the hydrogel formulation containing toxic monomers. The viability of cells inside the hydrogel is influenced by the porosity, free water content and mechanical stiffness of hydrogel. The major challenge is to protect the cells from monomers and free radicals during gelation. The nature of encapsulated cells largely depends on the bulk characteristics of the hydrogel substrates. In the present hydrogels systems, the encapsulated cardiomyoblast cells appear with spherical morphology inside the hydrogels compared to the cells in 2D culture (Figure - 46). Koh *et al* (2002) have reported round morphology of 3T3 fibroblast cells encapsulated in PEG microgels. The shape and polarity of cells depend on the mechanical and physical characteristic of external microenvironment (Moraes *et al*, 2014). The cells can alter their morphology based on the shape of the lodging space in the matrix. In 3D culture system (even in tissues), the cell-matrix interaction and the tension state decides the polarity of cells in the microtubule dependent or independent pathways. Rhee *et al* reported that the fibroblast cells under low tension retain the microtubule-mediated cell shape including dendritic extensions, whereas higher tension drive towards the circular morphology and loss of polarity (Rhee *et al*,

2007). The tension on cells inside the hydrogels is higher than in 2D culture, which causes the loss of extended cell morphology in 3D culture. The simultaneous cell extension by integrins on both dorsal and ventral sides and the extra mechanical intrusion by the external matrix are also responsible for the cell plasticity in the 3D culture system.

5.8.1. Proliferation of encapsulated cells

The long-term viability of encapsulated cardiomyoblast cells is a challenge in designing synthetic cell carriers. Park *et al* (2009) have reported the stem cell-encapsulated OPF 10K hydrogel for cartilage tissue engineering with decreasing DNA content of encapsulated cells after 14 days of culture. Wu *et al* (2014) have reported negligible proliferation of encapsulated mesenchymal stem cell in PEGS-M hydrogel after 2 weeks, which was attributed to the absence of cell adhesion sites in the synthetic hydrogel. Nuttelman *et al* (2005) also reported the similar observation in mesenchymal stem cell-encapsulated PEG hydrogels; the viability of MSC decreases to 15% after 1 week of culture. Kim *et al* (2008) have reported photopolymerized PEGSDA hydrogels for rat MSC encapsulation. However, the percentage of viable cells inside the hydrogel is not increased even after 15 days of culture. At this scenario, the cardiomyoblast cells encapsulated in the present hydrogels undergo significant proliferation on culture. The density of cells inside the hydrogels after 30 days of culture is higher than the initially encapsulated density. In poly(propylene fumarate) based hydrogels, the PP6 and SP 17 hydrogels exhibit increasing the density of encapsulated cells on *in vitro* culture, which reaches slightly higher than the initially encapsulated density after 30 days of culture (Figure - 47). In sugar alcohol based hydrogels, the

proliferation of encapsulated cells is higher in PEAX-P hydrogels on first two weeks of culture, however, higher cell density is observed with mannitol containing PEAM-P hydrogels after 30 days of culture (Figure - 48). The proliferation of cells occurs slowly inside the PS50P hydrogel (Figure - 49).

Comparatively, higher cell density is observed in PEAM-P hydrogel prepared from mannitol-fumarate-poly ethylene adipate-fumarate-PEG comacromer after 30 days of culture. Tanahashi and Mikos, 2002 have studied the factors limiting smooth muscle cell adhesion on hydrogels. They have identified hydrophilicity of hydrogel as a retarding factor for cell adhesion. In the present comacromers, the monomer ratio effectively balances the hydrophilic and hydrophobic groups. The amphiphilic nature of the present comacromers can improve the interaction with proteins and enhance the cell adhesion and proliferation inside the hydrogels. Cui *et al* (2014) have reported less than 80% viability for cardiomyoblast cells encapsulated in tetraaniline conjugated PolyNIPAM hydrogel after 7 days of *in vitro* culture. Dong *et al* (2016) have studied the cell encapsulation efficiency of a self-healing conductive hydrogel prepared from chitosan-graft-aniline tetramer and di benzaldehyde-terminated poly(ethylene glycol). They have studied the cell proliferation up to 3 days of *in vitro* culture. However, in the present studies, we have analyzed the long-term cell encapsulation efficiency of sulfonated polyaniline containing PS50P hydrogel for 30 days under static *in vitro* culture. The cells proliferate slowly inside the PS50P hydrogel compared to other hydrogels, which may be due to the poor interaction of polyaniline with protein in culture media. The viability of cells inside the hydrogel even in the absence of vasculature substantiates better channeling of

nutrients and gasses throughout the hydrogels, which is beneficial to retain the cell viability even under slow vascularisation conditions of infarct zone.

5.8.2. Live dead assay

Live dead assay is a qualitative confirmatory assay to ensure the viability of cells inside the hydrogels. Green fluorescing, viable H9c2 cardiomyoblast cells are observed inside the present hydrogels (Figure - 50, 51, 52). In poly(propylene fumarate) based hydrogels, SP 17 hydrogel exhibit comparatively higher cell density after 30 days of culture (Table - 14). The higher cell density is observed in sugar alcohol based PEAM-P hydrogel, which confirms the results obtained from MTT assay (Table - 14). The lower viable cell density is observed in PS50P hydrogel, which confirms the poor proliferation of cells inside the hydrogel. The diffusion of oxygen in tissue-engineered scaffold reaches up to 100 μm depth from the surface (Moraes *et al*, 2014). However, the wider interconnected internal pores in the present hydrogels facilitate diffusion of media and oxygen beyond oxygen transfer limit, which assist cell viability even at deeper layers. In the present studies, mostly viable cells are observed inside the hydrogels from the surface to bottom. The absence of dead cells even after 30 days of culture reveals the potential application of hydrogel for long-term cell encapsulation.

5.8.3. Histological evaluation

The hemalum binds DNA and stains nucleus blue, whereas eosin stains connective tissue, cytoplasm and other extracellular substances in various shades of pink. The H&E staining of the present cell-encapsulated hydrogels reveals the presence of extracellular matrix proteins stained pink in color inside the hydrogels (Figure - 53). H & E staining confirms the extracellular matrix modeling by the

viable cells inside the hydrogels. Clusters of cardiomyoblast cells with cytoplasm stained in dark red color are observed all over the hydrogels, which ascertain the proliferation of cells inside the hydrogel. The H&E stained internal sections of PEAM-P hydrogel prepared from mannitol-fumarate-poly ethylene adipate-fumarate-PEG comacromer exhibit uniform distribution of stained regions comparable to the native cardiac extracellular matrix.

In summary, among the poly(propylene fumarate) based hydrogels, SP 17 hydrogel exhibit elastic nature, higher free radical scavenging property and better encapsulated cell viability as a carrier. In sugar alcohol based hydrogels, PEAM-P hydrogel exhibit higher in vitro biomechanical ageing stability, free radical scavenging property, and viable encapsulated cell density compared to PEAX-P hydrogel. The polyaniline based PS50P hydrogel has electrical conductivity and elastic characteristics desirable for the cardiac application.

CHAPTER 6

SUMMARY AND CONCLUSIONS

6 Summary and conclusions

The ischemic myocardial injury is the primary cause of recurrent heart failure and cardiac arrest. The current pharmacological and device-based cardiac therapy fails to prevent ventricular remodeling and recurrent heart failure. Cell-based regenerative therapy is the practical solution for post-infarcted myocardial repair. Recently, various biocompatible materials have emerged as cell carriers to augment safe delivery of potential cells for cardiac regenerative therapy. Among these materials, the hydrogels are preferred due to the soft tissue-like viscoelasticity, high water holding capacity and porous internal morphology. The injectable hydrogels augment minimally invasive cell delivery in a one-step procedure. However, the hydrogels for cardiac applications must satisfy stringent and diagonally opposite physical characteristics, which is difficult to optimize with biological materials. The hydrogels derived from synthetic polymers are preferred for cardiac cell therapy. However, these hydrogels are rarely explored for cell encapsulation due to the poor cell adhesion, proliferation and toxicity of monomers when mixed with selected population of cells. Even with protective cell carriers, the oxidative stress at infarct border zone induces apoptosis in delivered cells. Therefore, the major objectives of the present study were to

develop biocompatible, synthetic and injectable hydrogel materials with inherent free radical scavenging property for long-term cardiac cell encapsulation.

The oligomeric polyester comacromers were synthesized for hydrogel preparation. Three types of comacromers based on poly (propylene fumarate), sugar alcohol and polyaniline were synthesized by melt condensation reaction, which includes poly(propylene fumarate- co- ethylene glycol) (PP), poly(propylene fumarate-co-sebacate-co-ethylene glycol) (SP), mannitol-fumarate-poly(ethylene adipate)-fumarate-PEG (PEAM), xylitol-fumarate-poly(ethylene adipate)-fumarate-PEG (PEAX), polyaniline emeraldine salt conjugated fumarate-PEG-sebacate (PANIE-P) and sulfonated polyaniline conjugated fumarate-PEG-sebacate (PANIS-P) comacromers. Poly(propylene fumarate) is an unsaturated linear polyester that degrades into fumaric acid and propylene glycol. Sugar alcohols like xylitol and mannitol are condensed with the poly(ethylene adipate)-fumarate comacromer to PEAX and PEAM comacromers. The sugar alcohols have inherent oxyradical scavenging property which imparts free radical scavenging property to the hydrogels. The electrically conducting polyaniline is condensed with the fumarate-PEG-sebacate oligomer to synthesize electrically responsive, water-soluble comacromer. The electroactive hydrogels can impart better electrical coupling and alignment of engrafted cells with the surrounding myocardium.

The FT-IR and ^{1}H-NMR analysis of comacromers confirmed the formation of polyesters and the presence of fumarate double bonds, which is responsible for *in situ* crosslinking. The FT-IR and ^{1}H-NMR analysis supported by UV-Visible spectroscopy confirmed the conjugation of polyaniline with the

fumarate-PEG-sebacate oligomer. The injectable hydrogels were prepared by free radical initiated crosslinking of comacromers with poly(ethylene glycol) diacrylate by conventional two-component APS/TEMED system. PP6, SP 17, PEAM-P, PEAX-P, PE50P and PS50P hydrogels were prepared from PP, SP, PEAM, PEAX, PANIE-P and PANIS-P comacromers respectively. The gelation time and rise in temperature during gelation of hydrogels were suitable for *in situ* application.

The studies on swelling characteristics of the present hydrogels account for the hydrophilic and porous nature. Higher equilibrium water content in hydrogels impart better diffusion of extracellular fluids containing essential nutrients into the hydrogel matrix, which is beneficial for the maturation and proliferation of cells inside the hydrogel. PP6 and PS50P hydrogels exhibit comparatively higher equilibrium water content in poly(propylene fumarate) based and polyaniline based hydrogels respectively. In sugar alcohol based hydrogels, both PEAX-P and PEAM-P hydrogels exhibit similar water affinity.

DSC analysis of swollen hydrogels showed a higher fraction of freezable free water content than bound water inside the hydrogels. The PEAM-P hydrogel has comparable fractions of free and bound water at equilibrium swelling. The alcohol groups associated with mannitol forms hydrogen bonds with water on swelling, which is responsible for a higher fraction of bound water in PEAM-P hydrogel. The free water present in the hydrogels ensures the uninterrupted cycling of nutrients, metabolites and essential gasses inside the hydrogel matrix, which is favorable to retain the viability of encapsulated cells under slow

vascularisation conditions. The bound water can improve the interaction of cells with hydrogel matrix.

The ESEM analyses of the present hydrogels reveal the smaller surface pores and wide internal interconnected pores. The smaller surface pores limit the water diffusion and reduce the hydrolytic degradation of the bulk hydrogel. The wider interconnected pores improve the nutrient diffusion all over the hydrogel within a short duration. Moreover, the porosity of hydrogels may improve vascularization after implantation. The size of the surface pores influences the size of the blood vessels, while the interconnectivity of internal pores influences the blood vessel density. The PEAM-P and PE50P hydrogels have aligned internal pores, which are suitable for the growth and proliferation of cardiomyocytes and endothelial cells.

The studies on mechanical strength and stress-strain behavior of hydrogels reveal mechanical stability and elastic characteristics desirable for cardiac applications. The present hydrogels have Young modulus in the range of native myocardium. The PEAM-P and PS50P hydrogels, which exhibit higher mechanical stiffness in the range of native myocardium even after 30 days of *in vitro* ageing, confirm better mechanical stability. The PP6, SP 17 and PEAM-P hydrogels do not collapse at compressive stress higher than the maximum stress observed with the native myocardium. The hydrogels exhibit J-shaped stress-strain graph, which indicates higher extension at smaller compressive stress substantiates the elastic nature. The SP 17, PE50P and PS50P hydrogels exhibit maximum extensibility without collapsing at 60% compression and plastic deformation. The higher stiffness with elastic nature can prevent the collapse of

hydrogel even under strong contraction and relaxation dynamics of the myocardium.

The evaluation of electrical resistance of polyaniline-based hydrogels confirmed electrical conductivity. The present polyaniline-based hydrogels have an electrical conductivity higher than the native myocardium, which is suitable for the myocardial applications. The electrical conductivity of PANIE-P/PEGDA and PANIS-P/PEGDA based hydrogels is increased with the increase of the concentration of comacromers. The hydrogels with sulfonated polyaniline exhibit comparatively higher conductivity. The sulfonation of PANI causes the conformational transition of PANI backbone from the compact coil to the expanded coil, which increases the charge transfer and electrical conductivity.

The MTT assay of L929 cells incubated with the extracts from the present hydrogels proved the cytocompatibility of hydrogels as per ISO10993-5, annexure C. The observations from direct contact assay and live-dead assay confirmed the compatibility of the present hydrogels with L929 cells. The compatibility of the present hydrogels with blood cells is revealed with the hydrogels exhibiting negligible hemolysis, which is acceptable for *in vivo* application, especially the PEAM-P and PS50P hydrogels.

The biochemical assays on different free radicals are conducted with the present hydrogels to assess the scavenging property. The PP6, SP 17, PEAX-P, PEAM-P and PS50P hydrogels exhibit DPPH radical scavenging percentage comparable to ascorbic acid. The PEAX-P, PEAM-P and PS50P hydrogels exhibit hydroxyl radical scavenging property, with comparatively higher scavenging

effect by PEAM-P hydrogel. The present hydrogels exhibit a moderate scavenging effect on nitric oxide radicals, which is beneficial to control the transition of nitric oxide radical concentration from physiological to pathological level at inflamed or infarcted tissues. The present hydrogels, especially PEAM-P and PEAX-P hydrogels exhibit higher reducing power, as a measure of antioxidant property.

The *in vitro* studies on cardiomyoblast cells treated with stress inducing media in the presence of hydrogels confirmed the protective effect of hydrogels over cardiomyoblast cells from deleterious active hydroxyl radicals. The viability of cells treated with stress inducing media is maintained in the presence of the present hydrogels. The cells treated with PEAM-P and SP 17 hydrogels exhibit 75% and 86% cell viability, which is comparatively higher than ascorbic acid-treated cells. The live-dead assay and DCFH-DA assay confirmed the protective effect of PEAM-P and SP 17 hydrogels over cardiomyoblast cells under oxidative stress.

As the hydrogels are crosslinked networks, the mechanism of free radical scavenging will be different and complicated compared to other soluble antioxidant molecules. The scavenging mechanism is proposed as 1) neutralization of free radicals through free π electrons associated with uncrosslinked fumarate double bonds in comacromer. 2) The sugar alcohols have inherent oxyradical scavenging property, which increases with increase in the number of aliphatic hydroxyl groups. The mannitol and xylitol groups present in comacromer contributes to the radical scavenging property of hydrogels. 3) The free water associated with hydrogels has a significant role in free radical dilution.

The higher equilibrium water content of hydrogel is favorable for radical dilution. Moreover, the hydrogels are crosslinked structures with a huge number of reactive centers available for reducing even higher concentration of a different type of free radicals. Therefore, the present hydrogels, especially PEAM-P hydrogel, can easily mitigate the oxidative stress at the infarct zone followed by ischemic injury.

The studies on proliferation and viability of cardiomyoblast cells encapsulated inside the present hydrogels reveal long-term viability, significant proliferation and uniform distribution of cells inside the hydrogels. The density of cells inside the hydrogels after 30 days of culture was higher than the initially encapsulated density. Comparatively, higher cell density was observed in PEAM-P hydrogel after 30 days of culture. The viability of encapsulated cells even at deeper layers substantiate the proper diffusion of media and oxygen throughout the hydrogel matrix supported by wide interconnected internal porosity. H & E staining confirmed the extracellular matrix modeling by the viable cells inside the hydrogels. The H&E stained internal sections of PEAM-P hydrogel showed a uniform distribution of stained regions comparable to the native cardiac extracellular matrix.

Overall, PEAM-P hydrogel is preferable with synergistic properties of biomechanical stability, free radical scavenging ability and cell proliferation for cardiac regenerative therapy.

6.1. Future prospects of the investigation

The success of cardiac regenerative therapy relies on the safe delivery of cells in the injectable formulation to the infarct zone of the myocardium. The injectable hydrogels can be delivered via an intracoronary, trans-endocardial or epicardial method to the myocardium. The regurgitation of injectable formulation into the blood and chance of emboli formation is higher for the trans-endocardial method. Recently, an alternative method; subxiphoid trans-epicardial approach, is reported to deliver the cells to the myocardium, which avoid the chances of emboli formation. In the present study, PEAM-P hydrogel prepared from mannitol-fumarate-poly (ethylene adipate)-fumarate-PEG comacromer has favorable characteristics for cardiac cell therapy. The future studies aim to standardize the PEAM-P hydrogel for delivery through subxiphoid trans-epicardial method.

The present PEAM-P hydrogel has adequate biomechanical stability and inherent free radical scavenging property and long-term viability of encapsulated cells, which are the major requirements for cardiac application. Further, functionalizing the present PEAM-P hydrogel with cell adhesion peptides, RoY peptides, and angiogenic factors can improve the tissue formation and vascularization at infarct zone.

The myofibroblast at the infarct zone has lower electrical conduction compared to cardiomyocytes, which results in arrhythmia and myocardial remodeling. However, the myofibroblast has structural and functional characteristics close to cardiomyocytes. Therefore, the *in situ* differentiation of

myofibroblast at the infarct zone to functional cardiomyocytes can open up a practical therapeutic strategy. Therefore, the future studies aim to identify the suitable factors to induce differentiation of myofibroblasts to cardiomyocyte. Further, the standardized formulation of the candidate PEAM-P hydrogel can be employed to deliver the required factors at the infarct zone for cardiomyocyte generation. The combined action of bulking effect by the hydrogel matrix and cardiomyocyte generation by the delivered factors may improve the regenerative repair of the post-infarcted myocardium.

References

Annabi N, Nichol JW, Zhong X, *et al* (2010) Controlling the porosity and microarchitecture of hydrogels for tissue engineering. *Tissue Eng Part B Rev* 16:371–383.

Ayala A, Munoz MF, Argüelles S (2014) Lipid Peroxidation: Production, Metabolism, and Signaling Mechanisms of Malondialdehyde and 4-Hydroxy-2-Nonenal, Lipid Peroxidation: Production, Metabolism, and Signaling Mechanisms of Malondialdehyde and 4-Hydroxy-2-Nonenal. *Oxidative Med Cell Longev* 2014:e360438- e360469.

Balint R, Cassidy NJ, Cartmell SH (2014) Conductive polymers: Towards a smart biomaterial for tissue engineering. *Acta Biomater* 10:2341–2353.

Bolli R, Chugh AR, Amario D, *et al* (2011) Effect of Cardiac Stem Cells in Patients with Ischemic Cardiomyopathy: Initial Results of the SCIPIO Trial. *Lancet* 378:1847–1857.

Boyle A, McNiece I, Hare J (2010) Mesenchymal Stem Cell Therapy for Cardiac Repair. In: Lee RJ (ed) *Stem Cells Myocard. Regen.* Humana Press, pp 65–84

Bruggeman JP, de Bruin BJ, Bettinger CJ, Langer R (2008) Biodegradable poly(polyol sebacate) polymers. *Biomaterials* 29:4726–4735.

Bui AL, Horwich TB, Fonarow GC (2011) Epidemiology and risk profile of heart failure. *Nat Rev Cardiol* 8:30–41.

Burridge PW, Keller G, Gold JD, Wu JC (2012) Production of De Novo Cardiomyocytes: Human Pluripotent Stem Cell Differentiation and Direct Reprogramming. *Cell Stem Cell* 10:16–28.

Chandy T, Rao GHR, Wilson RF, Das GS (2003) The development of porous alginate/elastin/PEG composite matrix for cardiovascular engineering. *J Biomater Appl* 17:287–301.

Chang MY, Huang TT, Chen CH, *et al* (2016) Injection of Human Cord Blood Cells With Hyaluronan Improves Postinfarction Cardiac Repair in Pigs. *Stem Cells Transl Med* 5:56–66.

Chen K, Keaney JF (2012) Evolving concepts of oxidative stress and reactive oxygen species in cardiovascular disease. *Curr Atheroscler Rep* 14:476–483.

Chiu Y-C, Cheng M-H, Engel H, *et al* (2011) The role of pore size on vascularization and tissue remodeling in PEG hydrogels. *Biomaterials* 32:6045–6051.

Choi B, Loh XJ, Tan A, *et al* (2015) Introduction to *In situ* Forming Hydrogels for Biomedical Applications. In: Loh XJ (ed) *–In situ gelling polymer*. Springer Singapore, pp 5–35.

Christman KL, Fok HH, Sievers RE, *et al* (2004a) Fibrin glue alone and skeletal myoblasts in a fibrin scaffold preserve cardiac function after myocardial infarction. *Tissue Eng* 10:403–409.

Christman KL, Vardanian AJ, Fang Q, *et al* (2004b) Injectable fibrin scaffold improves cell transplant survival, reduces infarct expansion, and induces neovasculature formation in ischemic myocardium. *J Am Coll Cardiol* 44:654–660.

Colvin Adams M, Smith JM, Heubner BM, *et al* (2015) OPTN/SRTR 2013 Annual Data Report: heart. *Am J Transplant Off J Am Soc Transplant Am Soc Transpl Surg* 15 Suppl 2:1–28.

Crowder SW, Liang Y, Rath R, *et al* (2013) Poly(ε-caprolactone)-carbon nanotube composite scaffolds for enhanced cardiac differentiation of human mesenchymal stem cells. *Nanomed* 8:1763–1776.

Cui H, Liu Y, Cheng Y, *et al* (2014) *In vitro* study of electroactive tetraaniline-containing thermosensitive hydrogels for cardiac tissue engineering. *Biomacromolecules* 15:1115–1123.

Dai W, Wold LE, Dow JS, Kloner RA (2005) Thickening of the infarcted wall by collagen injection improves left ventricular function in rats: a novel approach to preserve cardiac function after myocardial infarction. *J Am Coll Cardiol* 46:714–719.

Dash R, Acharya C, Bindu PC, Kundu SC (2008) Antioxidant potential of silk protein sericin against hydrogen peroxide-induced oxidative stress in skin fibroblasts. *BMB Rep* 41:236–241.

Dhandayuthapani B, Yoshida Y, Maekawa T, *et al* (2011) Polymeric Scaffolds in Tissue Engineering Application: A Review, Polymeric Scaffolds in Tissue Engineering Application: A Review. *Int J Polym Sci Int J Polym Sci* 2011:e290602- e290621.

Dobner S, Bezuidenhout D, Govender P, *et al* (2009) A synthetic non-degradable polyethylene glycol hydrogel retards adverse post-infarct left ventricular remodeling. *J Card Fail* 15:629–636.

Dong R, Zhao X, Guo B, Ma PX (2016) Self-Healing Conductive Injectable Hydrogels with Antibacterial Activity as Cell Delivery Carrier for Cardiac Cell Therapy. *ACS Appl Mater Interfaces* 8:17138–17150.

Dvir T, Timko BP, Brigham MD, *et al* (2011) Nanowired three-dimensional cardiac patches. *Nat Nanotechnol* 6:720–725.

Elloumi-Hannachi I, Yamato M, Okano T (2010) Cell sheet engineering: a unique nanotechnology for scaffold-free tissue reconstruction with clinical applications in regenerative medicine. *J Intern Med* 267:54–70.

El-Sherbiny IM, Yacoub MH (2013) Hydrogel scaffolds for tissue engineering: Progress and challenges. *Glob Cardiol Sci Pract* 2013: 316–342.

Fariba Ganji SVF (2010) Theoretical Description of Hydrogel Swelling: A Review. *Iran Polym J* 19:375–398.

Fossatti D, José da Silva W, Queiroz de Mello RM (2011) Electrochromism and conductivity of sulfonated polyaniline films in propylene carbonate. *Mediterr J Chem* 1:180–191.

Francis MP, Sachs PC, Elmore LW, Holt SE (2010) Isolating adipose-derived mesenchymal stem cells from lipoaspirate blood and saline fraction. *Organogenesis* 6:11–14.

Fujimoto KL, Ma Z, Nelson DM, *et al* (2009) Synthesis, characterization and therapeutic efficacy of a biodegradable, thermoresponsive hydrogel designed for application in chronic infarcted myocardium. *Biomaterials* 30:4357–4368.

Gaffey AC, Chen MH, Venkataraman CM, *et al* (2015) Injectable shear-thinning hydrogels used to deliver endothelial progenitor cells, enhance cell engraftment, and improve ischemic myocardium. *J Thorac Cardiovasc Surg* 150:1268–1277.

Gálvez-Montón C, Prat-Vidal C, Roura S, *et al* (2013) Cardiac Tissue Engineering and the Bioartificial Heart. *Rev Esp Cardiol Engl Ed* 66:391–399.

Gepstein L, Ding C, Rahmutula D, *et al* (2010) *In vivo* assessment of the electrophysiological integration and arrhythmogenic risk of myocardial cell transplantation strategies. *Stem Cells Dayt Ohio* 28:2151–2161.

Gerecht S, Townsend SA, Pressler H, *et al* (2007) A porous photocurable elastomer for cell encapsulation and culture. *Biomaterials* 28:4826–4835.

Gheorghiade M, Colucci WS, Swedberg K (2003) β-Blockers in Chronic Heart Failure. *Circulation* 107:1570–1575.

Gizdavic-Nikolaidis M, Travas-Sejdic J, Bowmaker GA, *et al* (2004) The antioxidant activity of conducting polymers in biomedical applications. *Curr Appl Phys* 4:347–350.

Gnecchi M, Zhang Z, Ni A, Dzau VJ (2008) Paracrine Mechanisms in Adult Stem Cell Signaling and Therapy. *Circ Res* 103:1204–1219.

Go AS, Mozaffarian D, Roger VL, *et al* (2014) Heart Disease and Stroke Statistics--2014 Update: A Report From the American Heart Association. *Circulation* 129:e28–e292.

Grill HP, Zweier JL, Kuppusamy P, *et al* (1992) Direct measurement of myocardial free radical generation in an *in vivo* model: Effects of postischemic reperfusion and treatment with human recombinant superoxide dismutase. *J Am Coll Cardiol* 20:1604–1611.

Guarino V, Alvarez-Perez MA, Borriello A, *et al* (2013) Conductive PANi/PEGDA macroporous hydrogels for nerve regeneration. *Adv Healthc Mater* 2:218–227.

Guo W, Frey MT, Burnham NA, Wang Y (2006) Substrate Rigidity Regulates the Formation and Maintenance of Tissues. *Biophys* J 90:2213–2220.

Gutteridge JM, Halliwell B (1988) The deoxyribose assay: an assay both for "free" hydroxyl radical and for site-specific hydroxyl radical production. *Biochem J* 253:932–933.

Habib M, Shapira-Schweitzer K, Caspi O, *et al* (2011) A combined cell therapy and in-situ tissue-engineering approach for myocardial repair. *Biomaterials* 32:7514–7523.

Habib S, Ali A (2011) Biochemistry of Nitric Oxide. *Indian J Clin Biochem* 26:3–17.

Hasan A, Khattab A, Islam MA, *et al* (2015) Injectable Hydrogels for Cardiac Tissue Repair after Myocardial Infarction. *Adv Sci* 2:1-18.

Hastings CL, Roche ET, Ruiz-Hernandez E, *et al* (2015) Drug and cell delivery for cardiac regeneration. *Adv Drug Deliv Rev* 84:85–106.

Henslee AM, Yoon DM, Lu BY, *et al* (2014) Characterization of an injectable, degradable polymer for mechanical stabilization of mandibular fractures: use of injectable PPF formulations. *J Biomed Mater Res B Appl Biomater* 103: 529-38.

Hichem B, Kaddour G, Imene B (2014) Synthesis and *in vitro* bio degradation of poly(ethylene adipate- co-D,L-lactic acid) copolymers (PLEA). *Orient J Chem* 30:1061–1069.

Hsu W-T, Jui H-Y, Huang Y-H, *et al* (2015) CXCR4 Antagonist TG-0054 Mobilizes Mesenchymal Stem Cells, Attenuates Inflammation, and Preserves Cardiac Systolic Function in a Porcine Model of Myocardial Infarction. *Cell Transplant* 24:1313–1328.

Hunt JA, Chen R, van Veen T, Bryan N (2014) Hydrogels for tissue engineering and regenerative medicine. *J Mater Chem B* 2:5319–5338.

Ifkovits JL, Tous E, Minakawa M, *et al* (2010) Injectable hydrogel properties influence infarct expansion and extent of postinfarction left ventricular remodeling in an ovine model. *Proc Natl Acad Sci U S A* 107:11507–11512.

Janaswamy P, Walters TE, Nazer B, Lee RJ (2016) Current Treatment Strategies for Heart Failure: Role of Device Therapy and LV Reconstruction. *Curr Treat Options Cardiovasc Med* 18:57.

Janssens S, Dubois C, Bogaert J, *et al* (2006) Autologous bone marrow-derived stem-cell transfer in patients with ST-segment elevation myocardial infarction: double-blind, randomised controlled trial. *The Lancet* 367:113–121.

Jeswani G, Alexander A, Saraf S, *et al* (2015) Recent approaches for reducing hemolytic activity of chemotherapeutic agents. *J Control Release Off J Control Release Soc* 211:10–21.

Jiang XJ, Wang T, Li XY, *et al* (2009) Injection of a novel synthetic hydrogel preserves left ventricle function after myocardial infarction. *J Biomed Mater Res A* 90:472–477.

Jose GM, Radhakrishnan A, Muraleedhara Kurup G (2015) Antioxidant and antimitotic activities of sulfated polysaccharide from marine brown algae Padina tetrastromatica. *J Phytol.* 7: 39-51.

Kajstura J, Zhang X, Reiss K, *et al* (1994) Myocyte cellular hyperplasia and myocyte cellular hypertrophy contribute to chronic ventricular remodeling in coronary artery narrowing-induced cardiomyopathy in rats. *Circ Res* 74:383–400.

Kang KW, Kwak SH, Yun SY, Kim SK (2007) Evaluation of Antioxidant Activity of Sugar Alcohols Using TOSC (Total Oxy-radical Scavenging Capacity) Assay. *J. Toxicol.* 23: 143-150.

Kemp CD, Conte JV (2012) The pathophysiology of heart failure. *Cardiovasc Pathol* 21:365–371.

Kim J, Hefferan TE, Yaszemski MJ, Lu L (2009) Potential of hydrogels based on poly(ethylene glycol) and sebacic acid as orthopedic tissue engineering scaffolds. *Tissue Eng Part A* 15:2299–2307.

Kim J, Lee KW, Hefferan TE, *et al* (2008) Synthesis and evaluation of novel biodegradable hydrogels based on poly(ethylene glycol) and sebacic acid as tissue engineering scaffolds. *Biomacromolecules* 9:149–157.

Knollmann BC (2013) Induced Pluripotent Stem Cell–Derived Cardiomyocytes Boutique Science or Valuable Arrhythmia Model? *Circ Res* 112:969–976.

Komeri R, Thankam FG, Muthu J (2015) Influence of matrix and bulk behaviour of an injectable hydrogel on the survival of encapsulated cardiac cells. *RSC Adv* 5:31439–31449.

Komeri R, Muthu J (2016) *In situ* crosslinkable elastomeric hydrogel for long-term cell encapsulation for cardiac applications. *J Biomed Mater Res A*. 12: 2936-2944.

Komeri R, Thankam FG, Muthu J (2017) Free radical scavenging injectable hydrogels for regenerative therapy. *Mater Sci Eng C* 71:100–110.

Kortsmit J, Davies NH, Miller R, *et al* (2013) The effect of hydrogel injection on cardiac function and myocardial mechanics in a computational post-infarction model. *Comput Methods Biomech Biomed Engin* 16:1185–1195.

Kutty JK, Cho E, Soo Lee J, *et al* (2007) The effect of hyaluronic acid incorporation on fibroblast spreading and proliferation within PEG-diacrylate based semi-interpenetrating networks. *Biomaterials* 28:4928–4938.

Landa N, Miller L, Feinberg MS, *et al* (2008) Effect of injectable alginate implant on cardiac remodeling and function after recent and old infarcts in rat. *Circulation* 117:1388–1396.

Le Visage C, Gournay O, Benguirat N, *et al* (2012) Mesenchymal stem cell delivery into rat infarcted myocardium using a porous polysaccharide-based scaffold: a quantitative comparison with endocardial injection. *Tissue Eng Part A* 18:35–44.

Leonard SS, Harris GK, Shi X (2004) Metal-induced oxidative stress and signal transduction. *Free Radic Biol Med* 37:1921–1942.

Leor J, Tuvia S, Guetta V, *et al* (2009) Intracoronary injection of *in situ* forming alginate hydrogel reverses left ventricular remodeling after myocardial infarction in Swine. *J Am Coll Cardiol* 54:1014–1023.

Leri A, Kajstura J, Anversa P (2011) Role of Cardiac Stem Cells in Cardiac Pathophysiology: A Paradigm Shift in Human Myocardial Biology. *Circ Res* 109:941–961.

Li J, Shu Y, Hao T, *et al* (2013) A chitosan-glutathione based injectable hydrogel for suppression of oxidative stress damage in cardiomyocytes. *Biomaterials* 34:9071–9081.

Li L, Ge J, Guo B, Ma PX (2014) *In situ* forming biodegradable electroactive hydrogels. *Polym Chem* 5:2880–2890.

Liochev SI, Fridovich I (2002) The Haber-Weiss cycle -70 years later: an alternative view. *Redox Rep Commun Free Radic Res* 7:55–57.

Liu J, Wang H, Wang Y, *et al* (2014) Exendin-4 Pretreated Adipose Derived Stem Cells Are Resistant to Oxidative Stress and Improve Cardiac Performance via Enhanced Adhesion in the Infarcted Heart. *PLoS ONE* 9:e99756.

Lo B, Parham L (2009) Ethical Issues in Stem Cell Research. *Endocr Rev* 30:204–213.

Lovett M, Lee K, Edwards A, Kaplan DL (2009) Vascularization Strategies for Tissue Engineering. *Tissue Eng Part B Rev* 15:353–370.

Lu L, Quinn MT, Sun Y (2004) Oxidative stress in the infarcted heart: role of de novo angiotensin II production. *Biochem Biophys Res Commun* 325:943–951.

Lü S, Gao C, Xu X, *et al* (2015) Injectable and Self-Healing Carbohydrate-Based Hydrogel for Cell Encapsulation. *ACS Appl Mater Interfaces* 7:13029–13037.

Lundy SD, Gantz JA, Pagan CM, *et al* (2014) Pluripotent Stem Cell Derived Cardiomyocytes for Cardiac Repair. *Curr Treat Options Cardiovasc Med* 16:1–17.

Ma Y, de Castro Brás LE, Toba H, *et al* (2014) Myofibroblasts and the extracellular matrix network in post-myocardial infarction cardiac remodeling. *Pflüg Arch - Eur J Physiol*. 466:1113-27.

Mäkinen KK (2010) Sugar Alcohols, Caries Incidence, and Remineralization of Caries Lesions: A Literature Review. *Int J Dent*. 2010: 1-23.

Mamajanov I, MacDonald P, Ying J, *et al* (2014) Ester Formation and Hydrolysis during Wet–Dry Cycles: Generation of Far-from-Equilibrium Polymers in a Model Prebiotic Reaction. *Macromolecules* 47:1334–1343.

Maron BA, Leopold JA (2010) Aldosterone Receptor Antagonists. *Circulation* 121:934–939.

Martin AW, Eng G, Caridade SG, *et al* (2014) Electrically Conductive Chitosan/Carbon Scaffolds for Cardiac Tissue Engineering. *Biomacromolecules* 15:635–643.

Matsuo T, Masumoto H, Tajima S, *et al* (2015) Efficient long-term survival of cell grafts after myocardial infarction with thick viable cardiac tissue entirely from pluripotent stem cells. *Sci Rep* 5:16842-16856.

McDevitt TC, Woodhouse KA, Hauschka SD, *et al* (2003) Spatially organized layers of cardiomyocytes on biodegradable polyurethane films for myocardial repair. *J Biomed Mater Res A* 66:586–595.

Moad G, Solomon DH (2005) *Radical Reactions*. In: Chem. Radic. Polym. Second Ed. Elsevier Science Ltd, Amsterdam, pp 11–48

Molapo KM, Ndangili PM, Ajayi RF, *et al* (2012) Electronics of Conjugated Polymers (I): Polyaniline. *Int. J. Electrochem. Sci.*, 7: 11859 – 11875.

Moscona AA (1959) Tissues from dissociated cells. *Sci Am* 200:132–134.

Muehleder S, Ovsianikov A, Zipperle J, *et al* (2014) Connections Matter: Channeled Hydrogels to Improve Vascularization. *Front Bioeng Biotechnol.* 2: 52.

Muiznieks LD, Keeley FW (2013) Molecular assembly and mechanical properties of the extracellular matrix: A fibrous protein perspective. *Biochim Biophys Acta BBA - Mol Basis Dis* 1832:866–875.

Mukherjee S, Gualandi C, Focarete ML, *et al* (2011) Elastomeric electrospun scaffolds of poly(L-lactide-co-trimethylene carbonate) for myocardial tissue engineering. *J Mater Sci Mater Med* 22:1689–1699.

Nagueh SF, Shah G, Wu Y, *et al* (2004) Altered titin expression, myocardial stiffness, and left ventricular function in patients with dilated cardiomyopathy. *Circulation* 110:155–162.

Naseem KM (2005) The role of nitric oxide in cardiovascular diseases. *Mol Aspects Med* 26:33–65.

Nemir S, West JL (2010) Synthetic materials in the study of cell response to substrate rigidity. *Ann Biomed Eng* 38:2–20.

Nicodemus GD, Bryant SJ (2008) Cell Encapsulation in Biodegradable Hydrogels for Tissue Engineering Applications. *Tissue Eng Part B Rev* 14:149–165.

Nielsen S, Falk K, Gyberg A, *et al* (2015) Experiences and actions during the decision making process among men with a first acute myocardial infarction. *J Cardiovasc Nurs* 30:332–339.

Nimse SB, Pal D (2015) Free radicals, natural antioxidants, and their reaction mechanisms. *RSC Adv* 5:27986–28006.

Ott HC, Matthiesen TS, Goh S-K, *et al* (2008) Perfusion-decellularized matrix: using nature's platform to engineer a bioartificial heart. *Nat Med* 14:213–221.

Pastor N, Weinstein H, Jamison E, Brenowitz M (2000) A detailed interpretation of OH radical footprints in a TBP-DNA complex reveals the role of dynamics in the mechanism of sequence-specific binding. *J Mol Biol* 304:55–68.

Pham-Huy LA, He H, Pham-Huy C (2008) Free Radicals, Antioxidants in Disease and Health. *Int J Biomed Sci* 4:89–96.

Pillai HS, Ganapathi S (2013) Heart failure in South Asia. *Curr Cardiol Rev* 9:102–111.

Pok S, Vitale F, Eichmann SL, *et al* (2014) Biocompatible Carbon Nanotube–Chitosan Scaffold Matching the Electrical Conductivity of the Heart. *ACS Nano* 8:9822–9832.

Qazi TH, Rai R, Boccaccini AR (2014) Tissue engineering of electrically responsive tissues using polyaniline based polymers: a review. *Biomaterials* 35:9068–9086.

(Radisic M and Vunjak-Novakovic G. (2005) Cardiac tissue engineering. *J. Serb. Chem. Soc*. 70: 541-556 (2005)

Rai R, Tallawi M, Barbani N, *et al* (2013) Biomimetic poly(glycerol sebacate) (PGS) membranes for cardiac patch application. *Mater Sci Eng C* 33:3677–3687.

Reissis Y, García-Gareta E, Korda M, *et al* (2013) The effect of temperature on the viability of human mesenchymal stem cells. *Stem Cell Res Ther* 4:139.

Rony IK, Baten A, Bloomfield JA, *et al* (2015) Inducing pluripotency *in vitro*: recent advances and highlights in induced pluripotent stem cells generation and pluripotency reprogramming. *Cell Prolif* 48:140–156.

Sangameswaran B, Balakrishnan BR, Deshraj C, Jayakar B (2009) *In vitro* antioxidant activity of roots of Thespesia lampas Dalz and Gibs. *Pak J Pharm Sci* 22:368–372.

Sarker M, Chen XB, Schreyer DJ (2015) Experimental approaches to vascularisation within tissue engineering constructs. *J Biomater Sci Polym Ed* 26:683–734.

Seif-Naraghi SB, Singelyn JM, Salvatore MA, *et al* (2013) Safety and Efficacy of an Injectable Extracellular Matrix Hydrogel for Treating Myocardial Infarction. *Sci Transl Med* 5:173ra25–173ra25.

Shachar M, Cohen S (2003) Cardiac tissue engineering, ex-vivo: design principles in biomaterials and bioreactors. *Heart Fail Rev* 8:271–276.

Sheng CC, Zhou L, Hao J (2012) Current Stem Cell Delivery Methods for Myocardial Repair. *BioMed Res Int* 2013:e547902.

Shinde AV, Frangogiannis NG (2014) Fibroblasts in myocardial infarction: a role in inflammation and repair. *J Mol Cell Cardiol* 70:74–82.

Simpson DG, Terracio L, Terracio M, *et al* (1994) Modulation of cardiac myocyte phenotype *in vitro* by the composition and orientation of the extracellular matrix. *J Cell Physiol* 161:89–105.

Soukoulis V, Boden WE, Smith SC, O'Gara PT (2014) Nonantithrombotic Medical Options in Acute Coronary Syndromes Old Agents and New Lines on the Horizon. *Circ Res* 114:1944–1958.

Srivastava A, Mohanty SK (2013) Age and Sex Pattern of Cardiovascular Mortality, Hospitalisation and Associated Cost in India. *PLoS ONE* 8:e62134.

Stejskal J, Gilbert RG (2002) Polyaniline. Preparation of a conducting polymer(IUPAC Technical Report). *Pure Appl Chem*. 74: 857-867.

Stout DA, Yoo J, Santiago-Miranda AN, *et al* (2012) Mechanisms of greater cardiomyocyte functions on conductive nanoengineered composites for cardiovascular application. *Int J Nanomedicine* 7:5653–5669.

Struck E, Hagl S, Meisner H, Sebening F (1985) Heart transplantation: limitations and perspectives. *Z Für Kardiologie*. 6:59–63.

Sun Y (2009) Myocardial repair/remodelling following infarction: roles of local factors. *Cardiovasc Res* 81:482–490.

Takahashi K, Yamanaka S (2006) Induction of Pluripotent Stem Cells from Mouse Embryonic and Adult Fibroblast Cultures by Defined Factors. *Cell* 126:663–676.

Tanahashi K, Mikos AG (2002) Cell adhesion on poly(propylene fumarate-co-ethylene glycol) hydrogels. *J Biomed Mater Res* 62:558–566.

Temenoff JS, Athanasiou KA, Lebaron RG, Mikos AG (2002) Effect of poly(ethylene glycol) molecular weight on tensile and swelling properties of oligo(poly(ethylene glycol) fumarate) hydrogels for cartilage tissue engineering. *J Biomed Mater Res* 59:429–437.

Temenoff JS, Park H, Jabbari E, *et al* (2004) Thermally cross-linked oligo(poly(ethylene glycol) fumarate) hydrogels support osteogenic differentiation of encapsulated marrow stromal cells *in vitro*. *Biomacromolecules* 5:5–10.

Terracio L, Miller B, Borg TK (1988) Effects of cyclic mechanical stimulation of the cellular components of the heart: *in vitro*. *Vitro Cell Dev Biol J Tissue Cult Assoc* 24:53–58.

Thankam FG, Muthu J (2013) Biosynthetic alginate-polyester hydrogels with inherent free radical scavenging activity promote cellular response. *J Bioact Compat Polym* 28:557–573.

Thankam FG, Muthu J (2014) Biosynthetic hydrogels-Studies on chemical and physical characteristics on long-term cellular response for tissue engineering: Biosynthetic Hydrogels. *J Biomed Mater Res A* 102:2238–2247.

Tous E, Purcell B, Ifkovits JL, Burdick JA (2011) Injectable Acellular Hydrogels for Cardiac Repair. *J Cardiovasc Transl Res* 4:528–542.

Trombino S, Cassano R, Bloise E, *et al* (2009) Synthesis and antioxidant activity evaluation of a novel cellulose hydrogel containing trans-ferulic acid. *Carbohydr Polym* 75:184–188.

Tse S, Mazzola N (2015) Ivabradine (Corlanor) for Heart Failure: The First Selective and Specific If Inhibitor. *Pharm Ther* 40:810–814.

Tsur-Gang O, Ruvinov E, Landa N, *et al* (2009) The effects of peptide-based modification of alginate on left ventricular remodeling and function after myocardial infarction. *Biomaterials* 30:189–195.

Vandenburgh HH, Karlisch P, Farr L (1988) Maintenance of highly contractile tissue-cultured avian skeletal myotubes in collagen gel. *Vitro Cell Dev Biol J Tissue Cult Assoc* 24:166–174.

Venugopal JR, Prabhakaran MP, Mukherjee S, *et al* (2012) Biomaterial strategies for alleviation of myocardial infarction. *J R Soc Interface* 9:1–19.

Vidarsson H, Hyllner J, Sartipy P (2010) Differentiation of Human Embryonic Stem Cells to Cardiomyocytes for *In vitro* and *In vivo* Applications. *Stem Cell Rev Rep* 6:108–120.

Vunjak-Novakovic G, Tandon N, Godier A, *et al* (2010) Challenges in cardiac tissue engineering. *Tissue Eng Part B Rev* 16:169–187.

Wall ST, Walker JC, Healy KE, *et al* (2006) Theoretical impact of the injection of material into the myocardium: a finite element model simulation. *Circulation* 114:2627–2635.

Wang H, Liu Z, Li D, *et al* (2012) Injectable biodegradable hydrogels for embryonic stem cell transplantation: improved cardiac remodelling and function of myocardial infarction. *J Cell Mol Med* 16:1310–1320.

Wang H, Shi J, Wang Y, *et al* (2014) Promotion of cardiac differentiation of brown adipose derived stem cells by chitosan hydrogel for repair after myocardial infarction. *Biomaterials* 35:3986–3998.

Wang T, Wu DQ, Jiang XJ, *et al* (2009) Novel thermosensitive hydrogel injection inhibits post-infarct ventricle remodelling. *Eur J Heart Fail* 11:14–19.

Wang WE, Chen X, Houser SR, Zeng C (2013) Potential of cardiac stem/progenitor cells and induced pluripotent stem cells for cardiac repair in ischaemic heart disease. *Clin Sci* 125:319–327.

Weaver JD, Stabler CL (2015) Antioxidant cerium oxide nanoparticle hydrogels for cellular encapsulation. *Acta Biomater* 16:136–144.

Wichterle O, Lím D (1960) Hydrophilic Gels for Biological Use. *Nature* 185:117–118.

Williams AR, Hatzistergos KE, Addicott B, *et al* (2012) Enhanced Effect of Human Cardiac Stem Cells and Bone Marrow Mesenchymal Stem Cells to Reduce Infarct Size and Restore Cardiac Function after Myocardial Infarction. *Circulation.*112:131110.

Wu Y, Chen YX, Yan J, *et al* (2015) Fabrication of conductive polyaniline hydrogel using porogen leaching and projection microstereolithography. *J Mater Chem B* 3:5352–5360.

Xing Y, Lv A, Wang L, *et al* (2012) Engineered myocardial tissues constructed *in vivo* using cardiomyocyte-like cells derived from bone marrow mesenchymal stem cells in rats. *J Biomed Sci* 19:6.

Yamada S, Nelson TJ, Crespo-Diaz RJ, *et al* (2008) Embryonic stem cell therapy of heart failure in genetic cardiomyopathy. *Stem Cells* 26:2644–2653.

Yancy CW, Jessup M, Bozkurt B, *et al* (2016) 2016 ACC/AHA/HFSA Focused Update on New Pharmacological Therapy for Heart Failure: An Update of the 2013 ACCF/AHA Guideline for the Management of Heart Failure: A Report of the American College of Cardiology/American Heart Association Task Force on Clinical Practice Guidelines and the Heart Failure Society of America. *Circulation.* 134. DOI: 10.1161/CIR.0000000000000435.

Yang J-A, Yeom J, Hwang BW, *et al* (2014) *In situ*-forming injectable hydrogels for regenerative medicine. *Prog Polym Sci* 39:1973–1986.

Ye KY, Black LD (2011) Strategies for Tissue Engineering Cardiac Constructs to Affect Functional Repair Following Myocardial Infarction. *J Cardiovasc Transl Res* 4:575–591.

Yeong WY, Sudarmadji N, Yu HY, *et al* (2010) Porous polycaprolactone scaffold for cardiac tissue engineering fabricated by selective laser sintering. *Acta Biomater* 6:2028–2034.

Yoon SJ, Fang YH, Lim CH, *et al* (2009) Regeneration of ischemic heart using hyaluronic acid-based injectable hydrogel. *J Biomed Mater Res B Appl Biomater* 91:163–171.

You J-O, Rafat M, Ye GJC, Auguste DT (2011) Nanoengineering the heart: conductive scaffolds enhance connexin 43 expression. *Nano Lett* 11:3643–3648.

Zhao X, Li P, Guo B, Ma PX (2015) Antibacterial and conductive injectable hydrogels based on quaternized chitosan-graft-polyaniline/oxidized dextran for tissue engineering. *Acta Biomater* 26:236–248.

Zhou J, Chen J, Sun H, *et al* (2014) Engineering the heart: evaluation of conductive nanomaterials for improving implant integration and cardiac function. *Sci Rep* 4:3733.

Zhu Y, Wood NA, Fok K, *et al* (2016) Design of a Coupled Thermoresponsive Hydrogel and Robotic System for Postinfarct Biomaterial Injection Therapy. *Ann Thorac Surg*. 102: 780-6.

List of publications

1. **Remya Komeri** and Jayabalan Muthu. Injectable, cytocompatible, elastic, free radical scavenging and electroconductive hydrogel for cardiac cell encapsulation. Colloids Surf. B Biointerfaces. (2017). 157: 381–390. DOI: 10.1016/j.colsurfb.2017.05.073 (IF: 3.902)

2. **Remya Komeri**, Finosh Gnanaprakasam Thankam, Jayabalan Muthu. Free radical scavenging injectable hydrogels for regenerative therapy. Mater. Sci. Eng. C. (2017) 71: 100–110. http://dx.doi.org/10.1016/j.msec.2016.09.087. (IF: 3.42).

3. **Remya Komeri**, Jayabalan Muthu. In situ crosslinkable elastomeric hydrogel for long-term cell encapsulation for cardiac applications. J Biomed Mater Res Part A.(2016) 12: 2936-2944. DOI: 10.1002/jbm.a.35833. (IF: 3.263).

4. **Remya Komeri**, Jayabalan Muthu. Injectable hydrogel for antioxidant therapy and cell encapsulation. Front. Bioeng. Biotechnol. (2016). Doi : 10.3389 / conf. FBIOE. 2016.01.01876.

5. **Remya Komeri**, Finosh Gnanaprakasam Thankam, Jayabalan Muthu, Influence of matrix and bulk behaviour of an injectable hydrogel on the survival of encapsulated cardiac cells, RSC Adv. (2015), 5: 31439–31449. doi:10.1039/C4RA16254D. (IF: 3.6).

6. Sunita Prem Victor, K.Jibin, M.G.Gayathridevi, **Remya Komeri**, Vineeth.M.Vijayan, Jayabalan Muthu. Design and characterization of biodegradable macroporous hybrid inorganic-organic polymer for orthopedic applications. Mater. Sci. Eng. C. (2017), 77: 513-520. . (IF: 3.42).

7. Sunita.P.Victor, Willi Paul, Vineeth.M.Vijayan, **Remya Komeri**, Jayabalan Muthu, Chandra.P.Sharma. Neodymium doped hydroxyapatite theranostic nanoplatforms for colon specific drug delivery applications. Colloids Surf. B Biointerfaces. (2016),145: 539–547. (IF: 4.1).

8. Sunita Prem Victor, Vineeth.M.Vijayan, **Remya Komeri**, Shivaram Selvam, Jayabalan Muthu, Covalently cross-linked hydroxyapatite–citric acid–based biomimetic polymeric composites for bone applications, J. Bioact. Compat. Polym. Biomed. Appl. (2015), 1-17. doi:10.1177/0883911515585181. (IF: 1.56).

9. Vineeth.M.Vijayan, **Remya Komeri**, Sunita.P.Victor, Jayabalan Muthu, Photoluminescent PEG based comacromers as excitation dependent fluorophores for biomedical applications, Colloids Surf. B Biointerfaces. (2015), 135: 243–252. doi:10.1016/j.colsurfb.2015.07.027. (IF: 4.1).

10. **Remya Komeri** and Jayabalan Muthu. Tissue Engineering Strategies to Confront End Stage Heart Failure: Novel Approaches from Cell Therapy to Bioprinting. J.Cardiovascular Disease. (Under review)

Conference proceedings

1. **Remya Komeri** and Jayabalan Muthu. Injectable poly propylene fumarate-co-ethylene glycol)/PEGDA hydrogel for myocardial cell therapy. Polymer conference for Young researchers (PCYR-15) conference Society for Polymer Science India (SPSI), NIIST, Trivandrum. Invited talk. 18th December, 2015.

2. **Remya Komeri**, Jayabalan Muthu. Injectable Hydrogels With Inherent and Consistent Free Radical Scavenging Property for Cardiac Applications. Kerala Science Congress, Malappuram, January 28-30, 2016. (**Best paper award**)

3. **Remya Komeri** and Jayabalan Muthu. Injectable Hydrogel for Antioxidant Therapy and Cell Encapsulation. World Biomaterial Congress, Montreal, Canada. 17-22 May, 2016.

4. **Remya Komeri** and Jayabalan Muthu. The injectable, conducting hydrogel for cell therapy and cardiac applications. BiTerm conference, IIT, New Delhi. 15-17 April, 2016.

Curriculum vitae

Remya Komeri

Education

JRF/SRF	Biomaterials science at SCTIMST, Kerala, India.
(01/2014 to 01/2017)	Advisor: Dr. M. Jayabalan. Ph.D, D.Sc, FABMS
M.Sc (2011-2013)	Biotechnology with 9.08 CGPA and 3rd rank. Cochin University of Science and Technology, Kochi, Kerala, India.
B.Sc (2008-2011)	Biotechnology with 90 % and 1st rank. Karyavattom Govt. College, Kerala University, Kerala, India.
Awards:	Best paper award in 28th Kerala Science Congress held at Malappuram on January 28-30, 2016.

Home address

Kommeri house

Podikundu, milma road

P.O. Pallikunnu, Kannur - 670004

Phone: 9946835353

E-mail: remyakomeri@gmail.com